Targeted and Stimuli-Responsive Polymers as Chemotherapeutic Delivery Systems

by

Noreen Tasneem Zaman

B.Sc. Chemical Engineering
University of Calgary, 2000

Submitted to the Department of Chemical Engineering in
Partial Fulfillment of the Requirements for the Degree of

Doctor of Philosophy in Chemical Engineering

at the

MASSACHUSETTS INSTITUTE OF TECHNOLOGY

June 2008

Author: _____

Department of Chemical Engineering
March 4, 2008

Certified by: _____

Professor Jackie Y. Ying
Adjunct Professor of Chemical Engineering
Thesis Supervisor

Accepted by: _____

Professor William M. Deen
Professor of Chemical Engineering
Chairman, Departmental Committee for Graduate Studies

Targeted and Stimuli-Responsive Polymers as Chemotherapeutic Delivery Systems

by

Noreen Tasneem Zaman

B.Sc. Chemical Engineering
University of Calgary, 2000

Submitted to the Department of Chemical Engineering in
Partial Fulfillment of the Requirements for the Degree of
Doctor of Philosophy in Chemical Engineering

Abstract

Successful administration of chemotherapeutic agents for cancer treatment requires a balance between the efficacy and the safety of the drug. This often limits physicians to a very narrow therapeutic window. To avoid the harmful side-effects, chemotherapeutic agents may be administered at a suboptimal dose. This is not only a less effective treatment, but can lead to the development of drug resistance by cancerous cells. The therapeutic window can be increased through targeted, stimuli-responsive delivery, which increases the drug concentration at the diseased site, and releases or activates the drug only when it reaches the target. Cancer is a highly variable disease occurring in many organs. There is a need for delivery systems that are easily adaptable for a number of targets in different forms of cancers, and that can accommodate various cytotoxic drugs. The motivation of this project was to develop flexible synthesis procedures for the targeted delivery of chemotherapeutic agents. In this work, we have synthesized and tested three drug delivery systems.

The first system is a dextran-based polymer conjugate designed to preferentially deliver doxorubicin to hepatocytes. Doxorubicin has been conjugated to dextran of different molecular weights, with varying degrees of galactose substitution. The degree of doxorubicin substitution was maintained by performing the conjugation of doxorubicin and galactose in two sequential steps. The synthesis scheme was simple, efficient and easily adaptable to other therapeutic agents and targeting moieties with free amine groups. In cell culture studies on target hepatocytes, the dextran-doxorubicin-galactose (DDG) conjugates showed lower toxicity compared to doxorubicin, increased toxicity with higher molecular weight polymers, and greater toxicity with higher degree of galactose substitution. Experiments in the control cell lines showed increased toxicity for higher molecular weight polymers; however, there was no effect due to the presence of galactose. At diameters of 15–40 nm, the polymer conjugates were too large to enter the cell nuclei in large quantities; however, a sufficient amount of doxorubicin entered the nuclei to cause cell death. The higher molecular weight polymers were more effective as they had a higher chain loading of doxorubicin.

In spite of significant uptake of the targeted conjugates, the cytotoxicity of the first system was limited since the doxorubicin remained attached to the polymer. For the second

system, pH-sensitive dextran-doxorubicin conjugates of different molecular weights were synthesized. The doxorubicin was attached to the dextran backbone through a hydrazone bond. These polymer conjugates were stable at a physiological pH of 7.4, but released over 70% of the attached doxorubicin within 24 h at a pH of 5.0. The rate of release was found to be faster for the lower molecular weight polymers. In cell culture studies, the conjugates showed significant cytotoxicity. The effect of lower chain loading of doxorubicin for the lower molecular weight polymers was offset by the rapid initial release; these polymers showed slightly greater toxicity. Live confocal microscopy indicated that the conjugates were internalized by cells within minutes after incubation. Since release of doxorubicin from the conjugates was much slower than cellular trafficking, it is possible that the conjugates went through multiple endocytosis and exocytosis cycles before the doxorubicin was released. Doxorubicin from the dextran-hydrazone-doxorubicin (DHD) conjugates was found to localize almost exclusively in the nuclei of cells. Since doxorubicin attached to dextran with a stable bond showed limited localization in the nuclei, this indicated that doxorubicin from the acid-labile conjugates was released after internalization by cells. The cytotoxicity of the DHD conjugates was significantly greater than the stable DDG conjugates due to the release of doxorubicin inside cells.

In the third system, the targeting and pH-sensitivity functionalities were combined by expressing galactose on an amphiphilic, temperature- and pH-sensitive copolymer of *N*-isopropylacrylamide (NIPAAm), *N*,*N*-dimethylacrylamide (DMAAm) and 10-undecenoic acid (UA). The polymer self-assembled in aqueous medium, and was used to encapsulate paclitaxel. Various synthesis parameters were adjusted to yield polymers that achieved high drug loading and rapid release in a temperature- and pH-responsive manner. The appropriate lower critical solution temperature (LCST) was obtained by adjusting the content of DMAAm and UA to change the hydrophilicity of the polymer. The hydrophilicity of UA was dependent on pH and thus, made the polymer pH-sensitive. Galactose was attached to the end-group of the copolymer to target it to hepatocytes. The drug loading, particle size and release rate were affected by the polymer molecular weight. Paclitaxel was encapsulated in particles that released nearly 100% of the drug within 24 h at a pH of 5.0 at 37°C. In the target hepatocyte cell line, the stimuli-responsive, galactose-expressing particles were significantly more toxic than the non-stimuli-responsive as well as the non-targeted particles. In the control cell line, the presence of galactose did not have any effect on cytotoxicity.

In summary, we have synthesized three targeted drug delivery systems. The DDG conjugates successfully targeted hepatocytes by expressing galactose. The DHD conjugates would be retained in tumors due to the enhanced permeability and retention effect, and release the drug at the target site. The galactose-targeted paclitaxel-loaded particles synthesized from the temperature- and pH-sensitive polymer achieved a remarkable increase in toxicity in the target cell line, while maintaining base toxicity in the control cell line. Both the amount of drug delivered and the rate of release were found to be important in the efficacy of the drug delivery vehicles.

Thesis Supervisor:
Jackie Y. Ying
Adjunct Professor of Chemical Engineering

Acknowledgements

I would like to thank my thesis advisor Professor Jackie Ying for her advice, support and patience. I am deeply grateful for the opportunity to work with her on my dissertation. I have had the opportunity to work in her laboratories at both MIT and in Singapore with many bright and inspiring people. I also thank my Thesis Committee members, Professor William Deen, Professor John Essigmann and Professor Paula Hammond for providing many helpful discussions and suggestions over the years.

Working at the Nanostructured Materials Research Laboratory at MIT was a pleasure due to the people there. I would like to thank the following group members for making my time memorable: Dr. John Lettow, Dr. Edward Ahn, Dr. Jason Sweeney, Dr. Justin McCue, Dr. Neeraj Sangar, Dr. Su Seong Lee, Dr. Javier García-Martínez, Dr. Yee San Su, Dr. Suniti Moudgil, Dr. Todd Zion, Dr. Thomas Lancaster, Dr. Pemakorn Pitukmanorom, Dr. Xiaohua Huang, Dr. Tseh-Hwan Yong, Dr. Steven Weiss, Dr. Hong He, Dr. Jianyi Cui and Cindy Ren. I would like to thank Todd, Suniti, Tseh-Hwan and Cindy for numerous helpful discussions and suggestions. Linda Mousseau was a tremendous help with all the administrative tasks. Four undergraduate students have worked on this project at different times. I would like to thank Fred Tan, Bei Xian Tan, Shilpa Joshi and Melanie Worley for their contributions and for their enthusiasm for the project.

I would like to thank the Colton Laboratory at MIT for use of cell culture facilities. Parts of this work were conducted utilizing the W. M. Keck Foundation Biological Imaging Facility at the Whitehead Institute. I would also like to thank the staff and students at the Institute of Bioengineering and Nanotechnology (IBN) in Singapore for their generous help during my many visits there starting from the Summer of 2004. In particular, I would like to thank Dr. Yiyan Yang for many helpful discussions, and her collaboration in Chapter 4 of this thesis.

This research was supported by the Singapore-MIT Alliance, and IBN (Biomedical Research Council, Agency for Science, Technology and Research, Singapore).

On a personal note, I want to especially thank Cindy for her friendship and support while we were in Singapore. I would like to thank several of my friends for helping to keep my life balanced: Ghada, Jean, Saeeda, Charisma, Tanvir, Nehreen, Mishu, Shakib, Adnan, Saber and Sarwat.

I want to thank my family, without whom this thesis could not have been completed. A special acknowledgement goes to my parents Jasimuz and Salma Zaman, whose unconditional love, support and belief in me have been my motivation in every step of my life, not the least for my PhD. I also thank my brother Emon and sister-in-law Janifah for their love and encouragement, and for my niece Tanisha, who is the light of my life. I would also like to acknowledge my parents-in-law Anwarul and Shaneara Kabir, and my brother-in-law Safen Kabir for their constant encouragement and support. Last but not least, I want to thank my husband Sujan Kabir for his love, support and confidence in me.

Table of Contents

List of Figures

List of Tables

Chapter 1 – Background and Motivation

1.1 Limitations on Conventional Cancer Treatment

Cancer is the growth of a population of cells with a genetic abnormality, which results in unrestrained cell division. In the early stages, the cancerous cells accumulate to form a localized tumor. If the tumor is malignant and remains undetected, it can metastasize and form secondary tumors in other organs. Cancer is the second leading cause of death after heart disease in the USA. Over 10.5 million people in the USA have or have had some form of cancer, and over two million new cases are expected in 2007 [1]. The five-year relative survival rate for all types of cancer is only 66% [1]. Conventional treatment involves various combinations of surgery, radiation therapy and chemotherapy. Radiation and chemotherapy are used if the cancer is inoperable or metastasized, and also as follow-up to surgery. In addition, immunotherapy and hormone therapy have been used in the treatment of certain forms of melanoma, breast and prostate cancers [2].

Chemotherapeutic agents are cytotoxic drugs, which affect any cells in the body that are actively dividing. The side-effects can include nausea, vomiting, immunosuppression, mucositis, hepatotoxicity, nephrotoxicity, memory loss, anemia and even death. Several chemotherapeutic agents also have long-term side-effects in major organs such as the heart, lungs, kidneys and central nervous system [1]. To avoid these adverse effects, conventional chemotherapeutic agents must be administered at a safe, but suboptimal dose, which is insufficient to treat the cancer satisfactorily in one session [3]. Physicians have attempted to treat cancer using these lower doses over a longer period of time, however, this is often ineffective due to the development of drug resistance by the cancerous cells [3]. Currently, patients are given "combination chemotherapy" – multiple drugs at various doses to try to circumvent these problems.

Newer treatments such as tumor vaccines and small-molecule therapies avoid many of the side-effects by targeting surface or intracellular proteins specific to the cancer being treated. However, these methods can only deal with very specific diseases. Cytotoxic drugs can be used to treat several types of cancers, and would be highly effective if they entered only cancerous cells. The limitations in conventional cancer treatment can be alleviated by targeted drug

delivery, which is a vehicle that will preferentially carry the drug to the target site in the body, and thereby reduce the amount of drug in the rest of the body that can cause undesired side-effects. This would increase the range in which a drug is both safe and effective.

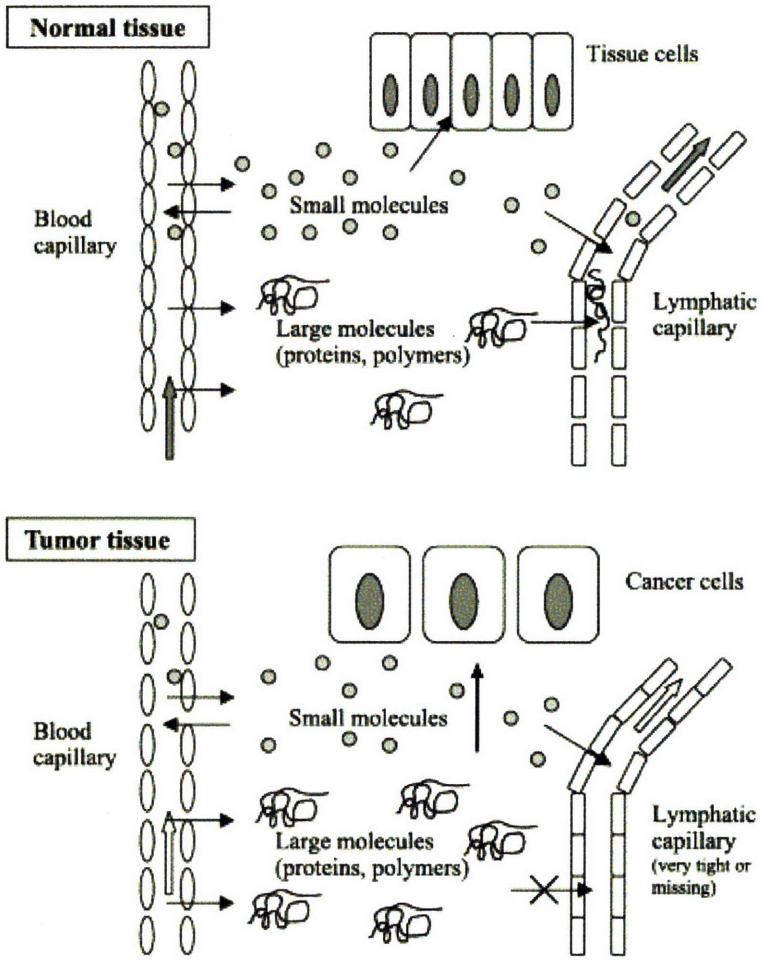

Fig. 1.1. Schematic illustration of differences between cancerous and healthy tissues [4].

There are a number of strategies that have been investigated to target tumors. Fig. 1.1 shows the basic physiological differences between healthy and cancerous tissues. As shown, tumors have leaky blood vessels and tight lymphatic capillaries, which allow them to take up and retain large molecules or particles. This is called the enhanced permeability and retention (EPR) effect, and has been used to passively target macromolecules or particles to tumors since uptake by normal tissue is comparatively lower. Yuan *et al.* conducted a study to determine size gaps between cells in tumor blood vessels. They found that while tumor vasculature permeability was

both temporally and spatially heterogeneous, the pore size ranged from 200-600 nm with a mean of 400 nm [5, 6]. Another difference between tumors and healthy tissue is that the pH in a tumor is on average 7.0 and widely variable, as compared to a pH of 7.4 in normal tissue [7]. Thirdly, cancerous cells may differ from normal cells in their protein expression and morphology, and in the ability to form new blood vessels or angiogenesis. Many researchers are utilizing one or more of these differences to achieve targeted treatment of cancer. A targeted drug delivery system can have several features, which are addressed in the next section.

1.2 Targeted Drug Delivery Systems

1.2.1 Drug Carrier

After administration, a targeted drug delivery vehicle must remain in circulation long enough to locate the target cells or organ, bind to them, and stimulate the appropriate response. This has been a challenge because drugs are usually low molecular weight molecules that are rapidly cleared from the plasma [8-10]. Residence time of drugs in the body can be increased by various means, including conjugation to polymers, and encapsulation in particles, micelles or liposomes.

Polymeric conjugates can enhance the performance of a drug in several ways. They increase the circulation time in the plasma, protect the drug from various enzymes and the immune system, and decrease non-specific toxicity [11, 12]. Chemical modification of polymers also allows addition of functionalities, such as receptor targeting and stimuli-responsive activation of the drug. Another advantage is that polymer-bound drugs are less likely to be expelled from multidrug-resistant cells [13]. Conversely, conjugation to a polymer results in reduced therapeutic effect compared to the free drug. Polymers that have been used for drug delivery include poly(lactic acid) (PLA), poly(glycolic acid), poly(ethylene glycol) (PEG), poly(L-lysine), poly(ethylene oxide), poly(ε-caprolactone) (PCL), N-isopropylacrylamide (NIPAAm), poly(methyl methacrylate), poly((N-2-hydroxypropyl)methacrylamide) (HPMA), chitosan and dextran, as well as various copolymers of these and other polymers [13-21].

Many researchers have studied the interaction of particles with cells both *in vitro* and *in vivo*. A critical parameter is the size of the particles. Micrometer-sized particles can induce an

immune response *in vivo* and are not taken up by many cell types [9]. Nanoparticles smaller than 100–150 nm have been found to be efficiently taken up in cell culture, perfusion and *in vivo* studies [22-24]. Our preliminary experiments using inert nanoparticles have shown that particles up to 200 nm diameter were taken up by hepatocytes in cell culture. Mitra *et al.* have synthesized chitosan nanoparticles of 100 nm diameter, and found that they were retained in tumors due to the EPR effect in a mouse cancer model [21].

PEG has been used by many researchers as the hydrophilic end of amphiphilic copolymers to form micelles for drug delivery. Micelles formed from PLA-PEG block copolymers were found to accumulate in the liver in *in vivo* studies [25]. When this copolymer was used to encapsulate doxorubicin, the micelles were stable and degraded over a period of five weeks [26]. These systems degrade very slowly and have no tunable release mechanism. Micelles formed from copolymers of PEG and PCL have been studied for the delivery of rapamycin. Rapamycin from these micelles was also released in a non-specific manner; however, they achieved full release in 6 days [27].

Liposomes can be used to deliver hydrophilic therapeutics. Some of the biggest challenges in liposomal delivery are that they are often leaky, have non-specific release, and fuse very easily with the cell membrane. Simoes *et al.* have worked on making liposomes stimuli-responsive using the pH-sensitive lipid phosphatidylethanolamine, and longer circulating by attaching PEG to the lipid to stabilize it in plasma. The liposome is also targeted to the H-2^k antigen, which is expressed on several types of tumors [28]. Zignani *et al.* imparted pH sensitivity to their egg phosphatidylcholine-cholesterol liposomes by incorporating NIPAAm copolymers into the lipid bilayer. They achieved 45% release after 16 h, and found that release was proportional to NIPAAm content [29].

1.2.2 Mechanism for Targeting

The key to successful targeting is to find a detectable difference between the target and the rest of the body. A promising method is protein-targeted delivery. In recent years, much attention has been given to ligand-binding receptor proteins, such as hormone and growth factor receptors, antigens (antibody receptors) and lectins (carbohydrate receptors) expressed on the cell surface in a tissue-specific manner. For example, macrophages and hepatocytes express

high concentrations of mannose and galactose binding sites, respectively [4, 30]. As mentioned before, cancer can cause a change in the expression of cell surface receptors. In particular, growth factor receptors, certain antigens and lectins are expressed on cancerous tissue at a higher concentration than on their healthy counterparts [13, 19, 31]. Transferrin and growth factors aid in cell division and their receptors are expressed in high concentrations in several types of cancers [32, 33]. The folate receptor is expressed in a high concentration in various forms of cancer, such as ovarian, lung, breast and colon cancer [34-36].

Targeting cancerous cells is challenging because the target cells can be spread throughout the whole body at a low concentration compared to the healthy cells. Also, the receptors being targeted are present on healthy cells as well, though at lower concentrations [37]. The success of this method is dependent on the higher local concentration of receptors on cancerous cells, resulting in more frequent binding of the drug delivery vehicle.

The antibody-antigen recognition system has been studied extensively recently, and a few drugs utilizing its potential are on the market or in clinical trials [10, 37, 38]. Some of the obstacles in antibody-targeted delivery include low tumor penetration, immunogenicity, poor internalization, and low and variable antigen density [31, 32]. Antibody-antigen binding has high affinity, which causes the drug delivery vehicle to bind strongly to the target. However, due to the strong binding, the vehicle may not be able to penetrate the tumor or tissue very effectively [37]. If an intact antibody is used for targeting, there would be a higher chance for the vehicle to be detected by the immune system and cleared rapidly [37, 39]. Antigens often recognize multiple antibodies that have a similar binding site, which lowers the specificity [39]. Since antibodies and antigens are proteins, their binding sites are dependent on the integrity of the three-dimensional amino acid structures. Processing of antibodies during synthesis of a delivery system may negatively affect this binding site, and lower the specificity and/or the binding affinity.

Despite all of these limitations, much research is being conducted in the area of antigen-targeted delivery, and a number of potential targets have been identified. Dillman *et al.* have worked on targets from several different types of cancers, including chronic lymphocytic leukemia and cutaneous T-cell lymphoma, and non-small cell lung carcinoma [40, 41]. They

synthesized conjugates of anti-human T-cell antibody and doxorubicin. They have also conjugated daunorubicin to the antibody with an acid-labile bond, and found improved performance in cell culture studies and a mouse model [42]. The HER2 receptor in breast cancer and tranferrin, and HER2/neu in immortalized breast cancer cell lines have been investigated. Doxorubicin-loaded liposomes expressing anti-HER2 were used to successfully treat tumors in animal models for breast cancer [43]. In breast cancer cell lines, certain combinations of immunotoxins targeting different antigens were found to have a synergistic cytotoxic effect [44]. Human chorionic gonadotropin receptors on breast cancer cell lines were also used as a target, and a ten-fold increase in cytotoxicity was observed using the targeted vehicle [45].

The lectin-carbohydrate system is a comparatively new area of study and shows great potential [9, 13, 19, 39, 46, 47]. It offers a few advantages over antibody-directed delivery. The dissociation constant for lectin-carbohydrate binding is in the millimolar to micromolar range, compared to the micromolar to picomolar range for antigen-antibody binding. The lower affinity between lectins and carbohydrates allows for greater tumor penetration [37, 48-51]. Also, the affinity can be increased with a higher density of carbohydrates expressed on the delivery vehicle [52]. A significant advantage of lectin targeting is that when carbohydrates on glycoproteins bind to their specific lectins, the resulting complex is taken into the cell by the process of receptor-mediated endocytosis (RME). RME is a rapid mechanism to internalize certain receptor-ligand complexes [53, 54]. Antigens usually do not undergo RME, however, they can get internalized by non-specific endocytosis, which is slower than RME [55]. Additionally, simple carbohydrates or carbohydrate chains are more robust and easier to work with than proteins. They are unlikely to become modified due to temperature, solvents or chemical processing.

Some potential lectin targets have been identified recently, such as the receptors for wheat germ agglutinin and peanut agglutinin on colon tissue for cancer or other diseases of the colon [17]. Colon adenocarcinomas have also been shown to express receptors for α-galactose, α-glucose and N-acetyl-β-glucosamine [52, 56]. Monsigny *et al.* have shown that murine leukemia cells express a high concentration of L-fucose receptors, and are studying the use of glycoconjugates for gene delivery [19]. Yamazaki *et al.* have attached glycoproteins to the surface of liposomes for targeted drug delivery [57].

1.2.3 Drug Release

A high percentage of macromolecules, proteins or particles taken up by endocytic pathways is trafficked to lysosomes and subsequently degraded [58]. However, chemotherapeutic agents must usually enter the nucleus of cells to cause cell cycle arrest or cell death. Whether the drug is conjugated to polymers or encapsulated within particles, micelles or liposomes, it must be released once it has reached the target site. If it is delivered in a conjugate form or in a slightly altered form due to synthesis, it must remain potent.

Fig. 1.2 is a schematic representation of RME of a hypothetical protein. After the ligand on the protein binds to its receptor on the cell surface, the complex is trapped in a clathrin-coated pit (1). Once enough receptor-ligand complexes occupy a coated pit, the clathrin polymerizes further and forms a separate vesicle in the cell cytosol (2). The clathrin then depolymerizes, allowing the vesicle to fuse with an endosome (3). The influx of H^+ and Cl^- ions cause a lowering of the pH of the endosome from 7.4 to ~ 5.0, causing the receptor and ligand to dissociate (4). The receptors are then usually recycled back to the cell surface as rapidly as every 10–20 min (5) [55]. The ligands may diffuse into the cytosol, or be transported to a lysosome, depending on its function in the cell.

Lysosomes contain many proteases and enzymes that may degrade the drug, therefore the drug must be released from the delivery vehicle in the endosome. Strategies for endosomal escape include endosomal disruption, enzyme-degradable crosslinkers and pH-sensitive release. Subbarao *et al.* performed studies on pH-dependent peptide disruption of lipid bilayers [59], which was put into use for endosomal disruption by researchers working on drug delivery. Murthy *et al.* have worked on a polymer with a PEG-shielded membrane-disruptive backbone. The PEG was released from the backbone in the low pH of the endosome, and the exposed acetal backbone broke open the endosome. Their experiments showed successful disruption of red blood cell membranes [58]. Duncan *et al.* have synthesized HPMA-drug conjugates with a peptide linker (Gly-Phe-Leu-Gly), which could be degraded by lysosomal proteases such as cathepsin B [60]. HPMA has also been conjugated to drugs using pH-sensitive hydrazone or *cis*-aconytil bonds. Its cytotoxicity in cell culture studies was found to be greater than for conjugates with an enzymatically degradable peptide [61]. Yoo *et al.* studied pH-sensitive release using two

synthesis strategies with a block copolymer of PLA and methoxy-poly(ethylene glycol). They found that the hydrazone bond performed much better than the acetal bond in terms of drug release and *in vitro* cytotoxicity. However, their polymer self-assembled to form micelles and released only ~ 40% of the drug over 24 h, and took up to 25 days to release the full amount [62].

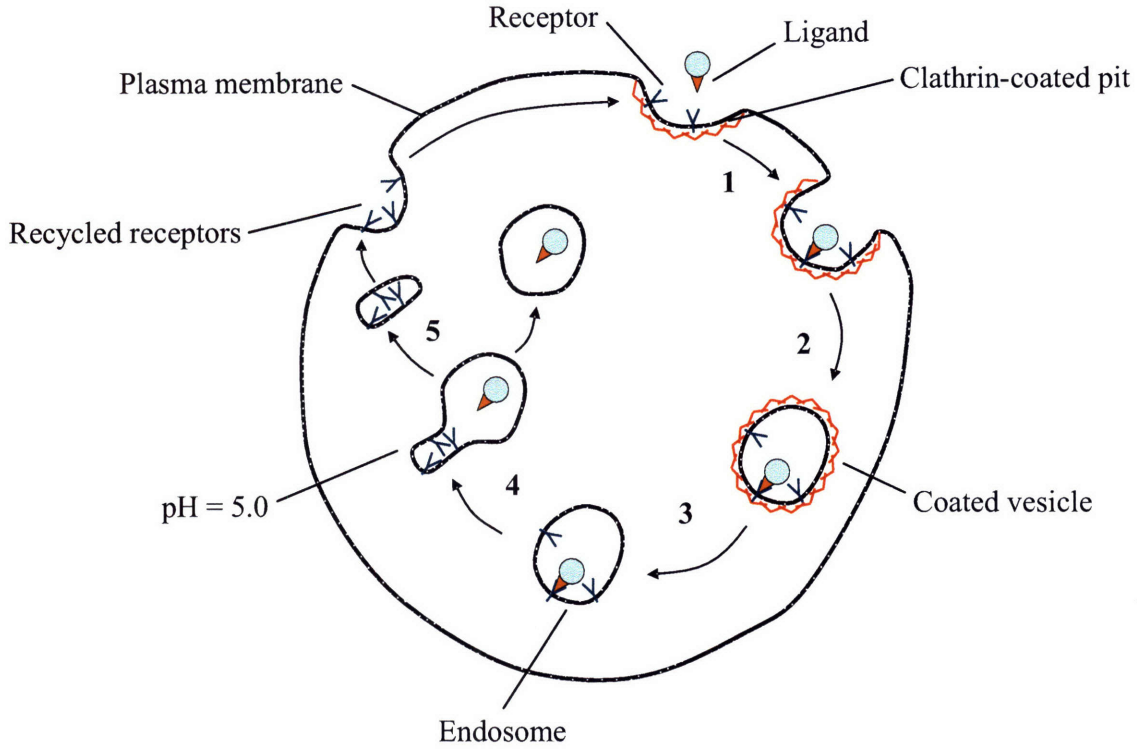

Fig. 1.2. Schematic of RME (adapted from [55]).

1.3 Project Goals

Cancer is a highly variable disease occurring in many organs. The variation is significant enough that cancer of each organ is treated as a separate disease. In spite of significant progress in the last few decades in the field of targeted drug delivery, more work is needed in improving target recognition, minimizing premature release, optimizing release at the target, and preserving drug efficacy despite chemical alteration [8, 12, 63]. There is a need for delivery systems that

are easily adaptable for a number of targets in different forms of cancers, and that can accommodate various cytotoxic drugs.

In this work, we have synthesized and tested three drug delivery systems for the delivery of chemotherapeutic agents. The first system is a dextran-based polymer conjugate designed to preferentially deliver doxorubicin to hepatocytes (Chapter 2). The second system is a pH-sensitive conjugate of dextran and doxorubicin, which releases the drug at low pH (Chapter 3). The third system is a temperature- and pH-sensitive copolymer that expresses a targeting moiety, and is used to encapsulate a hydrophobic drug and deliver it to hepatocytes in a pH-sensitive manner (Chapter 4).

1.4 References

[1] "Cancer Facts and Figures 2007", *American Cancer Society*, (2007).

[2] *Cancer: Principles & Practice of Oncology*, V. DeVita, Ed., 6th ed. Philadelphia: Lippincott, Williams & Wilkins, (2001).

[3] M. Yang, H. L. Chan, W. Lam, W. F. Fong, Cytotoxicity and DNA binding characteristics of dextran-conjugated doxorubicins, BBA Gen. Subjects 1380 (1998) 329–335.

[4] K. Ulbrich, V. Subr, Polymeric anticancer drugs with pH-controlled activation, Adv. Drug. Deliv. Rev. 56 (2004) 1023–1050.

[5] W. Monsky, D. Fukumura, T. Gohongi, M. Ancukiewcz, H. Weich, V. Torchilin, F. Yuan, R. Jain, Augmentation of transvascular transport of macromolecules and nanoparticles in tumors using vascular endothelial growth factor, Cancer Res. 59 (1999) 4129–4135.

[6] F. Yuan, M. Dellian, D. Fukumura, M. Leunig, D. Berk, V. Torchilin, R. Jain, Vascular permeability in a human tumor xenograft: Molecular size dependence and cutoff size, Cancer Res. 55 (1995) 3752–3756.

[7] I. Tannock, D. Rotin, Acid pH in tumors and its potential for therapeutic exploitation, Cancer Res. 49 (1989) 4373–4384.

[8] M. C. Garnett, Targeted drug conjugates: Principles and progress, Adv. Drug. Deliv. Rev. 53 (2001) 171–216.

[9] C. K. Kim, S. J. Lim, Recent progress in drug delivery systems for anticancer agents, Arch. Pharm. Res. 25 (2002) 229–239.

[10] R. Duncan, Polymer conjugates as anticancer nanomedicines, Nat. Rev. Cancer 6 (2006) 688–701.

[11] R. Mehvar, Dextrans for targeted and sustained delivery of therapeutic and imaging agents, J. Control. Release 69 (2000) 1–25.

[12] N. Munshi, P. De, A. Maitra, Size modulation of polymeric nanoparticles under controlled dynamics of microemulsion droplets, J. Colloid Interface Sci. 190 (1997) 387–391.

[13] L. Seymour, Soluble polymers for lectin-mediated drug targeting, Adv. Drug. Deliv. Rev. 14 (1994) 89–111.

[14] L. Seymour, K. Ulbrich, S. Wedge, I. Hume, J. Strohalm, R. Duncan, N-(2-Hydroxypropyl)methacrylamide copolymers targeted to the hepatocyte galactose-receptor: Pharmacokinetics in DBA2 mice, Br. J. Cancer 63 (1991) 859–866.

[15] R. Duncan, S. Dimitrijevic, E. Evagorou, The role of polymer conjugates in the diagnosis and treatment of cancer, STP Pharma. Sci. 6 (1996) 237–263.

[16] W. Amass, A. Amass, B. Tighe, A review of biodegradable polymers: Uses, current developments in the synthesis and characterization of biodegradable polyesters, blends of biodegradable polymers and recent advances in biodegradation studies, Polym. Int. 47 (1998) 89–144.

[17] Z.-R. Lu, J.-G. Shiah, S. Sakuma, P. Kopeckova, J. Kopecek, Design of novel bioconjugates for targeted drug delivery, J. Control. Release 78 (2002) 165–173.

[18] E. Gianasi, M. Wasil, E. Evagorou, A. Keddle, G. Wilson, R. Duncan, HPMA copolymer platinates as novel antitumour agents: *In vitro* properties, pharmacokinetics and antitumour activity *in vivo*, Eur. J. Cancer 35 (1999) 994–1002.

[19] M. Monsigny, A. Roche, P. Midoux, R. Mayer, Glycoconjugates as carriers for specific delivery of therapeutic drugs and genes, Adv. Drug. Deliv. Rev. 14 (1994) 1–24.

[20] K. Ulbrich, V. Subr, J. Strohalm, D. Plocova, M. Jelinkova, B. Rihova, Polymeric drugs based on conjugates of synthetic and natural macromolecules: I. Synthesis and physico-chemical characterization, J. Control. Release 64 (2000) 63–79.

[21] S. Mitra, U. Gaur, P. Ghosh, A. Maitra, Tumour targeted delivery of encapsulated dextran-doxorubicin conjugate using chitosan nanoparticles as carrier, J. Control. Release 74 (2001) 317–323.

[22] P. Rensen, L. Sliedregt, A. Ferns, E. Kieviet, S. van Rossenberg, S. van Leeuwen, T. van Berkel, E. Biessen, Determination of the upper size limit for uptake and processing of ligands by the asialoglycoprotein receptor on hepatocytes *in vitro* and *in vivo*, J. Biol. Chem. 276 (2001) 37577–37584.

[23] K. Ogawara, M. Yoshida, K. Higaki, T. Kimura, K. Shiraishi, M. Nishikawa, Y. Takakura, M. Hashida, Hepatic uptake of polystyrene microspheres in rats: Effect of particle size on intrahepatic distribution, J. Control. Release 59 (1999) 15–22.

[24] W. Zauner, N. Farrow, A. Haines, *In vitro* uptake of polystyrene microspheres: Effect of particle size, cell line and cell density, J. Control. Release 71 (2001) 39–51.

[25] S. Hagan, A. Coombes, M. Garnett, S. Dunn, M. Davies, L. Illum, S. Davis, S. Harding, S. Purkiss, P. Gellert, Polylactide-poly(ethylene glycol) copolymers as drug delivery systems. 1. Characterization of water dispersible micelle-forming systems, Langmuir 12 (1996) 2153–2161.

[26] E. Piskin, X. Kaitian, E. Denkbas, Z. Kucukyavuz, Novel PDLLA/PEG copolymer micelles as drug carriers, J. Biomater. Sci. Polym. Ed. 7 (1995) 359–373.

[27] M. Forrest, C.-Y. Won, A. Malick, G. Kwon., *In vitro* release of the mTOR inhibitor rapamycin from poly(ethylene glycol)-b-poly(ε-caprolactone) micelles, J. Control. Release 110 (2006) 370–377.

[28] S. Simoes, J. N. Moreira, C. Fonseca, N. Duzgunes, M. de Lima, On the formulation of pH-sensitive long circulation times, Adv. Drug. Deliv. Rev. 56 (2004) 947–965.

[29] M. Zignani, D. Drummond, O. Meyer, K. Hong, J.-C. Leroux, *In vitro* characterization of a novel polymeric-based pH-sensitive liposome system, Biochim. Biophys. Acta 1463 (2000) 383–394.

[30] L. Seymour, R. Duncan, J. Strohalm, J. Kopecek, Effect of molecular weight of N-(2-hydroxypropyl)methacrylamide copolymers on body distribution and rate of excretion after subcutaneous, intraperitoneal, and intravenous administration in rats, J. Biomed. Mater. Res. 21 (1987) 1341–1358.

[31] G. Dubowchik, M. Walker, Receptor-mediated and enzyme-dependent targeting of cytotoxic anticancer drugs, Pharmacol. Ther. 83 (1999) 67–123.

[32] M. Singh, A. Ferdous, M. Branham, G. Betageri, Trends in drug targeting for cancer treatment, Drug Deliv. 3 (1996) 289–304.

[33] C. Dufes, A. Schatzlein, L. Tetley, A. Gray, D. Watson, J.-C. Olivier, W. Couet, I. Uchegbu, Niosomes and polymeric chitosan based vesicles bearing transferrin and glucose ligands for drug targeting, Pharm. Res. 17 (2000) 1250–1258.

[34] J. Reddy, P. Low, Folate-mediated targeting of therapeutic and imaging agents to cancers, Crit. Rev. Ther. Drug Carrier Syst. 15 (1998) 587–627.

[35] J. Sudimack, R. Lee, Targeted drug delivery via the folate receptor, Adv. Drug. Deliv. Rev. 41 (2000) 147–162.

[36] H.–S. Yoo, T. Park, Folate-receptor-targeted delivery of doxorubicin nano-aggregates stabilized by doxorubicin-PEG-folate conjugate, J. Control. Release 100 (2004) 247–256.

[37] T. Allen, Ligand-targeted therapeutics in anticancer therapy, Nat. Rev. Cancer 2 (2002) 750–763.

[38] L. Brannon-Peppas, J. Blanchette, Nanoparticle and targeted systems for cancer therapy, Adv. Drug. Deliv. Rev. 56 (2004) 1649–1659.

[39] A. S. Kearney, Prodrugs and targeted drug delivery, Adv. Drug. Deliv. Rev. 19 (1996) 225–239.

[40] R. Dillman, D. Shawler, D. Johnson, D. Meyer, J. Koziol, J. Frincke, Preclinical trials with combinations and conjugates of T101 monoclonal antibody and doxorubicin, Cancer Res. 46 (1986) 4886–4891.

[41] D. Elias, L. Kline, B. Robbins, H. Johnson, K. Pekny, M. Benz, J. Robb, L. Walker, M. Kosty, R. Dillman, Monoclonal-antibody KS1/4-methotrexate immunoconjugate studies in nonsmall cell lung-carcinoma, Am. J. Respir. Crit. Care. Med. 150 (1994) 1114–1122.

[42] R. Dillman, D. Johnson, D. Shawler, J. Koziol, Superiority of an acid-labile daunorubicin monoclonal antibody immunoconjugate compared to free drug, Cancer Res. 48 (1988) 6097–6102.

[43] J. Park, K. Hong, D. Kirpotin, G. Colbern, R. Shalaby, J. Baselga, Y. Shao, U. Nielsen, J. Marks, D. Moore, D. Papahadjopoulos, C. Benz, Anti-HER2 immunoliposomes:

Enhanced efficacy attributable to targeted delivery, Clin. Cancer Res. 8 (2002) 1172–1181.

[44] J. Crews, L. Maier, H. Yin, S. Hester, K. O'Briant, D. Leslie, K. DeSombre, S. George, C. Boyer, Y. Argon, R. Bast, A combination of two immunotoxins exerts synergistic cytotoxic activity against human breast-cancer cell lines, Int. J. Cancer 51 (1992) 772–779.

[45] G. Gebauer, T. Fehm, E. P. Beck, A. Berkholz, P. Licht, W. Jager, Cytotoxic effect of conjugates of doxorubicin and human chorionic gonadotropin (hCG) in breast cancer cells, Breast Cancer Res. Treat. 77 (2003) 125–131.

[46] H. J. Gabius, The sugar code in drug delivery, Adv. Drug. Deliv. Rev. 56 (2004) 421–424.

[47] N. Yamazaki, S. Kojima, N. V. Bovin, S. Andre, S. Gabius, H. J. Gabius, Endogenous lectins as targets for drug delivery, Adv. Drug. Deliv. Rev. 43 (2000) 225–244.

[48] L. Damian, D. Fournier, M. Winterhalter, L. Paquereau, Determination of thermodynamic parameters of Xerocomus chrysenteron lectin interactions with N-acetylgalactosamine and Thomsen-Friedenreich antigen by isothermal titration calorimetry, BMC Biochem. 6 (2005) 11.

[49] A. Mackiewicz, S. Mackiewicz, Determination of lectin-sugar dissociation constants by agarose affinity electrophoresis, Anal. Biochem. 156 (1986) 481–488.

[50] F. Schwesinger, R. Ros, T. Strunz, D. Anselmetti, H.-J. Guntherodt, A. Honegger, L. Jermutus, L. Tiefenauer, A. Pluckthun, Unbinding forces of single antibody-antigen complexes correlate with their thermal dissociation rates, Proc. Natl. Acad. Sci. U. S. A. 97 (2000) 9972–9977.

[51] L. Tao, R. Kennedy, Measurement of antibody-antigen dissociation constants using fast capillary electrophoresis with laser-induced fluorescence detection, Electrophoresis 18 (2005) 112–117.

[52] A. David, P. Kopeckova, J. Kopecek, A. Rubinstein, The role of galactose, lactose, and galactose valency in the biorecognition of N-(2-hydroxypropyl)methacrylamide copolymers by human colon adenocarcinoma cells, Pharm. Res. 19 (2002) 1114–1122.

[53] H. Lodish, A. Berk, S. Zipursky, P. Matsudaira, D. Baltimore, J. Darnell, *Molecular Cell Biology*, 4th ed. New York: W. H. Freeman & Co., (1999).

[54] F. Kratz, U. Beyer, M. Schutte, Drug-polymer conjugates containing acid-cleavable bonds, Crit. Rev. Ther. Drug Carrier Syst. 16 (1999) 245–288.

[55] J. Goldstein, M. Brown, R. Anderson, D. Russell, W. Schneider, Receptor-mediated endocytosis: Concepts emerging from the LDL receptor system, Annu. Rev. Cell. Biol. 1 (1985) 1–39.

[56] H. J. Gabius, R. Engelhardt, T. Hellmann, P. Midoux, M. Monsigny, G. A. Nagel, K. Vehmeyer., Characterization of membrane lectins in human colon carcinoma cells by flow cytofluorometry, drug targeting and affinity chromatography, Anticancer Res. 7 (1987) 109–112.

[57] N. Yamazaki, Y. Jigami, H. J. Gabius, S. Kojima, Preparation and characterization of neoglycoprotein-liposome conjugates: A promising approach to developing drug delivery materials applying sugar chain ligands, Trends Glycosci. Glycotechnol. 13 (2001) 319–329.

[58] N. Murthy, J. Campbell, N. Fausto, A. Hoffman, S. Stayton, Bioinspired pH-responsive polymers for the intracellular delivery of biomolecular drugs, Bioconjug. Chem. 14 (2003) 412–419.

[59] N. Subbarao, R. Parente, F. Szoka, Jr., L. Nadasdi, K. Pongracz, pH-dependent bilayer destabilization by an amphipathic peptide, Biochemistry 26 (1987) 2964–2972.

[60] R. Duncan, H. Cable, J. Lloyd, T. Rejmanova, J. Kopecek, Polymers containing enzymatically degradable bonds, 7. Design of oligopeptide side chains in poly [N-(2-hydroxypropyl) methacrylamide] copolymers to promote efficient degradation by lysosomal enzymes., Macromol. Chem. Physic. 184 (1983) 1997–2008.

[61] K. Ulbrich, T. Etrych, M. Jelinkova, B. Rihova, HPMA copolymers with pH-controlled release of doxorubicin: *In vitro* cytotoxicity and *in vivo* antitumor activity, J. Control. Release 87 (2003) 33–47.

[62] H.-S. Yoo, E. Lee, T. Park, Doxorubicin-conjugated biodegradable polymeric micelles having acid-cleavable linkages, J. Control. Release 82 (2002) 17–27.

[63] J. Davda, V. Labhasetwar, Characterization of nanoparticle uptake by endothelial cells, Int. J. Pharm. 233 (2002) 51–59.

Chapter 2 – Synthesis, Characterization and *In Vitro* Studies of Dextran-Galactose Conjugates for Targeted Doxorubicin Delivery to Hepatocytes

2.1 Introduction

Hepatocyte cell lines have been extensively studied and are well-known to express a high concentration of the asialoglycoprotein (ASGP) receptor. This receptor has a selective and high affinity for proteins or carbohydrate structures terminating with galactose [1]. Researchers have shown that ligand binding leads to receptor-mediated endocytosis of the complex [1-4]. In addition to being a well-characterized model system, hepatocytes are a good target for the treatment of various diseases such as lysosomal storage disease, hepatitis and parasitic diseases (e.g. malaria) [1]. Trere *et al.* have shown that while normal liver cells express the ASGP receptor in a polarized manner on the luminal and lateral faces, on human hepatocellular carcinomas there is increased expression of the receptor on all surfaces of the cells [2]. Additionally, it has been found that in freshly isolated hepatocytes, internalization of the receptor-ligand complex does not reduce the number of receptors available on the cell surface due to recycling. The ligand-receptor complex dissociates at a low pH, and the receptor is transported back to the cell surface before the endosome fuses with a lysosome [3]. Studies by Anderson *et al.* have confirmed that the uptake of polymer-galactose conjugates were temperature- and adenosine triphosphate (ATP)-dependent, and could be competitively inhibited, indicating that synthetic macromolecules expressing galactose also undergo receptor-mediated endocytosis [4].

Many researchers have studied the uptake of drugs, proteins, polymers and particles modified to express galactose, and found enhanced association with hepatocytes [5-8]. Galactose has been conjugated to a number of polymers including dextran, poly(ethylene glycol), poly((N-2-hydroxypropyl)methacrylamide) (HPMA) and poly(L-lysine) [5-10]. Both *in vivo* and *in vitro* testing have shown specific uptake of galactosylated moieties by the liver or by hepatocyte cell lines expressing the ASGP receptor. This enhanced interaction was found to be dependent on the concentration of galactose on the material being tested. Cairo *et al.* have performed binding studies on a multivalent receptor on polymer scaffolds, and shown that increasing the density of binding sites on a ligand increased the stoichiometry of interaction

(number of binding moieties per receptor), the rate of interaction and the receptor proximity [11]. Ogawara *et al.* studied uptake of bovine serum albumin (BSA) conjugated to galactose at varied stoichiometries in perfused rat liver. The hepatic clearance was found to increase significantly as the number of galactose residues per BSA molecule was increased [12] Several researchers have worked on conjugates of HPMA with galactose and doxorubicin and tested them *in vitro* and *in vivo*. The galactose-targeted material showed improved uptake compared with the non-targeted polymer [10, 13-15]. David *et al.* have studied the effect of galactose, lactose and a branched multiple-galactose molecule in hepatocellular carcinomas using HPMA [15]. Ohya *et al.* have worked on cisplatin delivery using branched galactose residues. Even though the cisplatin was modified in the synthesis, it was still found to be effective in cell culture [16]. Hashida *et al.* have studied the effect of molecular weight, galactose configuration, and dose on the delivery of galactose-attached polymers and proteins [17].

Doxorubicin is an anthracycline chemotherapeutic agent commonly used for various types of cancer including breast, ovarian, lung, liver, thyroid and gastric cancers, as well as different forms of lymphoma, osteocarcinoma, melanoma and leukemia. Doxorubicin is commercially available in a slightly hydrophilic form with a molecular weight of 581 g/mol. Upon administration, it rapidly clears from the plasma with a half-life of 3.6 min and is distributed into tissue [18]. There is a slower clearance from tissue (terminal half-life of ~ 26.5 h) by clearance and metabolism through the bile duct and kidneys [18]. Doxorubicin acts by entering cell nuclei and intercalating with DNA, which inhibits RNA and DNA polymerases [19]. It can also stabilize an intermediate complex between topoisomerase II and DNA. These in turn lead to the induction of apoptosis or programmed cell death [20]. In addition to being harmful for any cell in the body that is actively dividing, doxorubicin is specifically and irreversibly toxic to heart tissue. This is thought to occur due to the formation and accumulation of reactive oxygen species when doxorubicin interacts with iron in the heart cells. It has been found that dilative cardiomyopathy and congestive heart failure can develop within one year of doxorubicin administration. Late forms of cardiac dysfunction can also occur months or years after therapy [20]. Due to these reasons, the cumulative dose of doxorubicin and other similar anthracyclines must not exceed 550 mg/m^2 for each patient [21]. Conjugating doxorubicin to a polymer will increase its circulation time in the plasma and reduce uptake into non-target tissue.

Conjugating the polymer-bound doxorubicin to galactose will increase the uptake by cells expressing the ASGP receptor.

Dextran (poly(α-D-1,6 glucose)) was used as the polymeric carrier to selectively deliver doxorubicin to hepatocytes. Dextran has many advantages as a drug carrier: it is biocompatible, inexpensive, and commercially available at various molecular weights. It is FDA-approved and currently in clinical use for plasma volume expansion, peripheral flow promotion and as an antithrombolytic agent [22]. Dextran can be cleared from the body by the enzyme dextranase, which is present in the liver, spleen, kidneys and lower gastrointestinal tract of humans [22]. Dextran has several hydroxyl groups on each glucose unit, which facilitate functionalization by various methods.

Dextran has been conjugated to or used in the delivery of various chemotherapeutic agents, anti-inflammatory agents, antibodies, proteins, antibiotics, immunosuppressants and imaging agents [1, 10, 22-25]. There are several methods that can be used to attach galactose and doxorubicin onto the dextran backbone for the drug delivery system [9, 23]. Preliminary synthesis trials were performed, and the periodate oxidation method was chosen due to the simplicity of this reaction, high yield and ease of characterization. Both doxorubicin and galactose could be conjugated to dextran through this method. The goal for this study was to develop a versatile synthesis that could incorporate different targeting moieties and drugs. This conjugate utilized a highly functional polymer, and conjugated the drug and targeting moiety through amine groups, which are very common in therapeutics.

2.2 Experimental Methods

2.2.1 Materials

Sodium periodate ($NaIO_4$), sodium borohydride ($NaBH_4$), galactosamine, calf-thymus DNA (ct-DNA), doxorubicin and paraformaldehyde were obtained from Sigma-Aldrich. Dextran with molecular weights of 10, 40 and 170 kilodaltons (kDa) were also obtained from Sigma-Aldrich. OmniPur 10× phosphate buffered saline (PBS) was used during synthesis at a 1:10 dilution. The cell lines BNL CL.2, NIH/3T3 and H-4-II-E, Dulbecco's Minimum Essential Medium (DMEM), Eagle's Minimum Essential Medium (EMEM), fetal bovine serum (FBS),

10,000 I.U./mL of Penicillin-10,000 μg/mL of Streptomycin, 0.25% of Trypsin/0.53 mM of ethylenediaminetetraacetic acid (EDTA), and the MTT Cell Proliferation Assay kit were obtained from American Type Culture Collection (ATCC). For cell culture studies, Dulbecco's 1× sterile PBS containing calcium and magnesium was obtained from VWR. The doxorubicin used for part of this project was a generous donation from Pharmacia & Upjohn (Pfizer).

2.2.2 Synthesis of Targeted Dextran-Doxorubicin-Galactose Conjugates

The synthesis scheme used to attach doxorubicin and galactose to the dextran chain is shown in Fig. 2.1.

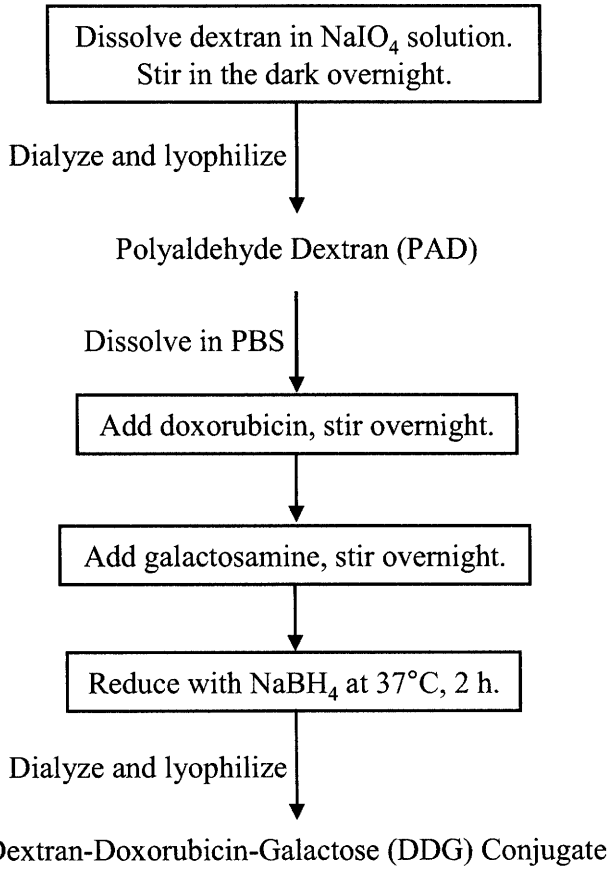

Fig. 2.1. Schematic of synthesis of targeted dextran-doxorubicin-galactose conjugates.

The conjugate was synthesized as follows. One gram of dextran was dissolved in 100 mL of 0.03 M of $NaIO_4$ in deionized (DI) water (50% molar ratio of periodate to glucose groups), and stirred in the dark overnight [26]. The partially activated polyaldehyde dextran

(PAD) was purified by dialysis against 1 L of DI water. The water was changed twice a day over 3 days, and the polymer was recovered by lyophilization. PAD (100 mg) was dissolved in 5 mL of 1× PBS (pH 7.4), reacted with doxorubicin (10 mg) overnight, and subsequently with galactosamine (varied amounts) overnight, and reduced with $NaBH_4$ (12 mg) at 37°C for 2 h. The resulting dextran-doxorubicin-galactose (DDG) conjugates were dialyzed against 500 mL of DI water. The water was changed twice a day over 3 days, and the conjugates were recovered by lyophilization.

The loading of doxorubicin was determined by measuring the absorbance at 485 nm on a UV-Vis microplate reader (VersaMax, Molecular Devices). The galactose content was determined from elemental analysis for nitrogen (Atlantic Microlab, Inc.). The presence of doxorubicin on dextran was verified by ^1H nuclear magnetic resonance (NMR) spectroscopy (Avance DMX 400 MHz, Bruker) in dimethyl sulfoxide (DMSO-d6) (3072 scans). The radius of gyration of the polymer conjugates was determined by static light scattering (Brookhaven Instruments Photon Correlation Spectrometer model BI-9000 AT).

2.2.3 Cell-Free Efficacy of Polymer-Bound Doxorubicin

Calf-thymus DNA was dissolved in 1× PBS (pH 7.4) at a concentration of 1 mg/mL. Doxorubicin and the polymer conjugates to be tested were also dissolved in 1× PBS at a normalized doxorubicin concentration of 12.5 μg/mL. The assay was carried out in a 96-well plate by adding 20 μL of the doxorubicin or polymer conjugate solution to a final ct-DNA concentration ranging from 0 to 0.9 mg/mL. Readings were taken on a fluorescence microplate reader (*f*Max, Molecular Devices; λ_{ex} = 488 nm, λ_{em} = 590 nm) immediately upon addition of the conjugates [27]. All experiments were performed in triplicate.

2.2.4 In Vitro Efficacy of Polymer Conjugates

The BNL CL.2 (mouse hepatocyte) and NIH/3T3 (mouse fibroblast) cell lines were cultured in DMEM supplemented with 10% of FBS and 1% of Penicillin-Streptomycin at 37°C in a 5% CO_2 atmosphere. The H-4-II-E (rat hepatocyte) cell line was cultured in EMEM supplemented with 10% of FBS and 1% of Penicillin-Streptomycin under identical growth conditions.

For uptake and cytotoxicity studies, cells were plated in triplicate at 400/mm^2 for the BNL CL.2 and H-4-II-E cell lines, and at 50/mm^2 for the NIH/3T3 cell line in 6-well plates, and allowed to adhere for 10–14 h. The medium was then replaced with complete medium containing doxorubicin or polymer conjugates at various concentrations, and incubated for 24 h. At the end of the experiment, the cell layer was gently washed three times with cold PBS, and the cells were harvested with Trypsin-EDTA solution and divided into two aliquots to measure the fluorescence and cell viability. The fluorescence due to the uptake of doxorubicin or conjugates was evaluated by running an aliquot of the samples through a flow cytometer (FACScan, Becton Dickinson; FL2-H: λ_{ex} = 488 nm, λ_{em} = 590 nm). To determine the killing efficiency, the other aliquot of the cells was replated in 96-well plates, and allowed to adhere for 8–10 h. The medium was replaced with 100 μL of fresh medium and 10 μL of the MTT reagent (3-(4,5-dimethylthiazol-2-yl)-2,5-diphenyltetrazolium bromide), and the plate was incubated for 1 or 2 h. One hundred microliters of sodium dodecyl sulfate were then added, and the cells were incubated for another 10 or 12 h. The absorbance was measured at 570 nm. The standard curves for viable cell numbers were obtained by performing the MTT assay on a known cell concentration curve, measured by hemacytometer.

Microscopy studies were conducted in chamber slides (Lab-Tek Chambered Coverglasses, NUNC) using a nominal doxorubicin concentration of 3.6 μM, and incubating for 4, 8 or 24 h. Cells were fixed with 1% of paraformaldehyde solution in 1× PBS for 1 h, followed by 2% of paraformaldehyde for 30 min. Images were obtained with a Zeiss Axiovert 200 Fluorescence Microscope.

2.3 Results and Discussion

2.3.1 Synthesis and Characterization of Polymer Conjugates

A schematic of the synthesis and structure of the dextran-doxorubicin-galactose conjugates is shown in Fig. 2.2. The degree of substitution of doxorubicin varied from 1.0% to 2.5%, and that of galactose varied from 3.5% to 11% for conjugates with different molecular weights. Fig. 2.3 showed the degree of substitution of galactosamine, and Table 2.1 showed the average degree of substitution of doxorubicin for conjugates at different molecular weights. Conjugation efficiency based on the amount loaded of each reactant varied from 15% to 54% for

doxorubicin and from 2% to 16% for galactosamine. Fig. 2.4 showed the ^{1}H-NMR spectra of dextran and DDG at a molecular weight of 170 kDa. The glucosidic protons appeared on the NMR spectrum in several bands between 3.0 and 5.0 ppm. The following peaks, numbered according to the molecular structure, were attributed to doxorubicin: (1) methoxy protons at 3.95 ppm, (2) phenyl protons between 6.0 and 8.0 ppm (inset), and (3) phenolic protons at 13.3 and 14.1 ppm (inset). Peaks due to galactosamine could not be distinguished in the NMR spectrum as they were masked by the glucosidic protons on the dextran backbone.

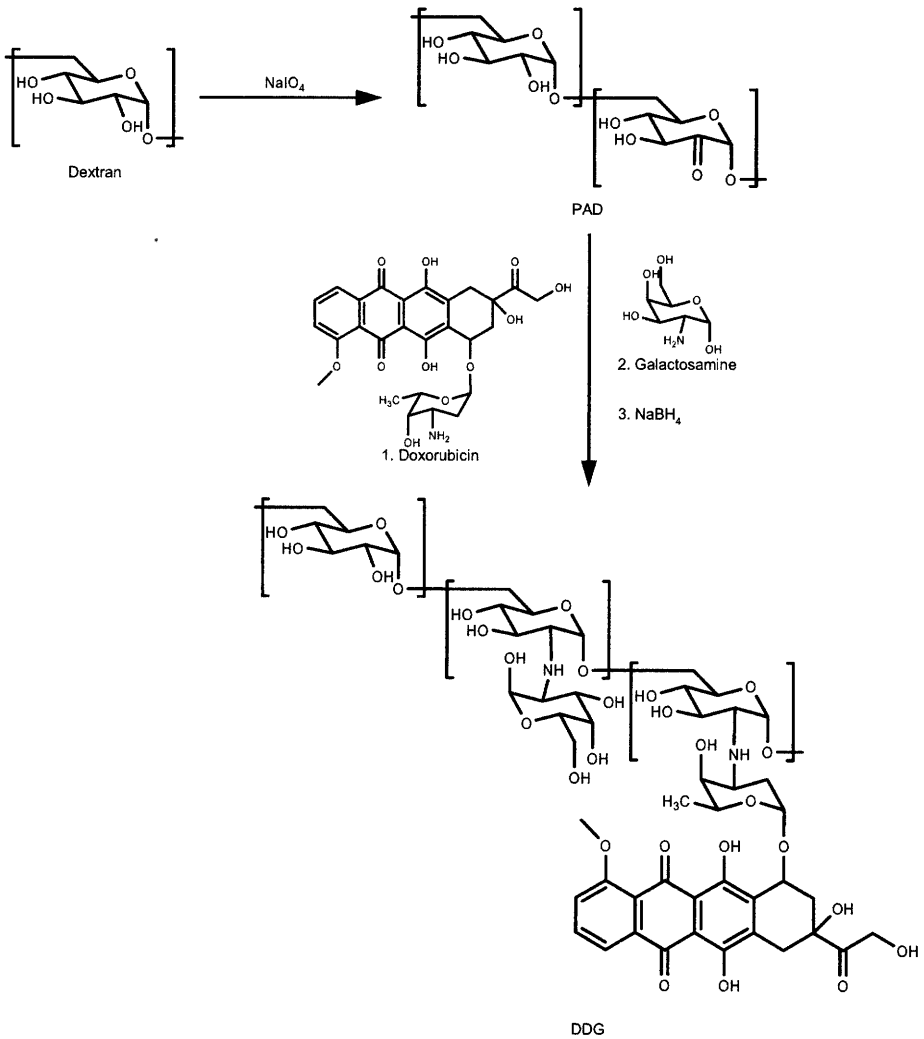

Fig. 2.2. Synthesis of the dextran-doxorubicin-galactose conjugates.

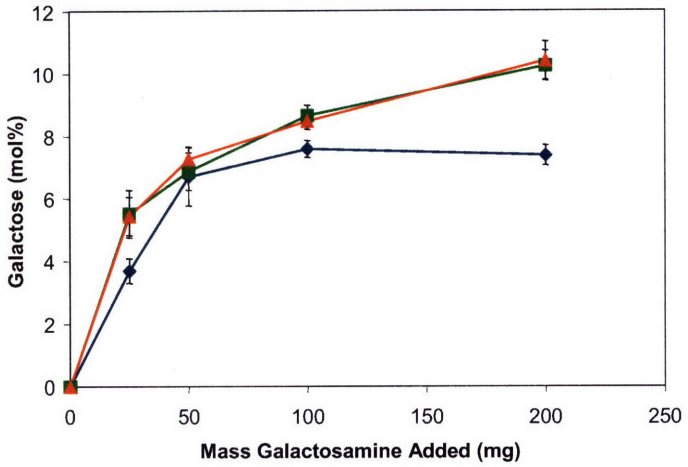

Fig. 2.3. Degree of galactose substitution per glucose monomer for DDG conjugates with molecular weights of (♦) 10 kDa, (■) 40 kDa and (▲) 170 kDa. Values are mean ± standard deviation; n = 3.

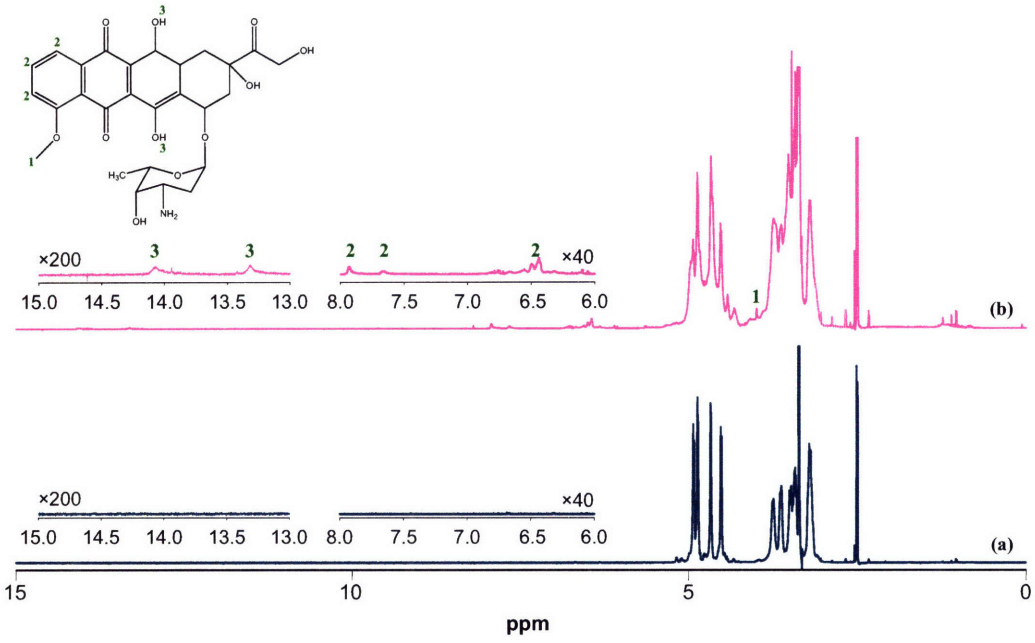

Fig. 2.4. ^{1}H-NMR spectra of (a) dextran and (b) DDG with a molecular weight of 170 kDa. Peaks were marked with numbers according to those given on the molecular structure of doxorubicin.

Table 2.1. Degree of doxorubicin substitution per glucose monomer for DDG conjugates with the molecular weights indicated. Values are mean ± standard deviation; n = 3.

Molecular Weight (kDa)	Doxorubicin (mol%)
10	1.2 ± 0.2
40	1.5 ± 0.1
170	1.5 ± 0.2

Periodate oxidation of the dextran hydroxyl groups was used to attach both doxorubicin and galactose to the polymer chain. Only 50% of the glucose groups were activated so as to maintain the water-solubility of the conjugates. The aldehyde groups on PAD reacted with the primary amines on doxorubicin and galactosamine to form imine bonds, which were reduced with $NaBH_4$ to form amine bonds. The reactions with doxorubicin and galactosamine were performed in two different steps to ensure relatively constant doxorubicin substitution for varied galactose substitutions. Simultaneous reaction would have resulted in decreasing doxorubicin substitution with increasing galactosamine introduced. In this case, increasing the amount of doxorubicin added to the reaction mixture would have raised the degree of substitution of doxorubicin slightly, but would result in a low reaction efficiency of 1–15%. Thus, the two-step reaction was preferred since it maintained a relatively constant degree of substitution of doxorubicin, while improving the substitution efficiency significantly. The dextran-doxorubicin conjugates were identified as DD followed by the molecular weights, while the DDG conjugates were designated with the molecular weights and degrees of galactose substitution. For example, DDG 40 kDa 6.9 referred to a DDG conjugate with 40 kDa molecular weight and 6.9 mol% galactose substitution.

2.3.2 Cell-Free Testing of Polymer-Bound Doxorubicin

Doxorubicin acted by entering the nuclei of cells and intercalating with the DNA. A fluorescence-based cell-free assay was used to examine if the dextran-bound doxorubicin remained effective [27]. When doxorubicin was bound to DNA, its fluorescence would be quenched. The degree of fluorescence quenching (F/F_o) at a particular DNA concentration was determined by taking the ratio of that fluorescence reading (F) to the reading in the absence of DNA (F_o). The assay indicated that all our conjugates intercalated with DNA. As seen in Fig.

2.5, conjugates with various molecular weights and galactose substitutions exhibited fluorescence quenching, though not to the same extent as free doxorubicin. The extent of quenching increased with the polymer molecular weight. The conjugates with a molecular weight of 170 kDa could undergo almost complete quenching, whereas those with molecular weights of 10 kDa and 40 kDa showed at most ~ 50% quenching. The fluorescence quenching also decreased slightly with galactose substitution at 170 kDa. The doxorubicin substitutions for the conjugates are shown in Table 2.2.

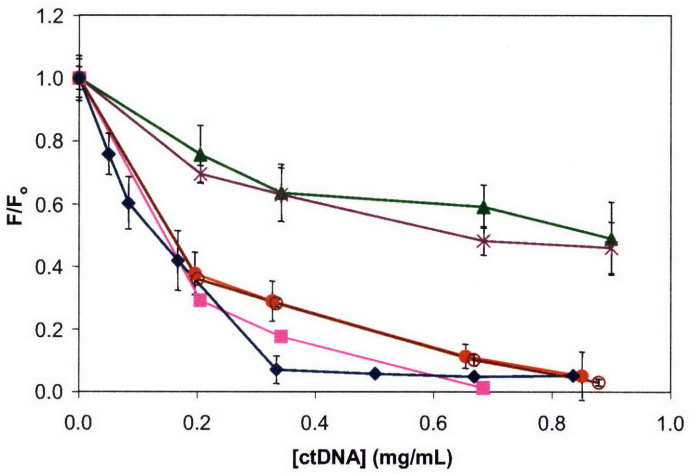

Fig. 2.5. Fluorescence quenching of doxorubicin in the presence of ct-DNA for (♦) doxorubicin, (×) DD 10 kDa, (▲) DD 40 kDa, (■) DD 170 kDa, (○) DDG 170 kDa 7.4, and (●) DDG 170 kDa 10.4. Values are mean ± standard deviation; n = 3.

It has been shown that when doxorubicin intercalates with double-stranded DNA, the DNA "buckles" into a distorted helix. This distorted structure is stabilized by a number of electrostatic interactions, including hydrogen bonding between the hydrogen on the amino sugar on doxorubicin and a thiamine base in the minor groove of DNA [28]. The reduction observed in the fluorescence quenching of the conjugates compared to that of doxorubicin was attributed partly to the occupation of the amine group in the synthesis reaction. Additional effect observed with conjugates of low molecular weights might be due to the reduced degrees of substitution of doxorubicin (see Table 2.2). To achieve a normalized doxorubicin concentration, it was necessary to use a greater mass of the lower molecular weight polymers. Consequently, there was more polymer in solution to interfere with the binding between doxorubicin and DNA. In contrast, all of the conjugates with 170 kDa molecular weight achieved close to 100% quenching

in spite of having varying doxorubicin substitutions. They carried a significantly larger number of doxorubicin molecules on each polymer chain as compared to the conjugates with 10 kDa and 40 kDa molecular weights. The proximity of the doxorubicin molecules on the same polymer chain might have also contributed to the higher degree of fluorescence quenching in the former. Once one doxorubicin molecule intercalated with DNA, the remaining molecules on the same polymer chain were brought into the immediate vicinity of the DNA and were more likely to be bound, resulting in greater fluorescence quenching.

Table 2.2. Degree of substitution and number of doxorubicin molecules per polymer chain for conjugates in Fig. 2.5.

Molecular Weight (kDa)	Galactose Substitution (mol%)	Doxorubicin Substitution (mol%)	Doxorubicin/Polymer Chain
10	0	1.7	1
40	0	1.9	5
170	0	2.1	26
170	7.3	1.4	15
170	10.4	1.7	18

2.3.3 In Vitro Studies

Table 2.3 lists the polymer conjugates used for the *in vitro* experiments. The amount of conjugate added was normalized in doxorubicin content for these experiments.

2.3.3.1 Uptake of Doxorubicin in the BNL CL.2 Cell Line

Flow cytometry was used to determine the excess fluorescence of cells incubated with either doxorubicin or conjugates. Floating cellular debris or dead cells were removed from the media during sample preparation for flow cytometry. Cells were gated according to light scattering parameters to isolate the live cell population. A slight shift in side scatter was observed for cells treated with some of the conjugates. The histogram profiles for all experiments were almost exclusively unimodal. Fig. 2.6 shows the histograms obtained from the

FACScan FL2-H detector for several uptake experiments. It was found that the fluorescence of cells increased as the doxorubicin content was increased in the experiments.

Table 2.3. Conjugates used in *in vitro* studies.

Sample	Molecular Weight (kDa)	Doxorubicin Substitution (mol%)	Galactose Substitution (mol%)
1	10	1.1	0
2	10	1.4	3.7
3	10	1.2	5.6
4	10	1.3	7.6
5	40	1.5	0
6	40	1.4	5.5
7	40	1.5	6.9
8	40	1.7	10.2
9	170	1.6	0
10	170	1.4	5.4
11	170	1.4	7.3
12	170	1.7	10.4

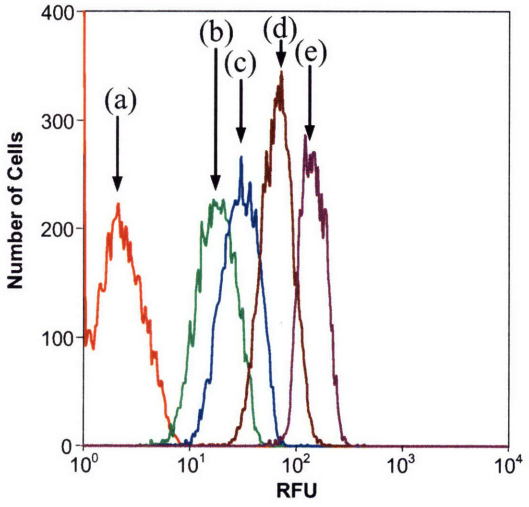

Fig. 2.6. Doxorubicin-associated fluorescence of BNL CL.2 cells incubated for 24 h with (a) no treatment, and DDG 170 kDa conjugates with galactose substitutions of (b) 0, (c) 5.4, (d) 7.3 and (e) 10.4 mol% at a nominal doxorubicin concentration of 9 μM.

Figs. 2.7–2.10 show the ratio of the fluorescence of BNL CL.2 cells incubated with doxorubicin or conjugates to the fluorescence of untreated cells. Fig. 2.7 indicates that the uptake of free doxorubicin was much higher than the uptake of the conjugates, which appeared to approach a plateau as doxorubicin content in the cell incubation medium was increased. Since there was less association with the polymer conjugates than with doxorubicin, the conjugates were expected to have less non-specific toxicity than free doxorubicin.

Fig. 2.7 also illustrates that the uptake of doxorubicin increased for higher molecular weight polymers. As mentioned previously, the chain loading of doxorubicin increased with the conjugate's molecular weight (see Table 2.2). Therefore, if one molecule of the 170 kDa polymer entered the cell, it increased the fluorescence to a much greater extent than the 10 kDa polymer.

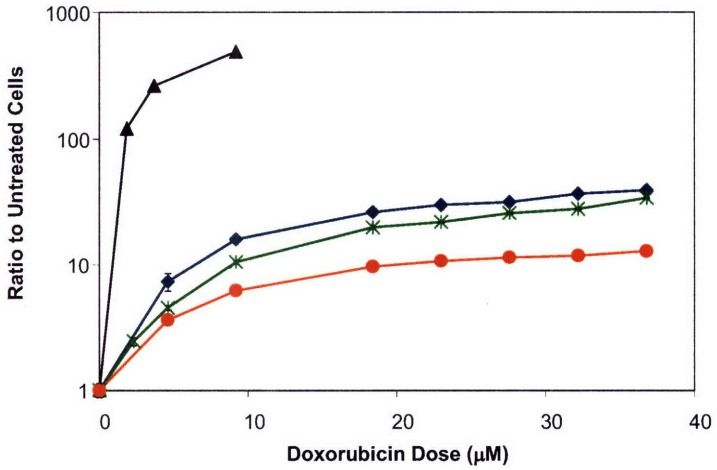

Fig. 2.7. Doxorubicin-associated fluorescence ratio of BNL CL.2 cells incubated for 24 h with (▲) doxorubicin, and DD conjugates with molecular weights of (●) 10 kDa, (✳) 40 kDa and (◆) 170 kDa. Values are mean ± standard deviation; n = 3.

The doxorubicin uptake also increased with the degree of substitution of galactose for conjugates of all molecular weights (see Figs. 2.8–2.10). BNL CL.2 cells are known to express a high concentration of the ASGP receptor on the surface [29-32], and a higher degree of substitution of galactose on the conjugates would be expected to increase the cell uptake.

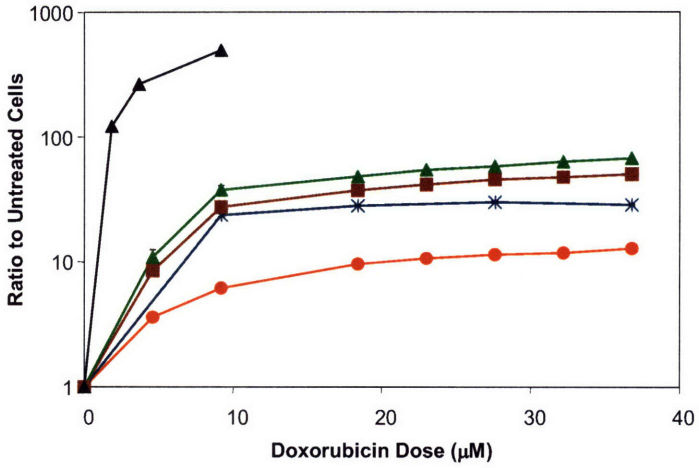

Fig. 2.8. Doxorubicin-associated fluorescence ratio of BNL CL.2 cells incubated for 24 h with (♦) doxorubicin, and DDG 10 kDa conjugates with galactose substitutions of (●) 0, (✳) 3.7, (■) 6.7 and (▲) 7.6 mol%. Values are mean ± standard deviation; n = 3.

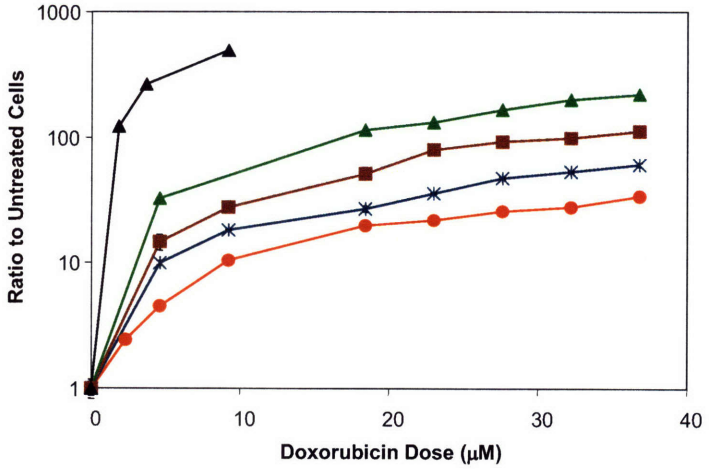

Fig. 2.9. Doxorubicin-associated fluorescence ratio of BNL CL.2 cells incubated for 24 h with (♦) doxorubicin, and DDG 40 kDa conjugates with galactose substitutions of (●) 0, (✳) 5.5, (■) 6.9 and (▲) 10.2 mol%. Values are mean ± standard deviation; n = 3.

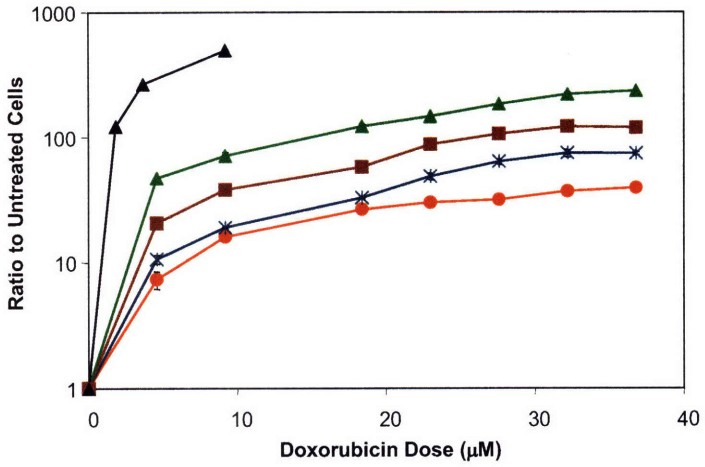

Fig. 2.10. Doxorubicin-associated fluorescence ratio of BNL CL.2 cells incubated for 24 h with (♦) doxorubicin, and DDG 170 kDa conjugates with galactose substitutions of (●) 0, (✳) 5.4, (■) 7.3 and (▲) 10.4 mol%. Values are mean ± standard deviation; n = 3.

2.3.3.2 Cytotoxicity Studies on the BNL CL.2 Cell Line

Cell viability was measured using the MTT assay, which is a standard colorimetric assay for measuring cell proliferation. The MTT tetrazolium salt was reduced to insoluble, purple formazan crystals in the mitochondria of cells. The crystals were solubilized with sodium dodecyl sulfate, and the amount was quantified by measuring absorbance. The amount of precipitate formed was directly proportional to the number of living cells, which with regard to this assay was defined as cells that were metabolically active. Even though the MTT assay did not provide a direct measure of the action of doxorubicin, it was employed since it was a simple and rapid method for quantifying cell viability.

The concentration corresponding to 50% of cell death (LC_{50}) was determined from the slope and intercept of the straight line obtained by inverting the dose vs. cell death data from the cytotoxicity studies. The LC_{50} values obtained by this method were corroborated by determination with a logistic model, as well as visual confirmation from the dose-response curves.

Cytotoxicity profiles of the polymer conjugates corresponded well with the trends observed for cell uptake. Fig. 2.11 showed the dose response curve of doxorubicin and non-targeted DD conjugates with different molecular weights. All the polymer conjugates were less

toxic to cells than free doxorubicin. The LC_{50} for DD 10 kDa was 36.4 μM, which was much higher than that for free doxorubicin (1.8 μM). The toxicity was higher for conjugates with higher molecular weights. The LC_{50} values for DD 40 kDa and DD 170 kDa were 30.9 and 25.6 μM, respectively (see Table 2.4).

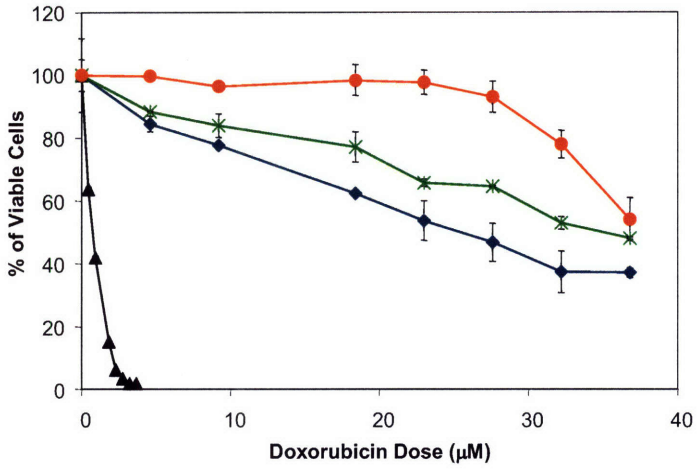

Fig. 2.11. Dose response curves of BNL CL.2 cells incubated for 24 h with (▲) doxorubicin, and DD conjugates with molecular weights of (●) 10 kDa, (✳) 40 kDa and (◆) 170 kDa. Values are mean ± standard deviation; n = 3.

The DD conjugates were much less toxic than free doxorubicin for a number of reasons. There was less uptake of doxorubicin in its polymer-bound form at the same concentration as shown in Figs. 2.7–2.10. Additionally, after internalization, the conjugates needed to enter the nucleus to cause cell death. Proteins or metabolites of up to 40 kDa can passively enter the nucleus through the nuclear pore complex (NPC) in mammalian cells, and the NPC transport channel can dilate up to 40 nm in response to certain cellular signals [33]. Our DD conjugates with molecular weights of 10 kDa and 40 kDa were small enough for individual polymer chains to have passively diffused into the nucleus. However, these conjugates carried a lower chain loading of doxorubicin than DD 170 kDa. Also, according to static light scattering measurements, the radius of gyration of the conjugates ranged from 15 nm to 40 nm, indicating that the conjugates might have aggregated into larger structures. This implied that DD 10 kDa and DD 40 kDa did not have a size advantage in terms of nuclear uptake. Another possible reason for the lower toxicity of the DD conjugates could be their less effective intercalation to DNA as compared to free doxorubicin (Fig. 2.5).

Table 2.4. LC_{50} of DD and DDG conjugates in BNL CL.2 cells.

MW = 10 kDa		MW = 40 kDa		MW = 170 kDa	
Drug	LC_{50} (μM)	Drug	LC_{50} (μM)	Drug	LC_{50} (μM)
DD	36.4	DD	30.9	DD	25.6
DDG 3.7	33.3	DDG 5.5	24.7	DDG 5.4	18.6
DDG 6.7	25.4	DDG 6.9	15.5	DDG 7.3	13.1
DDG 7.6	21.2	DDG 10.2	10.1	DDG 10.4	8.6

Targeted conjugates were significantly more toxic than the non-targeted conjugates of the same molecular weight (Table 2.4 and Figs. 2.12–2.14). The toxicity of the conjugates increased with an increase in the degree of galactose substitution for all three molecular weights. DDG 170 kDa 10.4 has a particularly low LC_{50} value of 8.6 μM.

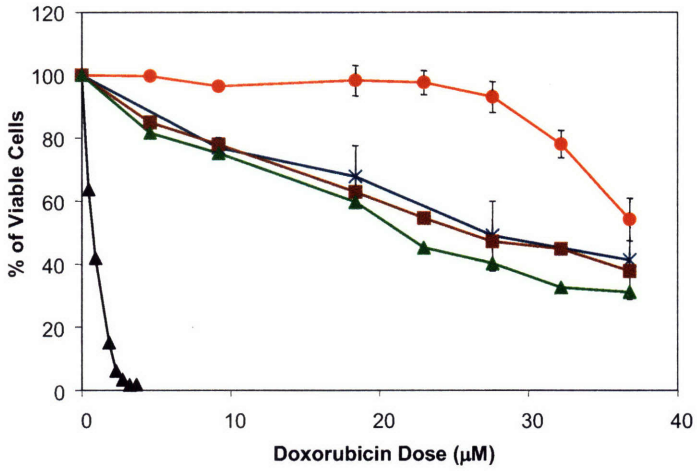

Fig. 2.12. Dose response curves of BNL CL.2 cells incubated for 24 h with (♦) doxorubicin, and DDG 10 kDa conjugates with galactose substitutions of (●) 0, (✕) 3.7, (■) 6.7 and (▲) 7.6 mol%. Values are mean ± standard deviation; n = 3.

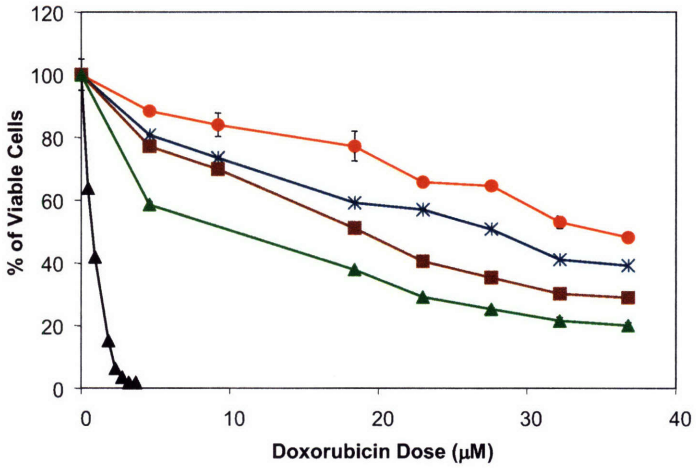

Fig. 2.13. Dose response curves of BNL CL.2 cells incubated for 24 h with (♦) doxorubicin, and DDG 40 kDa conjugates with galactose substitutions of (●) 0, (✳) 5.5, (■) 6.9 and (▲) 10.2 mol%. Values are mean ± standard deviation; n = 3.

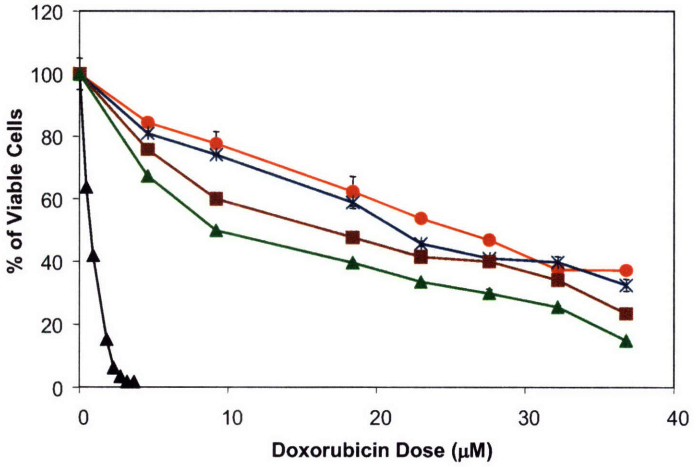

Fig. 2.14. Dose response curves of BNL CL.2 cells incubated for 24 h with (♦) doxorubicin, and DDG 170 kDa conjugates with galactose substitutions of (●) 0, (✳) 5.4, (■) 7.3 and (▲) 10.4 mol%. Values are mean ± standard deviation; n = 3.

Fig. 2.15 shows the light and fluorescence micrographs of hepatocytes incubated with doxorubicin and DDG 170 kDa 10.4. The free doxorubicin was localized almost exclusively in the nuclei of cells. In contrast, DDG 170 kDa 10.4 was found throughout the entire cell, with localization occurring outside the nucleus as well. More localization in the nuclei was observed after incubating the cells with polymer conjugates for 24 h.

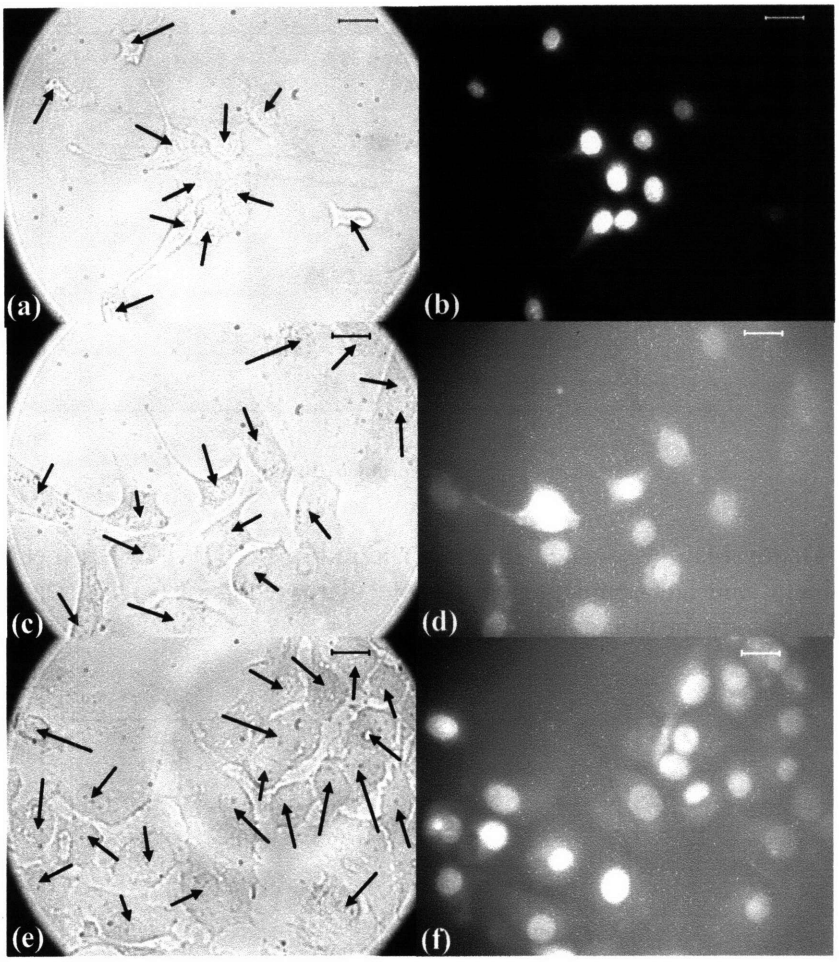

Fig. 2.15. Light (left) and fluorescence (right) micrographs of BNL CL.2 cells incubated with (a,b) doxorubicin for 8 h, and DDG 170 kDa 10.4 for (c,d) 8 h and (e,f) 24 h at a nominal doxorubicin concentration of 3.6 μM. Scale bar = 25 μm. Nuclei were marked with arrows on the light micrographs.

2.3.3.3 Uptake of Doxorubicin in the Control Cell Line

The uptake of doxorubicin and polymer conjugates was also determined in the NIH/3T3 cell line, which are mouse fibroblasts with no specificity for galactose uptake. Fig. 2.16 shows that doxorubicin uptake was significantly higher than the uptake of the DD conjugates. There was greater uptake of the DD conjugates of increasing molecular weights, as was observed also for the BNL CL.2 cell line. Fig. 2.17 shows the uptake of DDG 170 kDa conjugates with different galactose substitutions. As expected, the uptake of the conjugates in the NIH/3T3 cell line was not affected by the degree of substitution of galactose.

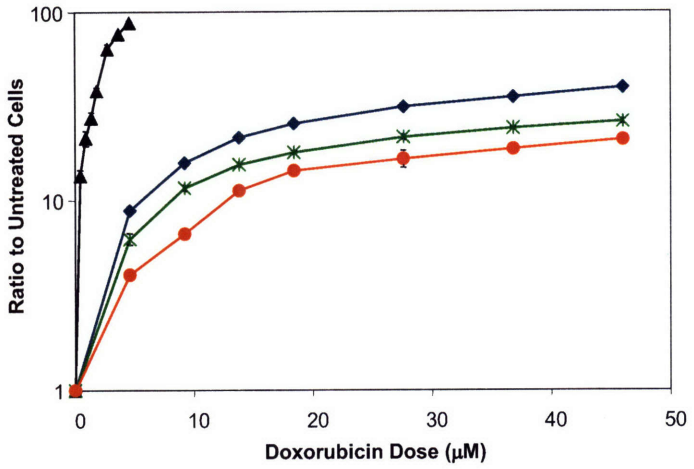

Fig. 2.16. Doxorubicin-associated fluorescence ratio of NIH/3T3 cells incubated for 24 h with (▲) doxorubicin, and DD conjugates with molecular weights of (●) 10 kDa, (✳) 40 kDa and (◆) 170 kDa. Values are mean ± standard deviation; n = 3.

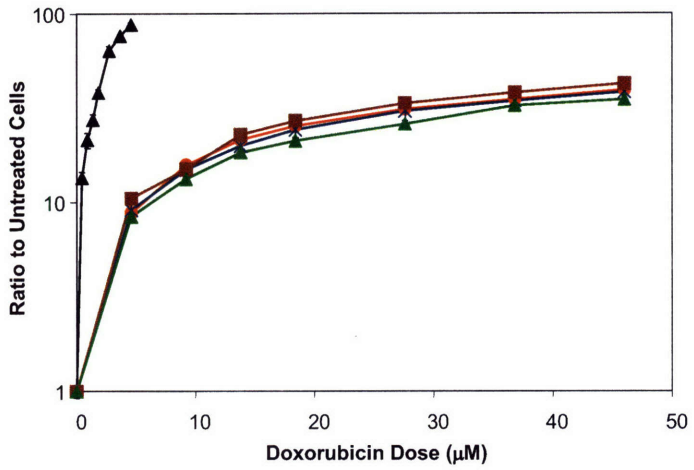

Fig. 2.17. Doxorubicin-associated fluorescence ratio of NIH/3T3 cells incubated for 24 h with (♦) doxorubicin, and DD 170 kDa conjugates with galactose substitutions of (●) 0, (✳) 5.4, (■) 7.3 and (▲) 10.4 mol%. Values are mean ± standard deviation; n = 3.

2.3.3.4 Cytotoxicity Studies in the Control Cell Lines

The cytotoxicity trends followed the uptake profiles for the NIH/3T3 cell line. There was a slight decrease in the LC_{50} with increasing molecular weight of polymer (see Fig. 2.18 and Table 2.5). Fig. 2.19 shows that there was negligible difference in LC_{50} due to the degree of substitution of galactose.

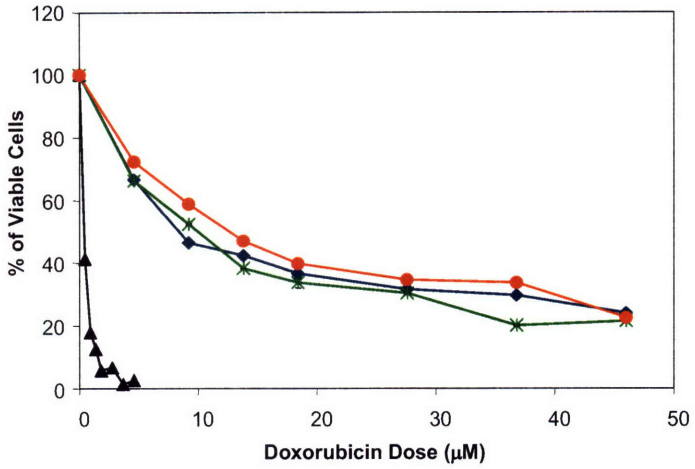

Fig. 2.18. Dose response curve of NIH/3T3 cells incubated for 24 h with (▲) doxorubicin, and DD conjugates with molecular weights of (●) 10 kDa, (✳) 40 kDa and (◆) 170 kDa. Values are mean ± standard deviation; n = 3.

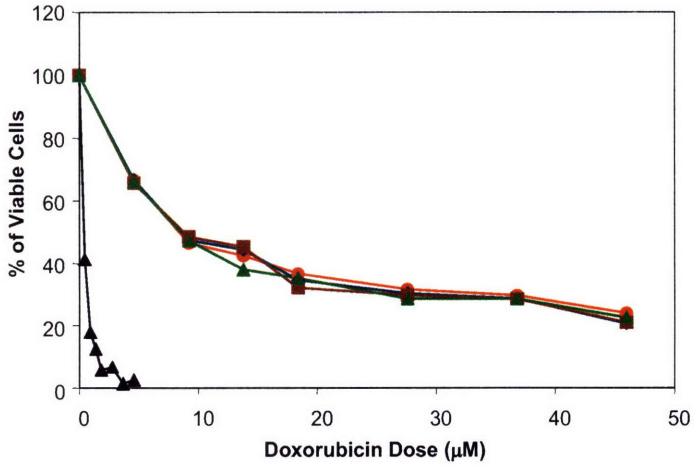

Fig. 2.19. Dose response curve of NIH/3T3 cells incubated for 24 h with (♦) doxorubicin, and DDG 170 kDa conjugates with galactose substitutions of (●) 0, (✳) 5.4, (■) 7.3 and (▲) 10.4 mol%. Values are mean ± standard deviation; n = 3.

The cytotoxicity of DDG conjugates was also tested in H-4-II-E, a rat hepatocyte cell line that has a low expression of galactose binding sites (< 5000 galactose binding sites per cell) [34]. In this cell line, the degree of substitution of galactose also had no effect on the LC_{50} (see Fig. 2.20 and Table 2.6).

Table 2.5. LC_{50} of doxorubicin, DD and DDG conjugates in NIH/3T3 cells.

Drug	LC_{50} (μM)
Doxorubicin	0.37
DD 10 kDa	10.7
DD 40 kDa	9.0
DD 170 kDa	7.4
DDG 170 kDa 5.4	7.7
DDG 170 kDa 7.3	7.4
DDG 170 kDa 10.4	7.5

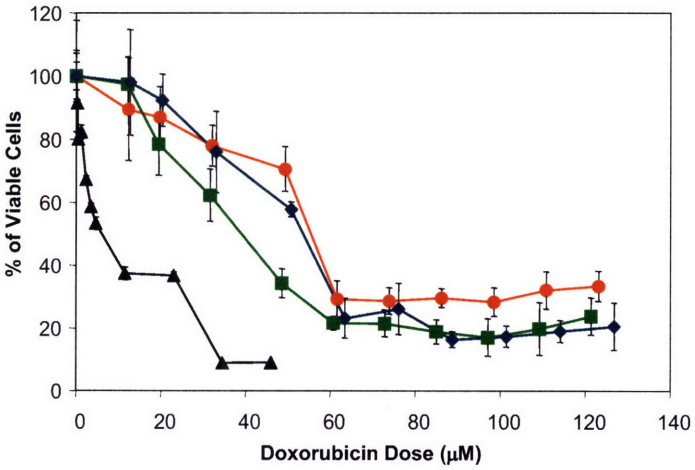

Fig. 2.20. Dose response curve of H-4-II-E cells incubated for 24 h with (▲) doxorubicin, and DDG 170 kDa conjugates with galactose substitutions of (●) 0, (■) 4.5 and (◆) 7.7 mol%. Values are mean ± standard deviation; n = 3.

Table 2.6. LC_{50} of doxorubicin, DD and DDG conjugates in H-4-II-E cells.

Drug	LC_{50} (μM)
Doxorubicin	5.0
DD 170 kDa	47.1
DDG 170 kDa 4.5	47.1
DDG 170 kDa 7.7	52.6

2.3.4 *Effect of Galactose Substitution on LC_{50} in Target and Control Cell Lines*

Fig. 2.21 demonstrates the reduction in LC_{50} achieved with galactose substitution on the target BNL CL.2 cells. The ratio of the LC_{50} for a DDG conjugate to that for the untargeted DD conjugate with the same molecular weight were plotted against the galactose substitution. With galactose substitution, the dose of doxorubicin needed to achieve the same cytotoxic effect was reduced by as much as 42% for DDG 10 kDa, and by as much as 66% for DDG 40 kDa and DDG 170 kDa. The normalized reductions observed for the DDG conjugates of different molecular weights were quite similar at a given degree of galactose substitution.

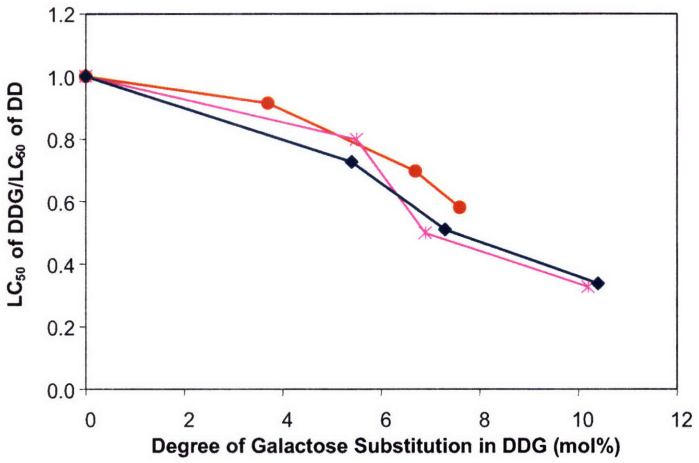

Fig. 2.21. Change in LC_{50} on BNL CL.2 cells incubated for 24 h with DDG conjugates with molecular weights of (●) 10 kDa, (✳) 40 kDa and (◆) 170 kDa, as a function of galactose substitution.

The ratio of the LC_{50} for DDG 170 kDa conjugates to that for the DD 170 kDa conjugate was also compared for the three different cell lines. Fig. 2.22 illustrates that the galactose substitution had no effect on the LC_{50} of DDG 170 kDa for the control NIH/3T3 and H-4-II-E cell lines. Increasing galactose substitution only gave rise to significant reduction in the LC_{50} for DDG 170 kDa on the BNL CL.2 cells. This confirmed the successful targeting of BNL CL.2 cells by DDG conjugates, which were taken up by receptor-mediated endocytosis through the ASGP receptors in the BNL CL.2 cell line.

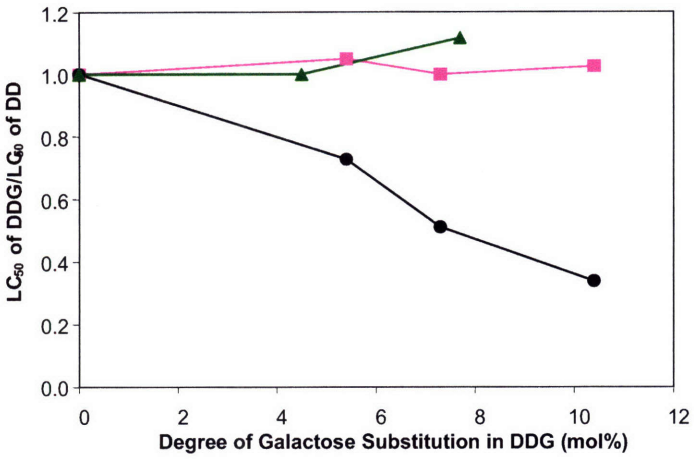

Fig. 2.22. Change in LC_{50} on (●) BNL CL.2, (■) NIH/3T3 and (▲) H-4-II-E cells incubated for 24 h with DDG 170 kDa conjugates, as a function of galactose substitution.

2.4 Summary

Doxorubicin and dextran have been prepared as polymer conjugates of different molecular weights, and different degrees of galactose substitution have been introduced to target hepatocytes. The degree of doxorubicin substitution was maintained by performing the doxorubicin conjugation and galactose conjugation in two sequential steps. The synthesis scheme was simple, efficient and easily adaptable to other therapeutic agents and targeting moieties with free amine groups.

In cell culture studies on the target cell line, the DDG conjugates showed lower toxicity compared to doxorubicin, increased toxicity with higher molecular weight polymers, and greater toxicity with higher degree of galactose substitution. Experiments in the control cell lines showed increased toxicity for higher molecular weight polymers; however, there was no effect due to the presence of galactose.

At diameters of 15–40 nm, the polymer conjugates were too large to enter the cell nuclei in large quantities, but sufficient conjugates entered the nuclei to cause cell death. The higher molecular weight polymers were more effective since they carried more doxorubicin molecules per polymer chain.

2.5 References

[1] L. Seymour, Soluble polymers for lectin-mediated drug targeting, Adv. Drug. Deliv. Rev. 14 (1994) 89–111.

[2] D. Trere, L. Fiume, L. B. De Giorgi, G. Di Stefano, M. Migaldi, M. Derenzini, The asialoglycoprotein receptor in human hepatocellular carcinomas: Its expression on proliferating cells, Br. J. Cancer 81 (1999) 404–408.

[3] K. Bridges, J. Harford, G. Ashwell, R. Klausner, Fate of receptor and ligand during endocytosis of asialoglycoproteins by isolated hepatocytes, Proc. Natl. Acad. Sci. U. S. A. 79 (1982) 350–354.

[4] D. Anderson, S. Vansteenkiste, E. Schacht, S. Sen, L. Seymour, *In vitro* binding specificity of glycosylated dextran to the asialoglycoprotein receptor of primary hepatocytes, Eur. J. Pharm. Sci. 3 (1995) 339–345.

[5] A. Groulet, M. Dorvillius, A. Pellegrin, J. Barbet, D. Baty, Pharmacokinetic and tumor-seeking properties of recombinant and nonrecombinant anti-carcinoembryonic antigen antibody fragments, Int. J. Cancer 100 (2002) 367–374.

[6] L. Fiume, C. Busi, G. Di Stefano, A. Mattioli, Targeting of antiviral drugs to the liver using glycoprotein carriers, Adv. Drug. Deliv. Rev. 14 (1994) 51–65.

[7] A. Kichler, F. Schuber, Comparative affinity of synthetic multi-antennary galactosyl derivatives for the Gal/GalNAc receptor of rat hepatocytes and peritoneal macrophages, J. Drug Target. 6 (1998) 201–205.

[8] K. Sagara, S. Kim, A new synthesis of galactose-poly(ethylene glycol)-polyethylenimine for gene delivery to hepatocytes, J. Control. Release 79 (2002) 271–281.

[9] A. S. Kearney, Prodrugs and targeted drug delivery, Adv. Drug. Deliv. Rev. 19 (1996) 225–239.

[10] R. Duncan, S. Dimitrijevic, E. Evagorou, The role of polymer conjugates in the diagnosis and treatment of cancer, STP Pharma. Sci. 6 (1996) 237–263.

[11] C. Cairo, J. Gestwicki, M. Kanai, L. Kiessling, Control of multivalent interactions by binding epitope density, J. Am. Chem. Soc. 124 (2002) 1615–1619.

[12] K. Ogawara, M. Nishikawa, Y. Takakura, M. Hashida, Pharmacokinetic analysis of hepatic uptake of galactosylated bovine serum albumin in a perfused rat liver, J. Control. Release 50 (1998) 309–317.

[13] K. Ulbrich, V. Subr, J. Strohalm, D. Plocova, M. Jelinkova, B. Rihova, Polymeric drugs based on conjugates of synthetic and natural macromolecules: I. Synthesis and physico-chemical characterization, J. Control. Release 64 (2000) 63–79.

[14] L. Seymour, K. Ulbrich, S. Wedge, I. Hume, J. Strohalm, R. Duncan, N-(2-Hydroxypropyl)methacrylamide copolymers targeted to the hepatocyte galactose-receptor: Pharmacokinetics in DBA2 mice, Br. J. Cancer 63 (1991) 859–866.

[15] A. David, P. Kopeckova, A. Rubinstein, J. Kopecek, Enhanced biorecognition and internalization of HPMA copolymers containing multiple or multivalent carbohydrate side-chains by human hepatocarcinoma cells, Bioconjug. Chem. 12 (2001) 890–899.

[16] Y. Ohya, H. Oue, K. Nagatomi, T. Ouchi, Design of macromolecular prodrug of cisplatin using dextran with branched galactose units as targeting moieties to hepatoma cells, Biomacromolecules 2 (2001) 927–933.

[17] M. Hashida, H. Hirabayashi, M. Nishikawa, Y. Takakura, Targeted delivery of drugs and proteins to the liver via receptor-mediated endocytosis, J. Control. Release 46 (1997) 129–137.

[18] K. Mross, U. Mayer, K. Hamm, K. Burk, D. Hossfeld, Pharmacokinetics and metabolism of iodo-doxorubicin and doxorubicin in humans, Eur. J. Clin. Pharmacol. 39 (1990) 507–513.

[19] D. Gustafson, J. Rastatter, T. Colombo, M. Long, Doxorubicin pharmacokinetics: Macromolecule binding, metabolism, and excretion in the context of a physiologic model, J. Pharm. Sci. 91 (2002) 1488–1501.

[20] G. Minotti, P. Menna, E. Salvatorelli, G. Cairo, L. Gianni., Anthracyclines: Molecular advances and pharmacologic developments in antitumor activity and cardiotoxicity, Pharmacol. Rev. 56 (2004) 185–229.

[21] E. Lefrak, J. Pitha, S. Rosenheim, J. Gottlieb, A clinicopathologic analysis of adriamycin cardiotoxicity, Cancer 32 (1973) 302–314.

[22] R. Mehvar, Dextrans for targeted and sustained delivery of therapeutic and imaging agents, J. Control. Release 69 (2000) 1–25.

[23] M. C. Garnett, Targeted drug conjugates: Principles and progress, Adv. Drug. Deliv. Rev. 53 (2001) 171–216.

[24] M. Yang, H. L. Chan, W. Lam, W. F. Fong, Cytotoxicity and DNA binding characteristics of dextran-conjugated doxorubicins, BBA Gen. Subjects 1380 (1998) 329–335.

[25] Y. Ohya, T. Masunaga, T. Baba, T. Ouchi, Synthesis and cytotoxic activity of dextran carrying cis-dichloro(cyclohexane-trans-l-1,2-diamine)platinum(II) complex, J. Biomater. Sci. Polym. Ed. 7 (1996) 1085–1096.

[26] A. Bernstein, E. Hurwitz, R. Maron, R. Arnon, M. Sela, M. Wilchek, Higher anti-tumor efficacy of daunomycin when linked to dextran: *In vivo* and *in vitro* studies, J. Natl. Cancer Inst. 60 (1978) 379–384.

[27] W. Lam, C. H. Leung, H. L. Chan, W. F. Fong, Toxicity and DNA binding of dextran-doxorubicin conjugates in multidrug-resistant KB-V1 cells: Optimization of dextran size, Anticancer Drugs 11 (2000) 377–384.

[28] C. A. Frederick, L. D. Williams, G. Ughetto, G. A. Vandermarel, J. H. Vanboom, A. Rich, A. H. J. Wang, Structural comparison of anticancer drug DNA complexes: Adriamycin and daunomycin, Biochemistry 29 (1990) 2538–2549.

[29] C. Plank, K. Zatloukal, M. Cotten, K. Mechtler, E. Wagner, Gene-transfer into hepatocytes using asialoglycoprotein receptor mediated endocytosis of DNA complexed with an artificial tetra-antennary galactose ligand, Bioconjug. Chem. 3 (1992) 533–539.

[30] M. M. Alauddin, A. Y. Louie, A. Shahinian, T. J. Meade, P. S. Conti, Receptor mediated uptake of a radiolabeled contrast agent sensitive to beta-galactosidase activity, Nucl. Med. Biol. 30 (2003) 261–265.

[31] M. A. Zanta, O. Boussif, A. Adib, J. P. Behr, *In vitro* gene delivery to hepatocytes with galactosylated polyethylenimine, Bioconjug. Chem. 8 (1997) 839–844.

[32] P. Q. Patek, J. L. Collins, M. Cohn, Transformed-cell lines susceptible or resistant to *in vivo* surveillance against tumorigenesis, Nature 276 (1978) 510–511.

[33] M. Rodriguez, C. Dargemont, F. Stutz, Nuclear export of RNA, Biol. Cell 96 (2004) 639–655.

[34] A. Schwartz, S. Fridovich, B. Knowles, H. Lodish., Characterization of the asialoglycoprotein receptor in a continuous hepatoma line, J. Biol. Chem. 256 (1981) 8878–8881.

Chapter 3 – Synthesis, Characterization and *In Vitro* Studies of Acid-Labile Dextran Conjugates for Doxorubicin Delivery

3.1 Introduction

When a drug is delivered as a conjugate with a polymer, an antibody or other macromolecule, it may have lower efficacy or a different mechanism of action compared to the free drug. Release or activation of the drug may be necessary to achieve the required effect. Hovorka *et al.* have demonstrated that doxorubicin stably conjugated to poly((N-2-hydroxypropyl)methacrylamide) (HPMA) has a different mechanism of action from free doxorubicin [1]. Free doxorubicin intercalated with nuclear and mitochondrial DNA, causing single- and double-stranded breaks, which started a cascade of signaling leading to apoptosis. Conversely, the HPMA-bound doxorubicin caused cell death mainly by necrosis and other cytocidal effects. Doxorubicin was not detected in the nucleus even after 72 h.

In Chapter 2, we synthesized a dextran-doxorubicin-galactose conjugate that was successful at targeting hepatocytes [2]. We did observe some nuclear localization of the conjugate even after only 8 h, and were able to observe an increase by 24 h. In cell-free buffer, the polymer had a very slight effect on the ability of doxorubicin to intercalate with DNA due to the occupation of the amino sugar group of doxorubicin. However, the cytotoxicity was limited since the size of the polymer conjugates reduced the nuclear uptake. The LC_{50} of the most toxic conjugate was 8.6 μM, compared to 1.8 μM for free doxorubicin. Therefore, a drug delivery vehicle that releases free doxorubicin inside the cell would be more effective.

Several methods for drug release have been investigated, which involved temperature-sensitive, membrane-disruptive, acid-labile and enzyme-degradable materials. Polymers of *N*-isopropylacrylamide (NIPAAm) are often used in micelles, liposomes and hydrogels for their temperature-sensitive behavior [3, 4]. Skirtach *et al.* have synthesized thermo-responsive polyelectrolyte multilayered shells doped with metal nanoparticles, which disrupted the membrane and led to release when treated with near infrared laser [5]. Hydrocarbon chains have also been utilized as membrane disruptive agents. Kyriakides *et al.* have synthesized poly(propylacrylic acid) (PPAA), which was effective at membrane disruption at a pH below 6.5, and tested it in *in vitro* studies and an *in vivo* excisional wound healing model. The propyl group

acted as a hydrophobic membrane destabilizer. They have also demonstrated the delivery of green fluorescent protein (GFP) in cell culture studies [6]. Doxorubicin and daunorubicin have been conjugated to human serum albumin or transferrin with a disulfide bond, which was reduced inside the cell to release the free drug. Over 50% of the conjugated drug was released within 24 h, and *in vivo* experiments have shown promising results [7]. Doxorubicin has also been conjugated to HPMA with enzymatically degradable peptide linkers, as well as acid-labile bonds [8-10]. In general, pH-sensitive release has been shown to be more toxic in cell culture studies than peptide-cleavable conjugates [7, 11].

In pH-responsive drug delivery, research has been conducted on polymer conjugates, hydrogels, particles, micelles, dendrimers and liposomes [12-22]. Polymers that have been used to form pH-sensitive conjugates included dextran, alginic acid, carboxymethyl cellulose, poly(amino acids), HPMA and poly(ethylene glycol) (PEG) [7]. Murthy *et al.* have synthesized "encrypted polymers" that mimicked the multi-functional design of biology. Their membrane-disruptive polymer was protected with pendant PEG groups attached with disulfide bonds. These bonds were reduced at low pH's and the PEG groups would dissociate from the polymer, which escaped from the endosome by disrupting the membrane [17]. Chiu *et al.* have attached acrylic acid to dextran to make it pH-sensitive for application in colon cancer treatment [20]. Yessine *et al.* have synthesized a NIPAAm copolymer with poly(methacrylic acid) and octadecyl acrylate. This formed a polyanion that changed from a coil to a globule conformation in acidic conditions; it was used to synthesize pH-sensitive liposomes that could escape from the endosome [21].

Carboxylic hydrazone, *cis*-aconityl and acetal are common acid-labile bonds that have been investigated extensively for use in drug delivery. Imine and ketal bonds have also been studied to a lesser extent [7, 10, 23]. The *cis*-aconityl bond has been utilized to form nanoaggregates between glycol and chitosan to deliver doxorubicin. About 20% of the drug was released from the delivery vehicle after 8 days. The aggregates had an average size of 250 nm, and were found to be retained in tumors in *in vivo* studies due to the enhanced permeability and retention (EPR) effect. There was also significant accumulation in the kidneys since the aggregates were not targeted to the tumors [24]. Some researchers have shown that the hydrazone bond was more effective than the *cis*-aconityl bond in cell culture experiments [9, 11].

One inherent disadvantage of using *cis*-aconityl was that the pendant *cis*-aconityl moiety could be lost in the side reactions, causing the drug conjugate to be less sensitive to pH [11]. Yoo *et al.* have conjugated doxorubicin to a copolymer of poly(lactic acid) and methoxy-PEG with acetal and hydrazone bonds. The micelles formed from the hydrazone-linked doxorubicin conjugate had higher overall release and greater cytotoxicity in cell culture studies [12].

A pH-sensitive dextran-doxorubicin conjugate would be more cytotoxic since it would release the drug in a free form. Also, due to the EPR effect, drug conjugates would tend to accumulate in tumors, and a pH-sensitive conjugate would release the drug inside the tumor [7]. Therefore, in addition to greater efficacy after cellular delivery, the pH-sensitive conjugates would also potentially be helpful specifically in treating tumors. The goal for this study was to attach doxorubicin to dextran in a pH-sensitive manner so that the drug would be released at a low pH. The hydrazone bond was chosen since it showed the most promising results in the literature.

3.2 Experimental Methods

3.2.1 Materials

Anhydrous dimethylformamide (DMF), anhydrous dimethylsulfoxide (DMSO), lithium chloride (LiCl), pyridine, 4-nitrophenylchloroformate (NPC), hydrazine, doxorubicin and bovine serum albumin (BSA) were obtained from Sigma-Aldrich. Dextran at molecular weights (MW's) of 10, 40, 70 and 170 kilodaltons (kDa) were also obtained from Sigma-Aldrich. OmniPur 10× phosphate buffered saline (PBS) was used during synthesis at a 1:10 dilution. Ethanol and diethyl ether and Dulbecco's 1× sterile PBS containing calcium and magnesium for cell culture studies were obtained from VWR. The murine hepatocytic cell line BNL CL.2, Dulbecco's Minimum Essential Medium (DMEM), fetal bovine serum (FBS), Penicillin-Streptomycin, 0.25% of Trypsin/0.53 mM of ethylenediaminetetraacetic acid (EDTA), and the MTT Cell Proliferation Assay kit were obtained from American Type Culture Collection (ATCC). LysoTracker Green, SYBR Green Nucleic Acid Stain, RNase A and propidium iodide (PI) were obtained from Invitrogen. Macro Fast DispoDialyzer cassettes (Harvard Apparatus) were used with a molecular weight cut-off (MWCO) of 5 kDa.

3.2.2 Synthesis of Acid-Labile Dextran-Hydrazone-Doxorubicin Conjugates

The synthesis scheme used to attach doxorubicin to the dextran chain with a pH-sensitive hydrazone bond is shown in Fig. 3.1. Dextran was activated with NPC following the method given by Ramirez *et al.* [25]. The reaction was performed in a dry nitrogen atmosphere, and the reagents were prepared as follows. Dextran was dried under vacuum at 100°C overnight. NPC was also dried under vacuum at room temperature overnight. A solution of 20 g/L of LiCl in DMF was purged with nitrogen overnight. In the first step, 1 g of vacuum dried dextran was dissolved in 100 mL of LiCl/DMF at 90°C. After the dextran had dissolved, the solution was transferred to an ice bath, and 0.5 g of pyridine and 1.2 g of NPC (both equimolar to glucose residues on dextran) were added. The reaction solution was kept in an ice bath for 4 h, and the resulting nitrophenyl carbonate-dextran was precipitated in a 4:1 volume mixture of ethanol and diethyl ether. The product was centrifuged, washed two more times with a 4:1 volume mixture of ethanol and diethyl ether, and dried under vacuum. The presence of the nitrophenyl group on dextran was confirmed by nuclear magnetic resonance (NMR) spectroscopy (Avance DMX 400 MHz, Bruker) in dimethyl sulfoxide (DMSO-d6) and photoacoustic Fourier-transform infrared (PA-FTIR) spectroscopy (Bio-Rad FTS60A).

1 g of the synthesized nitrophenyl carbonate-dextran was dissolved in 25 mL of anhydrous DMSO, and reacted with 2.0 g (10× molar ratio to glucose residues on dextran) of hydrazine [26]. The reaction was allowed to proceed for 3 h, and the dextran-hydrazide was purified by dialysis against 1 L of deionized (DI) water. The dialysis water was changed twice a day for three days. Dextran-hydrazide was recovered by lyophilization, and was characterized by NMR and PA-FTIR spectroscopies for the disappearance of the nitrophenyl carbonate group.

In the final step, 100 mg of dextran-hydrazide were dissolved in 5 mL of 1× PBS (pH 7.4). Doxorubicin (10 mg) and 1 drop of glacial acetic acid were added, and allowed to react for 48 h. The final dextran-hydrazone-doxorubicin (DHD) conjugate was purified by dialysis against 500 mL of 1× PBS (pH 7.4). The PBS was changed twice a day for three days, and the polymer conjugate was recovered by lyophilization. The degree of substitution of doxorubicin was determined by measuring the absorbance at 485 nm on a UV-Vis microplate reader (VersaMax, Molecular Devices).

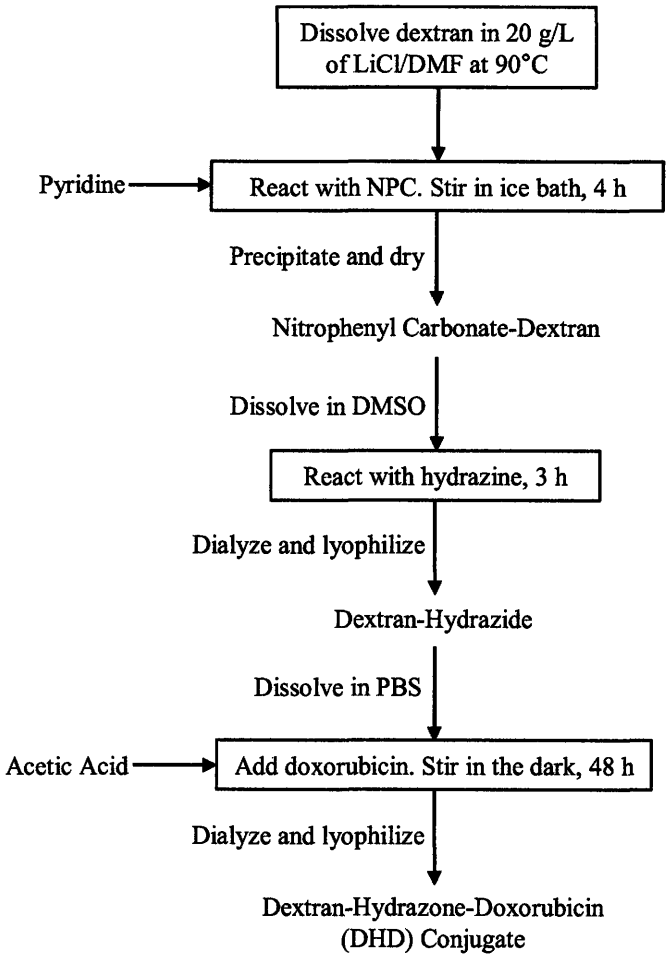

Fig. 3.1. Schematic of synthesis of dextran-hydrazone-doxorubicin conjugate.

3.2.3 Cell-Free Efficacy of Dextran-Hydrazone-Doxorubicin Conjugates

Calf-thymus DNA was dissolved in 1× PBS (pH 7.4) at a concentration of 1 mg/mL. Doxorubicin and the polymer conjugates to be tested were also dissolved in 1× PBS at a normalized concentration of 12.5 μg/mL of doxorubicin. The assay was performed in a 96-well plate by adding 20 μL of the doxorubicin or polymer conjugate solution to a final ct-DNA concentration ranging from 0 to 0.9 mg/mL. Readings were taken on a fluorescence microplate reader (*f*Max, Molecular Devices; λ_{ex} = 488 nm, λ_{em} = 590 nm) immediately upon addition of conjugates [27]. All experiments were performed in triplicate.

3.2.4 Doxorubicin Release from Acid-Labile Conjugates

The release of doxorubicin from the acid-labile DHD conjugate was tested in 0.1 M of sodium acetate buffer with 0.05 M of sodium chloride at pH's of 7.4 and 5.0. The DHD conjugates were dissolved in each buffer, transferred to a Macro Fast DispoDialyzer cassette, immersed in 5 mL of the buffers, and incubated at 37°C. At each time point, 0.75 mL of the dialysate was removed for analysis, and replaced with fresh buffer. Release was observed over 24 h. The amount of doxorubicin released was determined by measuring absorbance at 485 nm.

3.2.5 In Vitro Efficacy of Polymer Conjugates

The BNL CL.2 cell line was cultured in DMEM supplemented with 10% FBS and 1% Penicillin-Streptomycin at 37°C in 5% of CO_2.

For uptake and cytotoxicity studies, cells were plated at 400/mm^2 in six-well plates, and allowed to adhere for 10–14 h. The medium was then replaced with complete medium containing doxorubicin or polymer conjugates at various concentrations, and incubated for 24 h. At the end of the experiment, the cell layer was gently washed three times with cold PBS, and cells were harvested with Trypsin-EDTA. The fluorescence due to the uptake of doxorubicin or conjugates was evaluated by running the cell samples through a flow cytometer (Becton Dickinson FACScan, FL2-H; λ_{ex} = 488 nm, λ_{em} = 590 nm). All experiments were performed in triplicate.

To determine the killing efficiency, the harvested cells described in the preceding paragraph were replated in 96-well plates, and allowed to adhere for 8–10 h. The medium was replaced with 100 μL of fresh medium and 10 μL of the MTT reagent (3-(4,5-dimethylthiazol-2-yl)-2,5-diphenyltetrazolium bromide), and the plate was incubated for 1 or 2 h. 100 μL of sodium dodecyl sulfate were then added, and the cells were incubated for another 10 or 12 h. The absorbance was measured at 570 nm. The standard curves for cell viability were obtained by performing the MTT assay on a known cell concentration curve, measured by hemacytometer.

The DNA content of the treated cells was analyzed by flow cytometry. Cells were treated with doxorubicin or conjugates for 24 h at a nominal doxorubicin concentration of 3.6 μM. The cells were then harvested, washed twice with 1× PBS, redispersed in PBS, and fixed in cold ethanol overnight at 4°C. After fixation, the cells were washed twice with PBS containing 1% BSA, redispersed in the PBS solution, and PI and RNase were added to yield final concentrations of 50 μg/mL and 1 mg/mL, respectively. The cells were incubated at 37°C for 30 min and analyzed by flow cytometry.

The uptake of the conjugates was observed by performing live cell microscopy on a Zeiss LSM510 laser scanning confocal microscope. Cells were plated at 400/mm^2 in chambered slides (Lab-Tek Chambered Coverglasses, NUNC), and allowed to adhere for 10–14 h. LysoTracker Green was diluted in complete cell culture medium to a concentration of 100 nM, and used to stain the acidic intracellular vesicles. Cells were incubated with LysoTracker for 30 min at 37°C. The slides were placed in a temperature-, humidity- and CO_2-controlled chamber, and the images were obtained at 10-min intervals immediately after addition of free doxorubicin or conjugates at a nominal doxorubicin concentration of 9.0 μM.

Cells incubated with doxorubicin (nominal concentration = 3.6 μM) were fixed in paraformaldehyde, the nuclei were counterstained with SYBR Green, and confocal images were obtained after incubation for 4 or 8 h.

3.3 Results and Discussion

3.3.1 Synthesis and Characterization of Polymer Conjugates

A schematic of the reaction to form dextran-hydrazone-doxorubicin conjugates was shown in Fig. 3.2. The structure of nitrophenyl carbonate-dextran was confirmed by ^{1}H NMR and PA-FTIR spectra (Figs. 3.3 and 3.4). The glucosidic protons appeared on the NMR spectrum in several bands between 3.0 and 5.5 ppm. For nitrophenyl carbonate-dextran (Fig. 3.3(b)), the peaks from 7.5 to 8.5 ppm were attributed to the protons on the phenyl group. The nitrophenyl carbonate group was replaced during the reaction with hydrazine, as confirmed by the disappearance of the phenyl protons from the NMR spectrum of dextran-hydrazide (Fig. 3.3(c)). The final DHD conjugate (Fig. 3.3(d)) exhibited peaks due to phenyl protons between

6.5 to 7.8 ppm. The carbonate on nitrophenyl carbonate-dextran (Fig. 3.4(b)) showed a characteristic FTIR peak at 1770 cm^{-1}, which was not observed for dextran-hydrazide (Fig. 3.4(c)). The degrees of substitution of doxorubicin on conjugates of various MW's are listed in Table 3.1. This was controlled by the amount of doxorubicin added during the reaction, and did not increase significantly above 2.0 mol%. The efficiency of doxorubicin conjugation was between 5% and 8% for the different MW's.

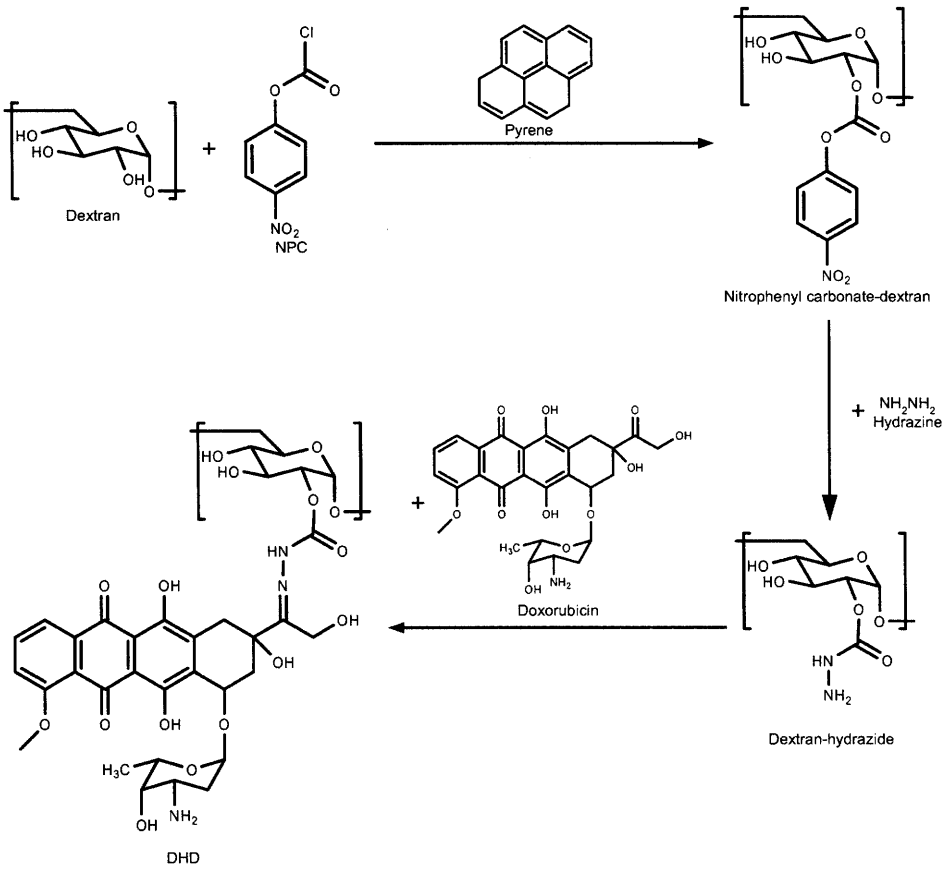

Fig. 3.2. Synthesis of the dextran-hydrazone-doxorubicin conjugates.

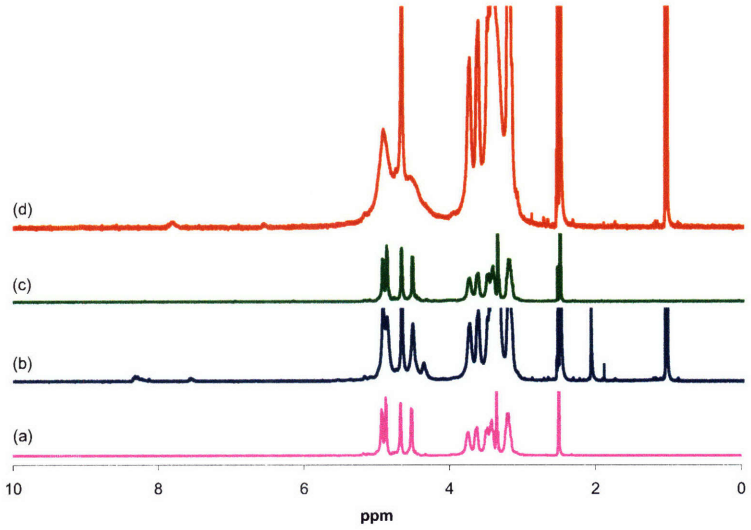

Fig. 3.3. ^{1}H NMR spectra of (a) dextran, (b) nitrophenyl carbonate-dextran, (c) dextran-hydrazide and (d) DHD with a MW of 10 kDa.

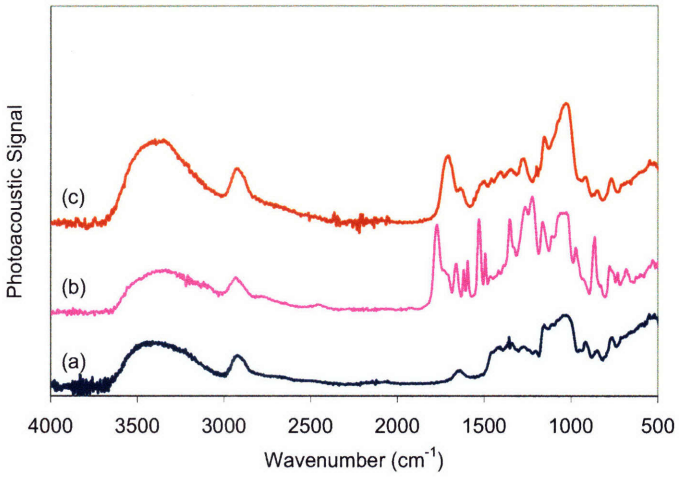

Fig. 3.4. PA-FTIR spectra of (a) dextran, (b) nitrophenyl carbonate-dextran and (c) dextran-hydrazide with a MW of 10 kDa.

Table 3.1. Degree of doxorubicin substitution per glucose monomer for DHD conjugates with various MW's. Values are mean ± standard deviation; n = 2.

Conjugate Molecular Weight (kDa)	Doxorubicin (mol%)
10	1.9 ± 0.2
40	1.9 ± 0.2
70	1.1 ± 0.9
170	1.1 ± 0.2

3.3.2 Cell-Free Testing of DHD Conjugates

3.3.2.1 DNA Binding Studies

The efficacy of doxorubicin can be lowered when it is bound to a macromolecule or released in an altered form. Therefore, the DNA binding efficiency of the acid-labile DHD conjugates and the doxorubicin released from the conjugates were examined using a fluorescence-based assay.

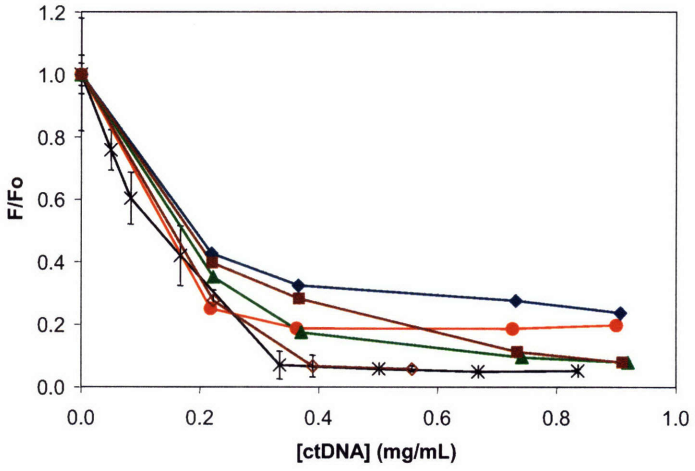

Fig. 3.5. Fluorescence quenching of doxorubicin in the presence of ct-DNA for (⋆) doxorubicin, DHD conjugates of MW's of (◆) 10 kDa, (●) 40 kDa, (■) 70 kDa and (▲) 170 kDa, and (◇) doxorubicin released from DHD 10 kDa. Values are mean ± standard deviation; n = 3.

The acid-labile DHD conjugates showed a significant degree of binding with ctDNA (Fig. 3.5). There was no clear trend in the effect of MW of the conjugates on the degree of

binding. It has been shown that the chromophore and amino-sugar groups of doxorubicin were involved in the intercalation with DNA [28]. In this case, the acetyl group of doxorubicin was occupied in the formation of the DHD conjugates. Since both of the DNA binding sites were free, a significantly improved degree of interaction was observed as compared to the previously synthesized dextran-doxorubicin (DD) conjugates [2]. Fig. 3.5 also shows the efficacy of doxorubicin that has been released from the 10 kDa conjugate at 37°C and a pH of 5.0. Fluorescence quenching of the released doxorubicin was almost identical to that of free doxorubicin.

3.3.2.2 pH-Responsive Release of Doxorubicin

Fig. 3.6 shows the release of doxorubicin from DHD conjugates at pH's of 5.0 and 7.4 at 37°C. At a pH of 5.0, the rate of release was significantly greater than that at the extracellular pH of 7.4 for all MW's, indicating that these conjugates would release the active drug inside an endosome or lysosome. There was some release from the conjugate at pH 7.4 as well, though the percentage released was significantly less than that at pH 5.0. The doxorubicin that was not released from the conjugate might have reacted by a different mechanism to form a stable amide bond with the dextran [29].

The release rate of doxorubicin from the conjugates of different MW's at a pH of 5.0 is shown in Fig. 3.7. The initial release rate at a pH of 5.0 from the 10 kDa polymer conjugate was up to 5-fold higher than the other conjugates. For both the 10 kDa and 40 kDa DHD conjugates, there was an initial increase in the rate for the first 6 h, followed by a decline. The 70 kDa and 170 kDa DHD conjugates showed a lower and highly variable release rate. The release rate in a pH 7.4 buffer remained relatively constant or declined over the 24 h period (data not shown). The initial release of doxorubicin from the 10 kDa DHD conjugate at a pH of 5.0 was about 5–10 times faster than that at a pH of 7.4. This was comparable to the release profiles for hydrazone-linked drugs reported in the literature [30].

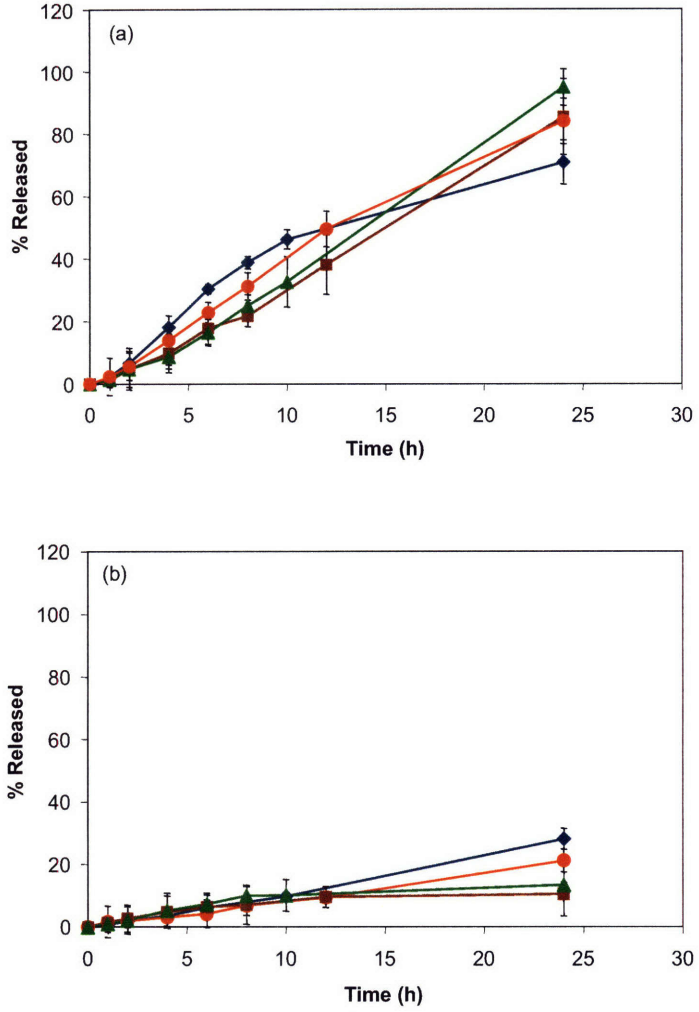

Fig. 3.6. Release of doxorubicin from DHD conjugates of MW's of (◆) 10 kDa, (●) 40 kDa, (■) 70 kDa and (▲) 170 kDa at a pH of (a) 5.0 and (b) 7.4. Values are mean ± standard deviation; n = 3.

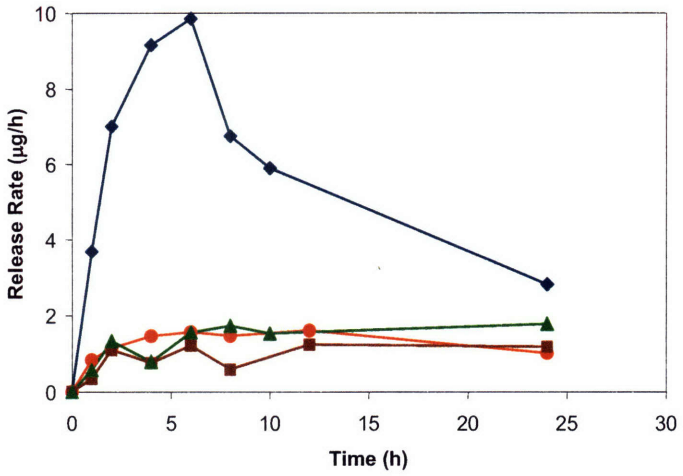

Fig. 3.7. Rate of doxorubicin release from DHD conjugates of MW's of (◆) 10 kDa, (●) 40 kDa, (■) 70 kDa and (▲) 170 kDa at a pH of 5.0.

3.3.3 In Vitro Studies

3.3.3.1 Doxorubicin Uptake

Flow cytometry was used to determine the excess fluorescence of cells incubated with either doxorubicin or polymer-bound doxorubicin conjugates. The relative fluorescence of cells incubated with the conjugates is illustrated in Fig. 3.8. The uptake of free doxorubicin was significantly greater than the uptake of the conjugates. The MW of the carrier polymer did not seem to have a significant effect on the uptake of the conjugates. The uptake of the acid-labile DHD conjugates was greater than the non-targeted DD conjugates at equivalent MW's (Fig. 2.7) [2]. A possible explanation for this was that doxorubicin was released from the DHD conjugate in acidic intracellular vesicles, which allowed it to enter the nucleus easily. In contrast, doxorubicin bound stably to dextran could be exocytosed before it had a chance to enter the nucleus.

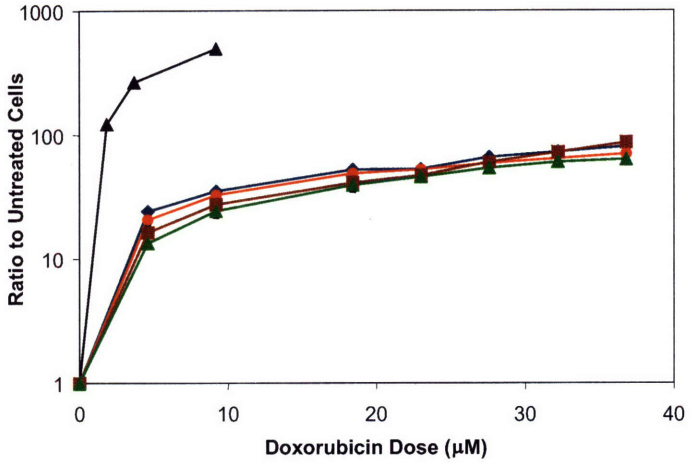

Fig. 3.8. Doxorubicin-associated fluorescence of cells incubated for 24 h with (▲) doxorubicin, DHD conjugates of MW's of (◆) 10 kDa, (●) 40 kDa, (■) 70 kDa and (▲) 170 kDa. Values are mean ± standard deviation; n = 3.

3.3.3.2 Cytotoxicity Studies

The cytotoxicity of the conjugates was determined using the MTT assay, which is a simple and rapid colorimetric method for measuring cell viability. The concentration corresponding to 50% cell death (LC_{50}) was determined from the slope and intercept of the straight line obtained by inverting the dose vs. cell death data from the dose response curves. The LC_{50} values obtained by this method were corroborated by determination with a logistic model.

Cytotoxicity profiles for the conjugates were shown in Fig. 3.9. The DHD conjugates were significantly more toxic than the stable DD conjugates. For example, the LC_{50} of DHD 10 kDa was 7.4 μM (Table 3.2), whereas LC_{50} of DD 10 kDa was 36.4 μM (Table 2.4) [2]. In our previous work, we observed a significant increase in toxicity with increasing MW of DD conjugates due to an increase in the chain loading (Table 2.4) [2]. However, we did not observe the same effect with the DHD conjugates. The higher MW conjugates had a greater doxorubicin loading, and would be able to carry more of the drug into the cell. However, as shown in Fig. 3.7, release from the DHD 10 kDa conjugate was much more rapid, and therefore, could lead to greater accumulation of doxorubicin inside the cells. This may be corroborated by the slightly greater uptake of DHD 10 kDa as observed in Fig. 3.8. Since these two effects opposed each other, the MW did not have a strong overall effect on cytotoxicity.

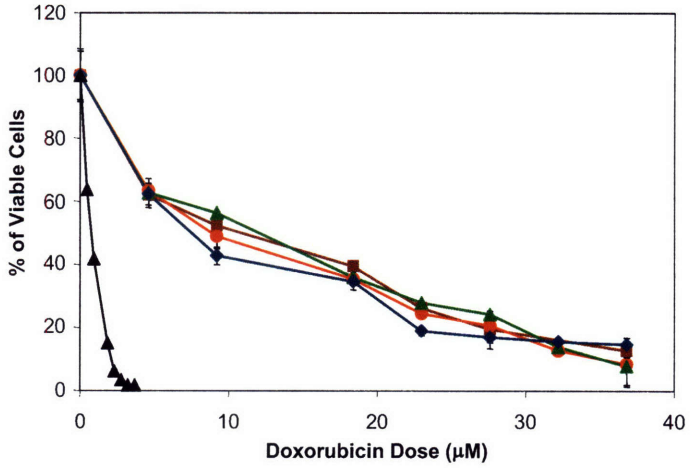

Fig. 3.9. Dose response curves of BNL CL.2 cells incubated for 24 h with (▲) doxorubicin, and DHD conjugates with MW's of (◆) 10 kDa, (●) 40 kDa, (■) 70 kDa and (▲) 170 kDa. Values are mean ± standard deviation; n = 3.

Table 3.2. LC_{50} of DHD conjugates in BNL CL.2 cells.

Conjugate MW (kDa)	LC_{50} (μM)
10	7.4
40	8.5
70	8.8
170	9.2

Ulbrich *et al.* have reported a comparison of cytotoxicity of free doxorubicin and pH-sensitive HPMA-doxorubicin conjugates in EL4 T cells [7]. They found that the doxorubicin attached through a hydrazone bond had a LC_{50} value of 7–34 times that of free doxorubicin. When they attached anti-Thy1.2 antibody to target the cells, the LC_{50} was the same as free doxorubicin. The DHD conjugates had LC_{50} values that were 4–5 times higher than that of free doxorubicin (1.8 μM). Attempts on galactose conjugation with the pH-sensitive synthesis were unsuccessful because the polymer became insoluble.

3.3.3.3 Cell Cycle Analysis

The DNA content of cells treated with free doxorubicin, DHD and DD conjugates were analyzed to investigate if treatment by free or conjugated doxorubicin yielded a difference in the cell cycle response. As shown in Table 3.3, free doxorubicin caused cell cycle arrest in the G2/M phase, with a significant increase in the number of cells in the S phase as well. Cells treated with the acid-labile DHD 10 kDa conjugate showed a response very similar to free doxorubicin. Cells treated with stably bound DD 10 kDa conjugate also exhibited G2/M phase arrest. However, the percentage of cells in the S phase did not increase, indicating that the mechanism of action of the DD conjugate differed from that of free doxorubicin and doxorubicin delivered by the DHD conjugate. We previously showed that the ability of the DD 10 kDa conjugates to intercalate with DNA was lower than that of free doxorubicin (Fig. 2.5) [2]. It is possible that due to the weaker DNA binding, cells treated with DD 10 kDa were able to undergo DNA replication in the S phase and enter mitosis, resulting in accumulation only in the G2/M phase of the cell cycle.

Table 3.3. Percentage of BNL CL.2 cells in different phases of the cell cycle before and after treatment with doxorubicin or conjugates.

Phase	Untreated	Doxorubicin	DHD 10 kDa	DD 10 kDa
G0/G1	84.5	14.1	12.0	28.2
S	4.6	16.0	14.9	2.1
G2/M	10.4	70.3	73.6	69.4

3.3.3.4 Internalization of Doxorubicin and Polymer Conjugates

Cancerous cells expel vast quantities of lactic acid, which results in the acidic environment in a tumor [31]. Therefore, a pH-sensitive delivery vehicle may release the drug before it is internalized by the cells. Live cell imaging was used in an attempt to examine the mechanism of action of the DHD conjugates.

LysoTracker is a fluorophore conjugated to a weak base that freely passes through the cell membrane and selectively localizes in low-pH intracellular vesicles. This green dye was

used to stain endosomes and lysosomes. The uptake of doxorubicin and DHD 10 kDa was followed by confocal microscopy for 1 h (Fig. 3.10). For both the free drug and the polymer conjugate, cellular uptake occurred within minutes. Free doxorubicin (red) was visible inside the nucleus within 30 min of incubation. However, cells incubated with DHD 10 kDa did not show nuclear uptake until at least 60 min after incubation. Also, for cells incubated with DHD 10 kDa, there was significant colocalization (yellow) of fluorescence from doxorubicin and LysoTracker, indicating that the polymer-conjugated doxorubicin was taken up by endocytic pathways. Free doxorubicin did not show much colocalization since the doxorubicin was able to diffuse freely through the cell.

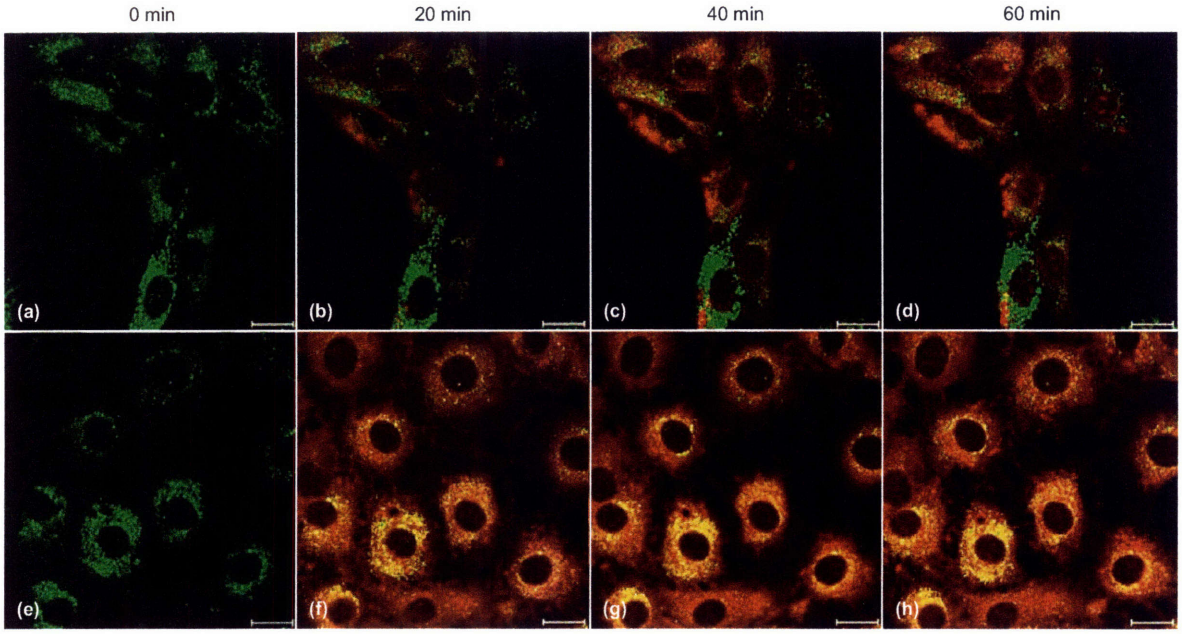

Fig. 3.10. BNL CL.2 cells incubated with (a–d) doxorubicin and (e–h) DHD 10 kDa at a nominal doxorubicin concentration of 9 μM at the stated times. Acidic intracellular vesicles were counterstained with LysoTracker Green. Scale bar = 20 μm.

From release studies at pH 5.0 (Fig. 3.5), it can be seen that a very small percentage of doxorubicin was released from the DHD conjugates within 1 h. Since the conjugates were taken into the cells within a few minutes, it is unlikely that they released doxorubicin outside the cell membrane. The DHD conjugates were possibly taken into the cells intact, and released doxorubicin in the intracellular vesicles. Since cellular trafficking occurs very rapidly, it was

possible that the conjugates underwent multiple endocytosis and exocytosis cycles before the doxorubicin was released.

Fig. 3.11 shows the confocal laser scanning microscopy images of BNL CL.2 cells incubated with doxorubicin, DHD 10 kDa and DD 10 kDa for 4 h, with the nuclei counterstained with SYBR Green. Free doxorubicin was localized exclusively in the nucleus, as observed from the co-localization of doxorubicin and SYBR Green fluorescence. The fluorescence micrographs of cells incubated with DHD conjugates also exhibited significant co-localization. In comparison, the DD conjugate showed much less co-localization. These micrographs confirmed that the doxorubicin on the DHD conjugates entered the nuclei efficiently, indicating that doxorubicin was released from the polymer in an intracellular vesicle.

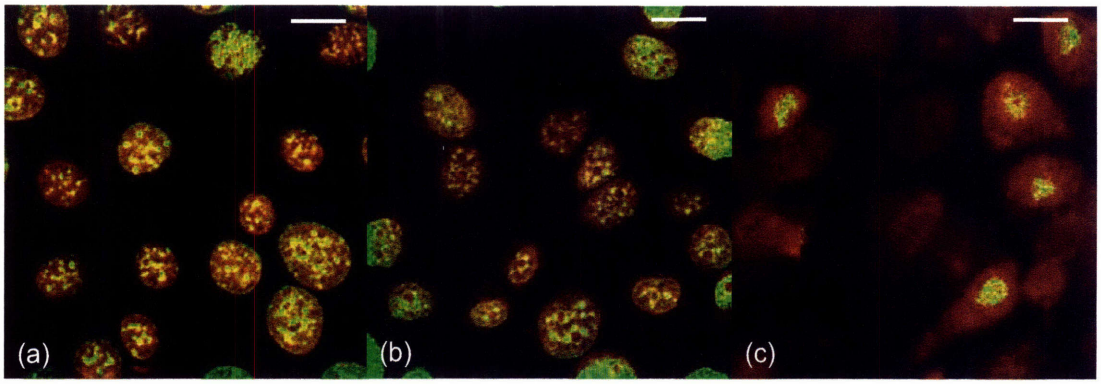

Fig. 3.11. BNL CL.2 cells incubated with (a) doxorubicin, (b) DHD 10 kDa and (c) DD 10 kDa for 4 h at a doxorubicin concentration of 3.6 μM. The nuclei were counterstained with SYBR Green. Scale bar = 10 μm.

3.4 Summary

In our previous work, we had synthesized galactose-expressing doxorubicin delivery vehicles, which were effective at targeting hepatocytes; however, the cytotoxicity was limited since the doxorubicin remained attached to the polymer. In this work, we prepared pH-sensitive dextran-doxorubicin conjugates of different MW's. Doxorubicin was attached through a hydrazone bond to the dextran backbone. These polymer conjugates were stable at a physiological pH of 7.4, but released over 70% of the attached doxorubicin within 24 h at a pH of 5.0. The rate of release was found to be much faster for the lower MW polymers. In cell culture studies, the conjugates showed significant cytotoxicity. The effect of lower chain loading

of doxorubicin in the lower MW polymers was offset by the rapid initial release rate of doxorubicin. Consequently, the lower MW polymers showed slightly greater toxicity.

Confocal microscopy images showed that the polymer conjugates were taken into the cells within minutes after incubation. Since release of doxorubicin from the conjugates occurred over hours, it was likely that intact conjugates were taken up by cells and the drug was released in intracellular vesicles. The conjugates might have gone through multiple endocytosis and exocytosis cycles before the doxorubicin was released.

Doxorubicin from the DHD conjugates was found to localize almost exclusively in the nuclei of cells. Since doxorubicin attached to dextran with a stable bond showed limited localization in the nuclei, this confirmed that doxorubicin from the acid-labile conjugates was released after internalization by cells. The cytotoxicity of the DHD conjugates was significantly greater than the stable conjugates due to the effective release of doxorubicin inside cells.

3.5 References

[1] O. Hovorka, M. St'astny, T. Etrych, V. Subr, J. Strohalm, K. Ulbrich, B. Rihova, Differences in the intracellular fate of free and polymer-bound doxorubicin, J. Control. Release 80 (2002) 101–117.

[2] N. T. Zaman, J. Y. Ying, Synthesis, characterization and *in vitro* studies of dextran-galactose conjugates for targeted doxorubicin delivery to hepatocytes, To be submitted to J. Control. Release.

[3] X. Z. Zhang, D. Q. Wu, C. C. Chu, Synthesis and characterization of partially biodegradable, temperature and pH sensitive Dex-MA/PNIPAAm hydrogels, Biomaterials 25 (2004) 4719–4730.

[4] J. Y. Wu, S. Q. Liu, P. W. S. Heng, Y.-Y. Yang, Evaluating proteins release from, and their interactions with, thermosensitive poly (N-isopropylacrylamide) hydrogels, J. Control. Release 102 (2005) 361–372.

[5] A. Skirtach, A. Javier, O. Kreft, K. Kohler, A. Alberola, H. Mohwald, W. Parak, G. Sukhorukov, Laser-induced release of encapsulated materials inside living cells, Angew. Chem. Int. Ed. 45 (2006) 4612–4617.

[6] T. Kyriakides, C. Cheung, N. Murthy, P. Bornstein, P. Stayton, A. S. Hoffman, pH-sensitive polymers that enhance intracellular drug delivery *in vivo*, J. Control. Release 78 (2002) 295–303.

[7] K. Ulbrich, V. Subr, Polymeric anticancer drugs with pH-controlled activation, Adv. Drug. Deliv. Rev. 56 (2004) 1023–1050.

[8] R. Duncan, Polymer conjugates as anticancer nanomedicines, Nat. Rev. Cancer 6 (2006) 688–701.

[9] T. Etrych, M. Jelinkova, B. Rihova, K. Ulbrich, New HPMA copolymers containing doxorubicin bound via pH-sensitive linkage: Synthesis and preliminary *in vitro* and *in vivo* biological properties, J. Control. Release 73 (2001) 89–102.

[10] M. C. Garnett, Targeted drug conjugates: Principles and progress, Adv. Drug. Deliv. Rev. 53 (2001) 171–216.

[11] R. J. Christie, D. W. Grainger, Design strategies to improve soluble macromolecular delivery constructs, Adv. Drug. Deliv. Rev. 55 (2003) 421–437.

[12] H.-S. Yoo, E. Lee, T. Park, Doxorubicin-conjugated biodegradable polymeric micelles having acid-cleavable linkages, Journal of Controlled Release 82 (2002) 17–27.

[13] S. Q. Liu, Y. W. Tong, Y.-Y. Yang, Incorporation and *in vitro* release of doxorubicin in thermally sensitive micelles made from poly(*N*-isopropylacrylamide-*co*-*N*,*N*-dimethylacrylamide)-β-poly(D,L-lactide -*co*-glycolide) with varying compositions, Biomaterials 26 (2005) 5064–5074.

[14] A. Potineni, D. M. Lynn, R. Langer, M. M. Amiji, Poly(ethylene oxide)-modified poly(β-amino ester) nanoparticles as a pH-sensitive biodegradable system for paclitaxel delivery, J. Control. Release 86 (2003) 223–234.

[15] M. Zignani, D. Drummond, O. Meyer, K. Hong, J.-C. Leroux, *In vitro* characterization of a novel polymeric-based pH-sensitive liposome system, Biochim. Biophys. Acta 1463 (2000) 383–394.

[16] S. Simoes, J. N. Moreira, C. Fonseca, N. Duzgunes, M. de Lima, On the formulation of pH-sensitive liposomes with long circulation times, Adv. Drug. Deliv. Rev. 56 (2004) 947–965.

[17] N. Murthy, J. Campbell, N. Fausto, A. Hoffman, S. Stayton, Bioinspired pH-responsive polymers for the intracellular delivery of biomolecular drugs, Bioconjug. Chem. 14 (2003) 412–419.

[18] M. Mahkam, M. Allahverdipoor, Controlled release of biomolecules from pH-sensitive network polymers prepared by radiation polymerization, J. Drug Target. 12 (2004) 151–156.

[19] I. S. Kim, I. J. Oh, Drug release from the enzyme-degradable and pH-sensitive hydrogel composed of glycidyl methacrylate dextran and poly(acrylic acid), Arch. Pharm. Res. 28 (2005) 983–987.

[20] H. C. Chiu, G. H. Hsiue, Y. P. Lee, L. W. Huang, Synthesis and characterization of pH-sensitive dextran hydrogels as a potential colon-specific drug delivery system, J. Biomater. Sci. Polym. Ed. 10 (1999) 591–608.

[21] M. A. Yessine, J. C. Leroux., Membrane-destabilizing polyanions: Interaction with lipid bilayers and endosomal escape of biomacromolecules, Adv. Drug. Deliv. Rev. 56 (2004) 999–1021.

[22] E. Lee, K. Na, Y. H. Bae, Polymeric micelle for tumor pH and folate-mediated targeting, J. Control. Release 91 (2003) 103–113.

[23] F. Kratz, U. Beyer, M. Schutte, Drug-polymer conjugates containing acid-cleavable bonds, Crit. Rev. Ther. Drug Carrier Syst. 16 (1999) 245–288.

[24] Y. Son, J.-S. Jang, Y. Cho, H. Chung, R.-W. Park, I. Kwon, I.-S. Kim, J. Park, S. Seo, C. Park, S. Jeong, Biodistribution and anti-tumor efficacy of doxorubicin loaded glycol-chitosan nanoaggregates by EPR effect, J. Control. Release 91 (2003) 135–145.

[25] J. C. Ramirez, M. Sanchez-Chaves, F. Arranz, Dextran functionalized by 4-nitrophenyl carbonate groups, Angew. Makromol. Chem. 225 (1995) 123–130.

[26] T. Etrych, P. Chytil, M. Jelinkova, B. Rihova, K. Ulbrich, Synthesis of HPMA copolymers containing doxorubicin bound via a hydrazone linkage. Effect of spacer on drug release and *in vitro* cytotoxicity, Macromol. Biosci. 2 (2002) 43–52.

[27] W. Lam, C. H. Leung, H. L. Chan, W. F. Fong, Toxicity and DNA binding of dextran-doxorubicin conjugates in multidrug-resistant KB-V1 cells: Optimization of dextran size, Anticancer Drugs 11 (2000) 377–384.

[28] C. A. Frederick, L. D. Williams, G. Ughetto, G. A. Vandermarel, J. H. Vanboom, A. Rich, A. H. J. Wang, Structural comparison of anticancer drug DNA complexes: Adriamycin and daunomycin, Biochemistry 29 (1990) 2538–2549.

[29] H.-S. Yoo, T. Park, Folate receptor targeted biodegradable polymeric doxorubicin micelles, Journal of Controlled Release 96 (2004) 273–283.

[30] K. Ulbrich, T. Etrych, M. Jelinkova, B. Rihova, HPMA copolymers with pH-controlled release of doxorubicin: *In vitro* cytotoxicity and *in vivo* antitumor activity, J. Control. Release 87 (2003) 33–47.

[31] I. Tannock, D. Rotin, Acid pH in tumors and its potential for therapeutic exploitation, Cancer Res. 49 (1989) 4373–4384.

Chapter 4 – Synthesis, Characterization and *In Vitro* Studies of a Temperature- and pH-Sensitive Polymer and its Use in Targeted Delivery of Paclitaxel to Hepatocytes

4.1 Introduction

Site-specific transport of drugs ensures that narrow therapeutic window drugs such as chemotherapeutic agents are localized at the target site. Site-specific release or activation of drugs after reaching the target site helps to ensure high therapeutic efficacy, and to maintain the mechanism of action of the free drug. The combination of site-specific delivery and release yields a drug delivery vehicle more effective than either one could be individually. Rihova *et al.* have conducted a significant amount of research on poly((N-2-hydroxypropyl)methacrylamide) (HPMA) conjugates for the delivery of chemotherapeutic agents. They have attached the pH-sensitive conjugate HPMA-hydrazone-doxorubicin to anti-thymocyte globulin to target T cell lymphoma EL4 cells. The *in vitro* toxicity of the targeted, pH-sensitive conjugate was comparable to that of free doxorubicin [1].

Drugs encapsulated in micelles, liposomes or particles are protected from degradation or prematured metabolism, and have longer plasma circulation times. If the release mechanism is stimuli-responsive, a therapeutic level of the drug can be sustained over days or even months [2]. There has been much research on folate targeted delivery since folate receptors are over-expressed on various forms of cancers [3]. Yoo *et al.* have formed biodegradable micelles from block copolymers of poly(D,L-lactic-*co*-glycolic acid) (PLGA) and poly(ethylene glycol) (PEG) [4]. Doxorubicin was attached to the PLGA end, and folate was attached to the PEG end of the block copolymers. Micelles were formed by utilizing the hydrophobic PLGA segment and free doxorubicin was encapsulated. The folate targeted micelles reduced the lethal median concentration in cell culture studies by 33%. *In vivo* studies have shown increased accumulation of doxorubicin in tumors due to folate receptor targeting, and significant regression of tumor size [4]. Lee *et al.* have synthesized folate targeted micelles that are fine-tuned to release at a pH between 6.6 and 7.2. They used poly(L-histidine) and poly(lactic acid)-PEG block copolymers to encapsulate doxorubicin. The L-histidine component was thought to aid in endosomal escape by fusing with the intracellular membranes [5]. Release studies and *in vitro* experiments in a

controlled pH environment showed rapid release in a narrow pH range and a corresponding increase in cytotoxicity that was comparable to free doxorubicin [5].

Poly(*N*-isopropylacrylamide) (NIPAAm) is a well-known temperature-sensitive polymer that is soluble in water below its lower critical solution temperature (LCST) of 32°C, but becomes hydrophobic and aggregates above that temperature. Though there is concern about the carcinogenic effects of acrylamides in food, research on polyacrylamides has shown them to be biocompatible [6, 7]. Much research has been conducted on the use of thermosensitive NIPAAm polymers and copolymers for drug delivery. Prednisone acetate, an anti-inflammatory drug, has been encapsulated in micelles formed from copolymers of NIPAAm and 10-undecenoic acid (UA). The micelles were found to be pH-responsive only at temperatures above 31°C, which was the LCST of the block copolymer [8]. Yang and co-workers have used poly(NIPAAm-*co*-dimethyl acrylamide) and PLGA block copolymers to encapsulate paclitaxel in micelles. The drug was released above the copolymer's LCST of 39.5°C, and the micelles had an LC_{50} value that was an order of magnitude lower than that of free paclitaxel [9]. Such a system could be utilized in drug delivery by local heating at the target site. They have also synthesized a copolymer of NIPAAm, *N*,*N*-dimethyl acrylamide (DMAAm) and UA with an LCST of ~ 37°C, and encapsulates doxorubicin in micelles [10].

We have adapted the last mentioned system, which was originally developed by Soppimath *et al.* [11]. An ideal drug delivery system would be thermo-responsive at low pH only. At physiological temperature and pH, the LCST would be greater than 37°C, but at a lower pH it would be lower than 37°C. It is well established in the literature that conjugating a polymer of NIPAAm to another hydrophilic polymer or moiety increases the phase transition temperature by increasing the hydrophilicity. On the other hand, attaching a hydrophobic moiety would have the opposite effect and decrease the LCST [12]. DMAAm was included in the polymer to increase the LCST of NIPAAm above 32°C. The UA served two functions. It contained a long hydrocarbon chain that allowed the polymer to form vesicles in the aqueous medium. In addition, the carboxylic acid group would trigger the temperature sensitivity of the NIPAAm. It would be protonated at a low pH, and the neutral charge would make it more hydrophobic. This would lower the LCST of NIPAAm, and the polymer would become

hydrophobic. We targeted these copolymers to hepatocytes by expressing galactose on the polymer.

The hydrophobic core of our particles was used to encapsulate paclitaxel – a hydrophobic chemotherapeutic agent of the taxane family that is often used for cancers that do not respond well to other conventional drugs. Paclitaxel is administered intravenously in Cremophor EL (a mixture of polyoxyethylated castor oil and dehydrated ethanol) to treat lung, ovarian, breast, head and neck cancers, and advanced forms of Kaposi's sarcoma [13, 14]. It has a plasma half-life as low as 6 min, and is cleared through hepatic metabolism, biliary excretion, fecal elimination and tissue binding. Its terminal half-life from organs and tissues varies from 14 to 50 h [14]. Paclitaxel acts by interfering with the assembly of the mitotic spindle, and preventing the chromosomes from segregating during cell division. This inhibits cell proliferation and leads to cell death. In cell culture studies, cell death has been found to occur via both apoptotic and non-apoptotic mechanisms [13, 15]. The side-effects for this drug include hypersensitivity, neutropenia, neurotoxicity, disturbance of cardiac rhythm and mucositis [14]. Delivery of paclitaxel is a challenge due to its extremely low solubility in aqueous medium. Encapsulating the drug in targeted micelles or particles with a hydrophilic shell would effectively increase its solubility and delivery to the target sites.

The goal for this study was to synthesize galactose-targeted copolymers of NIPAAm, DMAAm and UA with physical properties and thermo-responsiveness that would be appropriate for drug delivery. Paclitaxel would be encapsulated in polymeric particles, which would be examined for targeting and stimuli-responsive release in cell culture studies.

4.2 Experimental Methods

4.2.1 Materials

NIPAAm, DMAAm, UA, n-hexane, ammonium persulfate (APS), 2-aminoethanethiol hydrochloride (AET·HCl), sodium hydroxide (NaOH), sodium chloride (NaCl), dimethyl formamide (DMF), pyrene, D-lactose, sodium cyanoborohydride ($NaBH_3CN$), boric acid, *Ricinus communis* Agglutinin (RCA_{120}), HPLC grade tetrahydrofuran (THF), phenol, sulfuric acid, bovine serum albumin (BSA) and FITC-conjugated monoclonal anti-β-tubulin antibody

were obtained from Sigma-Aldrich. NIPAAm was further purified by crystallization in n-hexane. DMAAm and UA were also further purified by reduced pressure distillation. All other chemicals were used as received from Sigma-Aldrich. Acetone, methanol, chloroform, 10× phosphate buffered saline (PBS), and Dulbecco's 1× sterile PBS containing calcium and magnesium for cell culture studies were obtained from VWR. The cell lines BNL CL.2 and NIH/3T3, Dulbecco's Minimum Essential Medium (DMEM), fetal bovine serum (FBS), 10,000 I.U./mL of Penicillin-10,000 μg/mL of Streptomycin, 0.25% of Trypsin/0.53 mM of ethylenediaminetetraacetic acid (EDTA), and the MTT Cell Proliferation Assay kit were obtained from American Type Culture Collection (ATCC). Propidium iodide (PI) and RNase A were obtained from Invitrogen. Paclitaxel was purchased from LC Laboratories.

4.2.2 Polymerization of N-Isopropylacrylamide, N,N-Dimethylacrylamide and 10-Undecenoic Acid

Fig. 4.1 shows a schematic of the polymerization of NIPAAm, DMAAm and UA. NIPAAm and DMAAm (0.2 g) were dissolved in deionized (DI) water with the NIPAAm:DMAAm molar ratio varied from 1 to 5. UA (0.1 to 0.5× molar ratio to DMAAm) was dissolved in 1 M of NaOH solution and added to the solution of NIPAAm and DMAAm with total monomer concentrations ranging from 0.1 to 0.4 mg/mL. The pH was adjusted to between 6.5 and 6.8 by addition of dilute HCl. The mixture was then purged with nitrogen for 30 min. Solutions of APS (0.00125 to 0.00625× molar ratio to monomers) and AET·HCl (2× molar ratio to APS) were added dropwise sequentially, and the reaction proceeded under a nitrogen seal for 12–96 h. The polymer was precipitated by adding NaCl solution (10 M), subsequently dissolved in ethanol, and purified by dialysis in a membrane with a molecular weight cut-off (MWCO) of 2000 against DI water. The water was changed twice a day over 5 days, and the polymers were recovered by lyophilization.

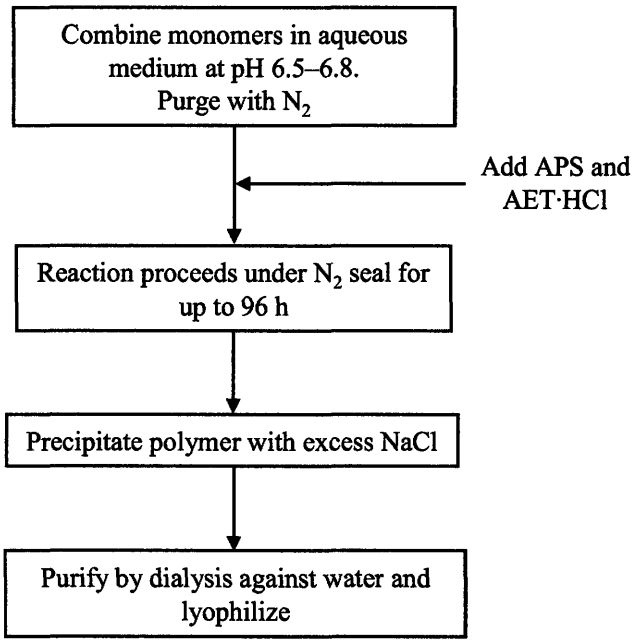

Fig. 4.1. Schematic of synthesis of poly(NIPAAm-*co*-DMAAm-*co*-UA) [11].

4.2.3 Characterization of Polymer

4.2.3.1 Composition and Physical Properties

Photoacoustic Fourier-transform infrared (PA-FTIR) spectroscopy (Bio-Rad FTS60A) and ^{1}H nuclear magnetic resonance (NMR) spectroscopy (Avance DMX 400 MHz, Bruker) were used to confirm the presence of all three monomers in the polymer. NMR was also used to determine the ratio of NIPAAm to DMAAm in the polymer. The content of UA was estimated from the number of carboxylic acid groups determined by acid-base titration. The polymer was dissolved in 0.01 M of NaOH at a concentration of 1 mg/mL. The solution was back-titrated with 0.01 M of HCl, and the moles of carboxylic acid groups on the polymer were determined from the volume of titration.

The molecular weights (MW's) and polydispersity indices (PI's) were determined by gel permeation chromatography (GPC) (Waters 2695D Separations Module, mobile phase of THF at 1.0 mL/min, relative to polystyrene standards) [11]. Differential scanning calorimetry (DSC) (TA Instruments DSC Q100) was used to determine the glass transition temperature (T_g) of the polymers. A sample of 10–15 mg was loaded in a standard pan. The temperature was initially

decreased to 0°C, and then raised to 200°C at a ramp of 20°C/min. The decomposition temperature (T_{dec}) was determined using thermal gravimetric analysis (TGA) (PerkinElmer Pyris 1 TGA). A sample of 5–10 mg was taken to a temperature of 700°C at a ramp of 10°C/min.

4.2.3.2 Lower Critical Solution Temperature

The LCST was determined by measuring the optical transmittance of a solution of blank particles as a function of temperature. A solvent extraction/evaporation method was used to form the particles. 10 mg of the polymer was dissolved in 1 mL of acetone, added drop-wise to 5 mL of DI water, and sonicated for 15 min. The acetone was allowed to evaporate by stirring for 6 h, and the particles were dialyzed in a 50,000 MWCO membrane against DI water. The particles were recovered by lyophilization, and redispersed in 1× PBS at a pH of 7.4 or 5.0 at a concentration of 5 mg/mL. Transmittance measurements were obtained with an ultraviolet-visible (UV-Vis) microplate reader (VersaMax, Molecular Devices) at 450 and 650 nm as a function of temperature between 25°C and 45°C. The particle solutions were allowed to stabilize at each temperature for 5 min before the measurement. The LCST was defined as the temperature at the inflection point of the transmittance curve [16].

4.2.3.3 Critical Aggregation Concentration

A fluorescent probe method was used to determine the critical aggregation concentration (CAC) of the polymers [17]. The probe, pyrene was dissolved in methanol at a concentration of 1 mM, and was subsequently diluted in water near its saturation of 6×10^{-7} M. Polymer solutions of concentrations ranging from 0.001 to 50 mg/mL were prepared in the pyrene/methanol/water solution. The solutions containing polymer were allowed to stabilize overnight on an orbital shaker at 100 rpm. Excitation spectra were measured on a Tecan Safire^2 from 300 to 360 nm with emission at 390 nm. The ratios of the emission at 344 nm to that at 335 nm were plotted against the concentration of the polymer. The CAC was defined as the concentration at the intersection between the two straight lines that defined the curve.

4.2.4 Incorporation of Galactose onto the Polymer Chain

The polymer (200 mg) was dissolved in a sodium borate buffer (200 mM, pH 9.0) at 1 mg/mL. D-lactose (up to 100× molar ratio to the amine groups on the polymer) and a 5-fold

excess of $NaBH_3CN$ relative to lactose were added to the polymer; the reaction was allowed to proceed for up to 48 h at 30°C [18]. The amount of lactose conjugated was determined using the phenol-sulfuric acid assay [19]. Lactose-conjugated polymer (2 mg/mL in DI water (1 mL)) was added to 1 mL of 5% phenol in DI water, followed by 5 mL of sulfuric acid. The absorbance was measured at 490 nm. The standard curve was determined using galactose.

4.2.5 Formation and Characterization of Paclitaxel-Loaded Particles

4.2.5.1 Synthesis of Paclitaxel-Loaded Particles

Paclitaxel-loaded particles were formed from a similar method as the synthesis of blank particles. Paclitaxel was added to the polymer/acetone solution with an initial paclitaxel:polymer weight ratio of 0.2 to 1.0. The excess paclitaxel that was not encapsulated by polymer was removed after dialysis by centrifugation at 3000 rpm for 1 min. The particles were recovered by decanting and lyophilizing the supernatant.

4.2.5.2 Characterization of Paclitaxel-Loaded Particles

The presence of paclitaxel in the particles was confirmed by ^1H NMR spectroscopy in D_2O and $CDCl_3$. The amount of paclitaxel loaded was measured by dissolving the particles in a 1:1 volume mixture of methanol and DMF, and measuring the absorbance at 261 nm. Drug loading was defined as the mass of paclitaxel loaded in the particles divided by the total mass of particles. The loading efficiency was defined as the mass of paclitaxel loaded in the particles divided by the mass of paclitaxel introduced during synthesis. Transmission electron microscopy (TEM) was conducted on a FEI Tecnai G^2 F20 electron microscope (200 kV) to examine the size and shape of the particles. Particle size was determined by sizing ~ 100 particles from each sample. The availability of galactose residues on the particle surface was investigated using a multivalent galactose-binding lectin RCA_{120}. The turbidity of a solution of 100 μg/mL of RCA_{120} and 100 μg/mL of particles was measured at 450 and 650 nm before and after the addition of 50 μL of 20 mg/mL of galactose [18]. The crystallinity of the particles was investigated using X-ray diffraction (XRD) (PANalytical X'Pert PRO).

4.2.5.3 Release of Paclitaxel

Paclitaxel-loaded particles were suspended in pH 5.0 or 7.4 buffer with an initial paclitaxel loading of 40 μg/mL. The particles were incubated at 37°C on an orbital shaker at 150 rpm. At each time point, the released paclitaxel was isolated by centrifuging the mixture at 3000 rpm for 1 min, and decanting the release buffer containing the particles. The paclitaxel was subsequently extracted with chloroform, which was evaporated, redissolved in a 1:1 volume mixture of methanol and DMF, and quantified by measuring the absorbance at 261 nm.

4.2.6 In Vitro Efficacy of Paclitaxel-Loaded Particles

The BNL CL.2 (mouse hepatocyte) and NIH/3T3 (mouse fibroblast) cell lines were cultured in DMEM supplemented with 10% FBS and 1% Penicillin-Streptomycin at 37°C in 5% of CO_2.

For cytotoxicity studies, cells were plated (n = 6) at 100/mm^2 in 96-well plates, and allowed to adhere for 10–14 h. The medium was then replaced with complete medium containing paclitaxel or paclitaxel-loaded particles at various concentrations, and incubated for 24 h. At the end of the experiment, the cell layer was gently washed three times with cold PBS and 100 μL of fresh medium. 10 μL of the MTT reagent (3-(4,5-dimethylthiazol-2-yl)-2,5-diphenyltetrazolium bromide) were then added, and the plate was incubated for 1 or 2 h. 100 μL of sodium dodecyl sulfate were then added, and the cells were incubated for another 10 or 12 h. The absorbance was measured at 570 nm. The standard curves for viable cell numbers were obtained by performing the MTT assay on a known cell concentration curve, measured by hemacytometer.

The time required for uptake of particles was determined by a timed cytotoxicity study. Cells were prepared as above, and incubated with paclitaxel or paclitaxel-loaded particles at a nominal paclitaxel concentration of 0.1 μM up to specific time-points. The medium was then replaced with drug-free complete medium, and the cell viability was determined using the MTT assay after a total incubation period of 24 h.

For microscopy studies, cells were plated at 100/mm^2 in chambered slides (Lab-Tek Chambered Coverglasses, NUNC) and allowed to adhere for 10–14 h. The medium was then replaced with complete medium containing paclitaxel or paclitaxel-loaded particles at a normalized concentration of 0.1 μM, and incubated for 24 h. The cell layer was gently washed three times with cold PBS, and fixed in cold methanol for 20 min at -20°C. The cells were subsequently washed three times with cold acetone and rehydrated in PBS for 30 min. They were incubated at room temperature for 1 h in 38 μg/mL of FITC-conjugated anti-β-tubulin antibody. The nuclei were counterstained with 1 μg/mL of PI for 30 min at room temperature. The cell layer was washed with PBS to remove excess markers. Confocal images were obtained on an Olympus IX71.

The DNA content of treated cells was analyzed by flow cytometry. Cells were treated with paclitaxel or paclitaxel-loaded particles for 24 h at a nominal paclitaxel concentration of 0.1 μM. The cells were then harvested, washed twice with calcium- and magnesium-free PBS, redispersed in PBS, and fixed in cold ethanol overnight at 4°C. After fixation, the cells were washed twice with PBS containing 1% of BSA, and redispersed in the PBS solution. PI and RNase were then added at final concentrations of 50 μg/mL and 1 mg/mL, respectively. The cells were incubated at 37°C for 30 min, and analyzed by flow cytometry (BD FACSCalibur).

4.3 Results and Discussions

4.3.1 Characterization of Poly(NIPAAm-co-DMAAm-co-UA)

4.3.1.1 Composition and Physical Properties

A schematic of the polymerization of NIPAAm, DMAAm and UA is illustrated in Fig. 4.2. The polymerization was confirmed by the absence of the monomer vinylic protons between 5.4 to 6.6 ppm in the ^{1}H NMR spectrum of poly(NIPAAm-*co*-DMAAm-*co*-UA) (Fig. 4.3(a)). The signals at 1.2 and 2.9 were attributed to the methyl protons of NIPAAm and DMAAm, respectively, and the integrated areas of these peaks were used to determine the molar ratio of the two monomers on the polymer. The peak at 4.0 ppm was due to the *iso*-propyl proton on NIPAAm, and the broad peaks between 1.5 to 2.6 ppm were from the methylene groups on NIPAAm and DMAAm. The PA-FTIR spectrum (Fig. 4.3(b)) exhibited peaks at ~ 1540, 1645

and 1711 cm^{-1}, which corresponded to the DMAAm amine (C–N), NIPAAm carbonyl (C=O) and UA carbonyl groups, respectively [10]. The peaks above 3000 cm^{-1} were due to the amine groups (N–H).

The compositions of the polymers used in *in vitro* studies are given in Table 4.1. The relative content of NIPAAm to DMAAm was easily controlled by the precursor ratio of the two monomers. The UA content in the final polymer could be adjusted by changing the molar ratios of APS:monomers and NIPAAm:DMAAm, and the total monomers concentration. The T_g of the polymers ranged from ~ 110°C to 140°C, and the decomposition temperatures were ~ 285–306°C (Table 4.1).

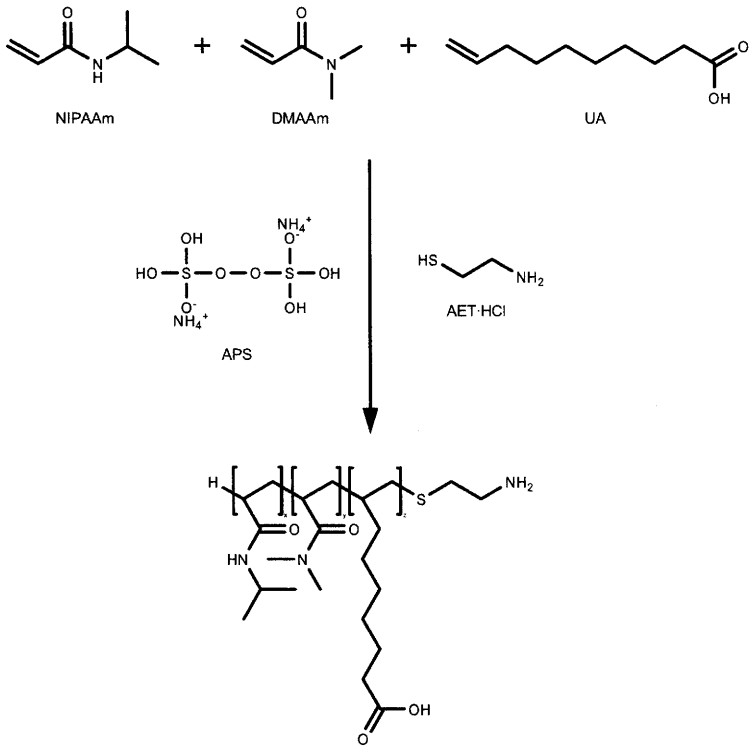

Fig. 4.2. Synthesis scheme of poly(NIPAAm-*co*-DMAAm-*co*-UA).

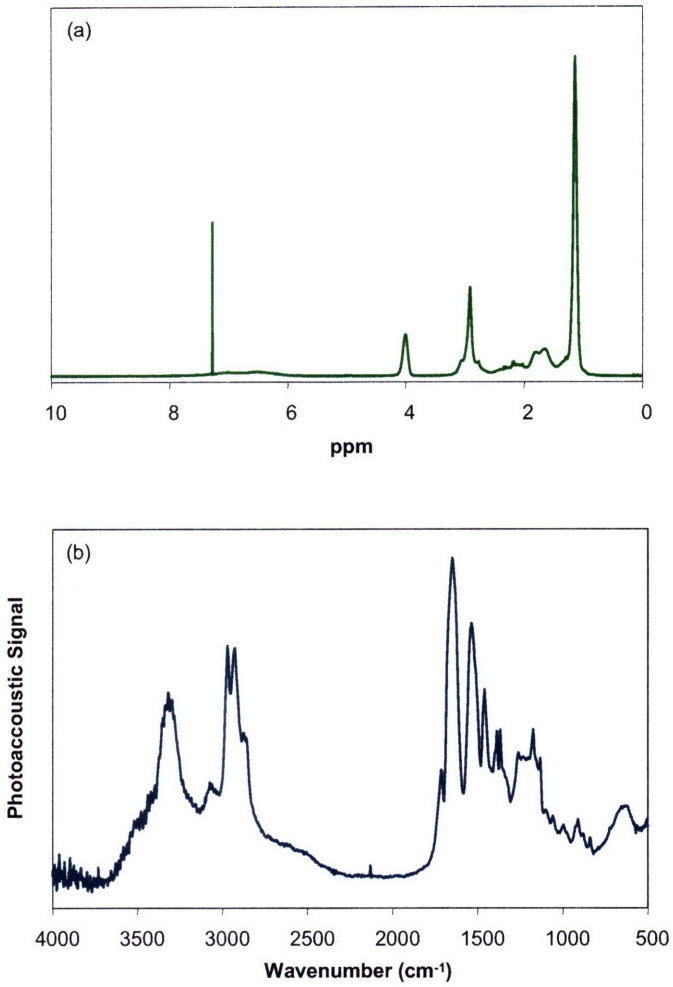

Fig. 4.3. (a) ^{1}H NMR and (b) PA-FTIR spectra of poly(NIPAAm-*co*-DMAAm-*co*-UA).

Table 4.1. Composition and physical properties of polymers used in *in vitro* studies.

NIPAAm (mol/mol)	DMAAm (mol/mol)	UA (mol/mol)	MW (kDa)		T_g (°C)	T_{dec} (°C)
			M_W	PI		
30	10	2	4.8	1.7	135	285
41	14	2	6.5	1.7	127	291
53	17	6	8.8	1.7	113	298
58	20	5	9.6	1.8	123	306
77	26	3	11.9	1.3	130	296

The MW's of the polymers ranged from 3 to 13 kDa. There was a large increase in MW when the reaction time was increased from 12 to 24 h, followed by a plateau. A period of at least 24 h was used to ensure the completion of polymerization. The MW could be increased by increasing the monomer concentration or decreasing the APS:monomer molar ratio (Fig. 4.4). Bokias *et al.* have also found that the MW's of poly(NIPAAm) and poly(acrylic acid) were proportional to the concentration of the monomer solution, and inversely proportional to the concentration of AET·HCl [20].

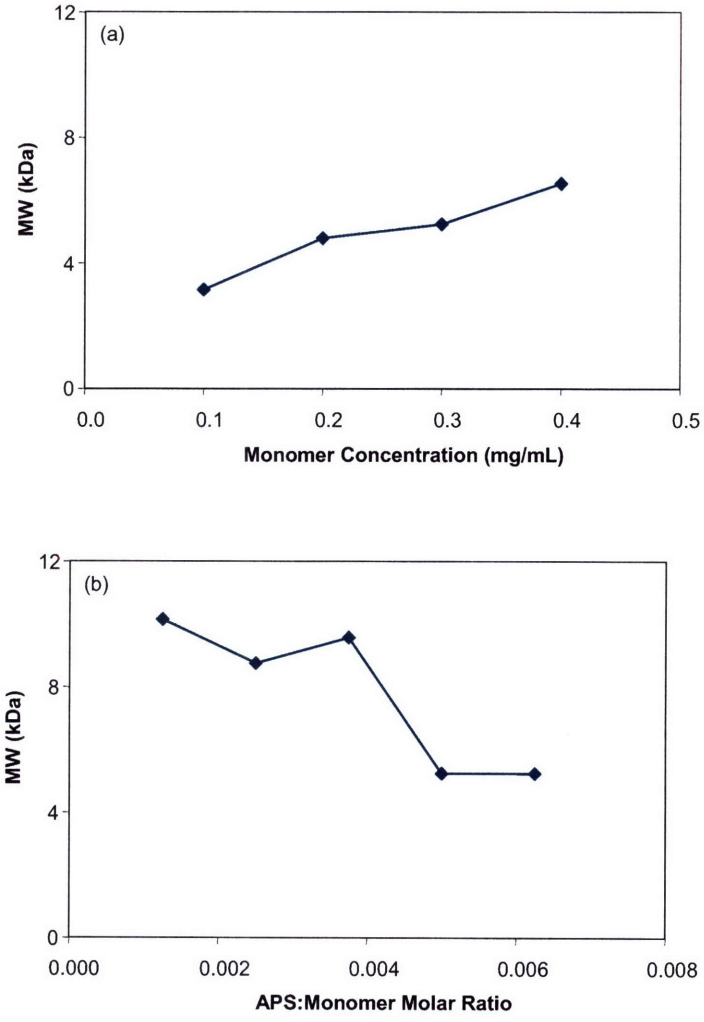

Fig. 4.4. MW's of polymers synthesized with varying (a) monomer concentrations and (b) APS:monomer molar ratios.

4.3.1.2 Effect of Polymer Composition on LCST

As the content of DMAAm in the copolymer was increased, the LCST also increased due to the increasing hydrophilicity of the polymer (Fig. 4.5(a)). At a pH of 7.4, the UA on the polymer was deprotonated, and had little effect on the LCST (Fig. 4.5(b)). However, at pH 5.0, the carboxyl groups were protonated, making the UA hydrocarbon chain more hydrophobic. This imparted sufficient hydrophobicity to the polymer, so that the LCST was lowered and the polymer was precipitated. As the content of UA was increased from 20 to 50 mg/g polymer, the difference in LCST at the two pH's also increased. Polymers with a NIPAAm:DMAAm ratio of ≥ 3 and a UA content of ≥ 50 mg/g met the LCST criteria for a drug delivery vehicle.

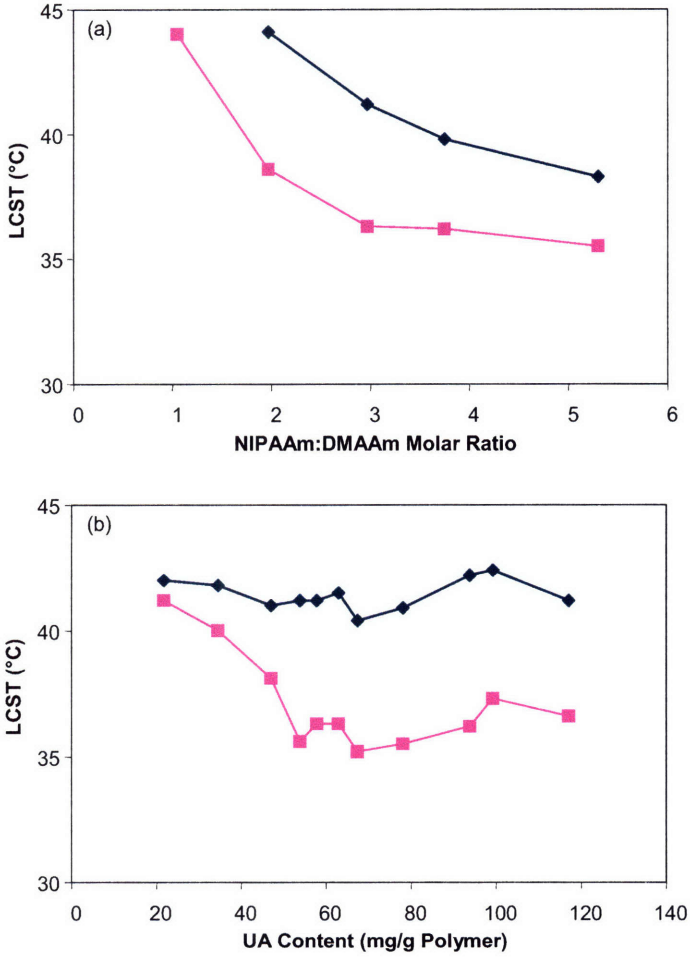

Fig. 4.5. LCST values of poly(NIPAAm-*co*-DMAAm-*co*-UA) with varying (a) NIPAAm:DMAAm molar ratios (UA content $\geq$ 50 mg/g polymer) and (b) UA contents (NIPAAm:DMAAm = 3) at a pH of (■) 5.0 and (◆) 7.4.

4.3.1.3 Effect of Polymer Composition on Critical Aggregation Concentration

The fluorescence of pyrene was quenched as it partitioned from an organic to an aqueous phase. This was quantified from the excitation spectrum by measuring the ratio of the emission (I_λ) at 344 nm to that at 335 nm. As the polymer concentration increased, pyrene was partitioned into the organic cores formed by aggregation of the hydrophobic UA groups, and the I_{344}/I_{335} ratio increased exponentially. The polymer concentration at the intersection of the two lines that defined the curve was taken as the CAC.

It was shown previously that for the range of LCST required for drug delivery, the polymers of interest must have a NIPAAm:DMAAm ratio of ≥ 3. The CAC of the polymers fitting that criteria were found to be independent of the NIPAAm:DMAAm ratio. As expected, the CAC decreased with increasing UA content (Fig. 4.6). The CAC values for the polymer were found to be significantly larger than other polymers used in drug delivery, implying that a higher loading of polymer would be necessary to form micelles or particles. However, a higher CAC value would improve particle stability and increase the maximum drug loading that could be achieved for a particular system [21]. The LCST and CAC values of the polymers chosen for *in vitro* studies are given in Table 4.2.

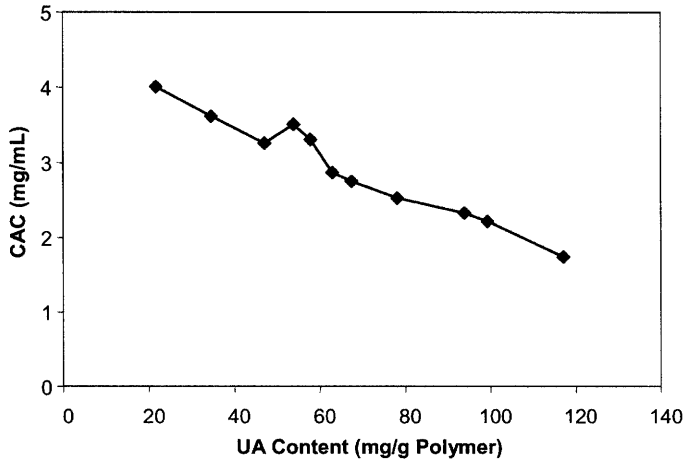

Fig. 4.6. CAC values of poly(NIPAAm-*co*-DMAAm-*co*-UA) with varying UA contents.

Table 4.2. LCST, CAC and galactose substitution of polymers used in *in vitro* studies.

Polymer MW (kDa)	LCST (°C)		CAC (mg/mL)	Galactose Substitution (mol/mol)
	pH 7.4	pH 5		
4.8	41	35	2.6	0.69
6.5	42	36	2.9	0.73
8.8	41	37	1.7	0.66
9.6	41	36	2.5	0.70
11.9	42	33	3.2	0.74

4.3.1.4 Characterization of Galactose-Conjugated Polymer

The polymers synthesized have an amine end-group due to the chain transfer agent, AET·HCl. This amine group was employed in a reaction with lactose to express galactose on each polymer chain. Lactose is a disaccharide of D-glucose and β-D-galactose with a β1-4 glycosidic link. Galactose is a non-reducing locked ring, whereas glucose is a hemiacetal, which can react with the amine groups on the polymer. The degree of galactose substitution was optimized with a lactose:polymer molar ratio of 10 and a reaction time of 48 h (Fig. 4.7). The galactose substitutions on the polymers used in this study are given in Table 4.2. The degree of expression of galactose on the particles was controlled by adjusting the ratio of galactose-substituted polymer used during particle synthesis. The particles were identified according to the percentage of galactose-substituted polymer used during synthesis (i.e. 0, 50, 75 or 100%).

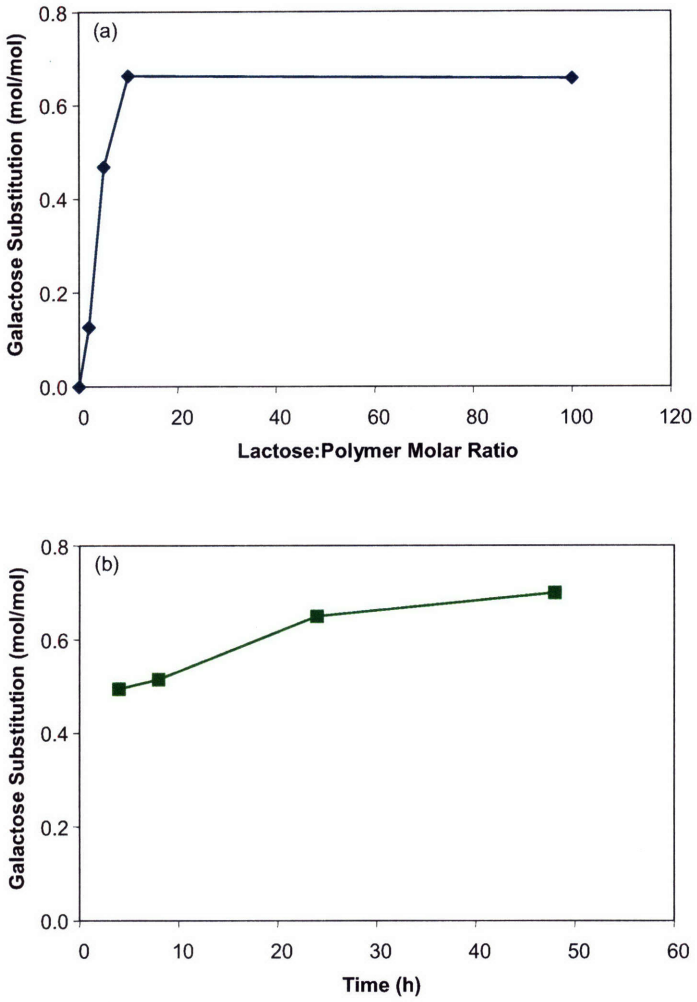

Fig. 4.7. Degrees of galactose substitution with varying (a) lactose:polymer molar ratios (reaction time = 48 h), and (b) reaction times (lactose:polymer molar ratio = 10).

4.3.2 Characterization of Paclitaxel-Loaded Particles

4.3.2.1 Encapsulation of Paclitaxel

NMR spectroscopy was used to investigate the structure of the paclitaxel-loaded particles (Fig. 4.8). In D_2O, the particles remained intact, and only the peaks due to the hydrophilic segments of the polymer were visible. $CDCl_3$ dissolved the particles and paclitaxel, and the peaks due to both the polymer and the hydrophobic paclitaxel were visible. This confirmed that paclitaxel had been encapsulated in the polymer particles.

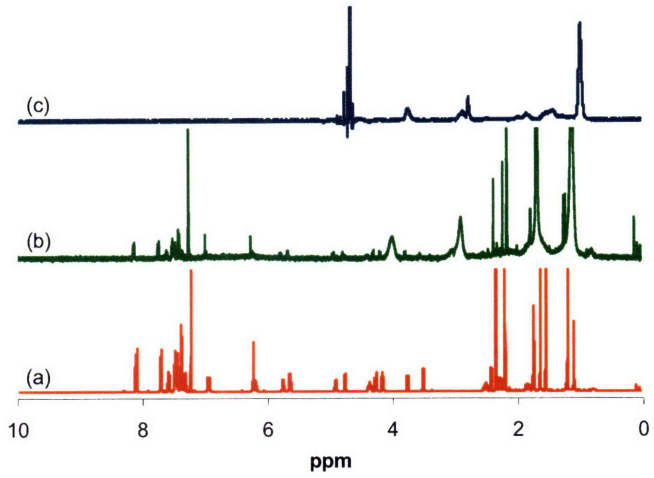

Fig. 4.8. ^{1}H NMR spectra of (a) paclitaxel in $CDCl_3$, (b) paclitaxel-loaded particles in $CDCl_3$, and (c) paclitaxel-loaded particles in D_2O.

Sonication, paclitaxel:polymer mass ratio, and acetone:water volume ratio were found to be important in determining the final paclitaxel loading in the particles. Particles that were not sonicated had a loading that was over 50% lower than those that were sonicated during synthesis. At a MW of 11.9 kDa, the loading increased from 10% to 25% with sonication. There was a slight increase in loading with the polymer MW.

Fig. 4.9(a) illustrates that the paclitaxel loading approached a plateau at a paclitaxel:polymer mass ratio of ~ 0.8. The efficiency of paclitaxel loading also increased and reached a maximum of 49% at a paclitaxel:polymer mass ratio of 0.8. The acetone:water volume ratio represented the speed of organic phase removal, and was a measure of the time for interaction between the drug and the hydrophobic elements of the polymer while in the organic phase. At low ratios, there was fast acetone removal, and less time to interact and structure the particles. The loading initially increased as the acetone:water volume ratio was increased. However, as the time of interaction was increased further, paclitaxel might partition with the acetone during the dialysis step, and precipitate out of solution leading to decreased loading. The paclitaxel loading efficiency reached a maximum of 83% at an acetone:water volume ratio of 0.1. At an acetone:water volume ratio of 0.2, the efficiency was 53%. For particle synthesis, a paclitaxel:polymer mass ratio of 0.8 and an acetone:water volume ratio of 0.2 were used to maximize the paclitaxel loading.

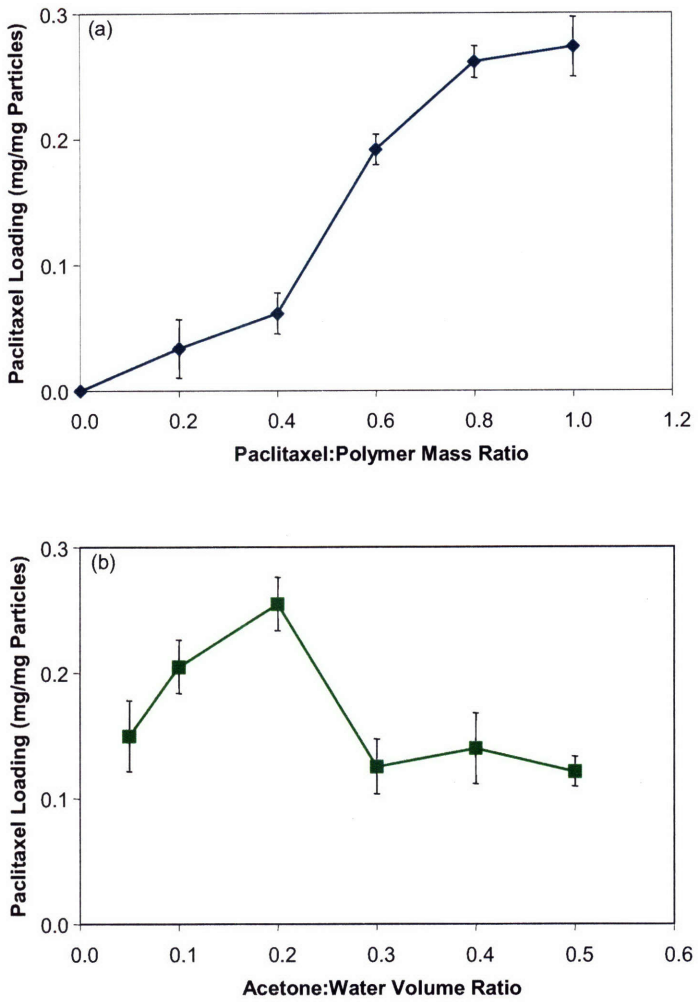

Fig. 4.9. Paclitaxel loadings of particles with varying (a) paclitaxel:polymer mass ratios (acetone:water volume ratio = 0.2), and (b) acetone:water volume ratios (paclitaxel:polymer mass ratio = 0.8). Polymer MW = 11.9 kDa. Values are mean ± standard deviation; n = 2.

4.3.2.2 Morphology of Paclitaxel-Loaded Particles

Transmission electron microscopy showed that the paclitaxel-loaded particles were cylindrical with high aspect ratios (Fig. 4.10). The diameters ranged from ~ 50 nm to 100 nm and the lengths varied from 200 nm to 1000 nm. There was an increase in particle length with increasing polymer MW (Table 4.3).

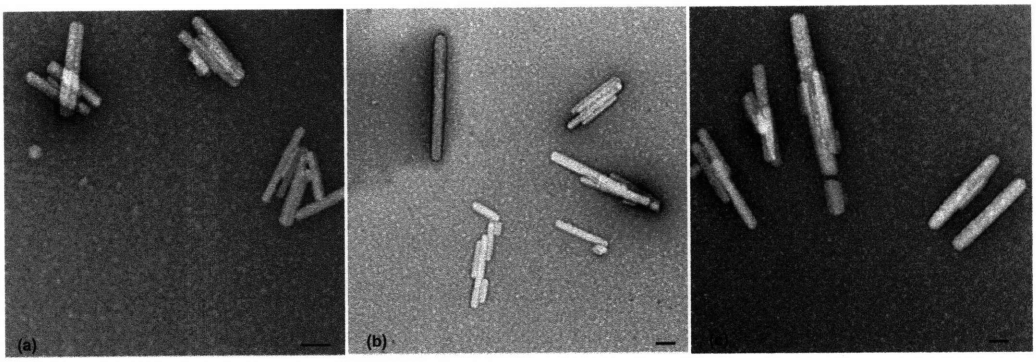

Fig. 4.10. TEM images of paclitaxel-loaded particles with MW's of (a) 4.8, (b) 6.5 and (c) 11.9 kDa. Scale bar = 100 nm.

Table 4.3. Length of paclitaxel-loaded particles.

MW (kDa)	Particle Length (nm)
4.8	363 ± 31
6.5	389 ± 90
8.8	528 ± 76
9.6	547 ± 84
11.9	556 ± 88

Most of the research on drug delivery vehicles has focused on the effects of particle size and surface chemistry of spherical particles. Until recently, there have not been many simple, reproducible methods to form non-spherical particles, and therefore, there has been little study on the effect of particle shape [2, 22, 23]. Euliss *et al.* [23] and Champion *et al.* [24] have recently developed methods that could be used to reproducibly synthesize large quantities of particles with shapes as varied as rods, cones, disks, pellets, vases and donuts. Particle morphology can affect the release and degradation properties, cellular interactions, flow properties and diffusion rate. Zero-order release has been achieved from hemispheres with release only from the flat face [25]. It has been shown recently that depending on the orientation during cellular interaction, one length scale might be more important than others. Additionally, the profile of the particle extending into flow conditions would determine the length of attachment [2]. Due to adhesive properties, non-spherical particles might be able to carry more

drugs into the cells than spherical particles [26]. Geng *et al.* have synthesized flexible worm micelles using PEG-poly(ethylethylene) or PEG-poly(caprolactone), and have shown that they remain in circulation in rodents up to one week, which was ten times longer than the spheres. The circulation time increased with the length of the micelles; under flow conditions, it was easier for cells to internalize shorter or spherical micelles [27]. More thorough research is required to investigate the advantages and disadvantages of using non-spherical particles in drug delivery. Recent work on nanotubes has shown great potential with regard to drug loading and release profiles from cylindrical particles [28].

The availability of galactose residues on the paclitaxel-loaded particles was investigated using a turbidity assay. RCA_{120} is a lectin from castor beans that has several galactose binding sites on each unit [29, 30]. If the lectins have binded galactose from different particles, it would cause particle aggregation, increasing the turbidity of the solution. Fig. 4.11 shows that the turbidity of a solution containing galactose-expressing particles decreased when an excess of free galactose was introduced into the mixture. This indicated that the galactose was available on the surface of the particles.

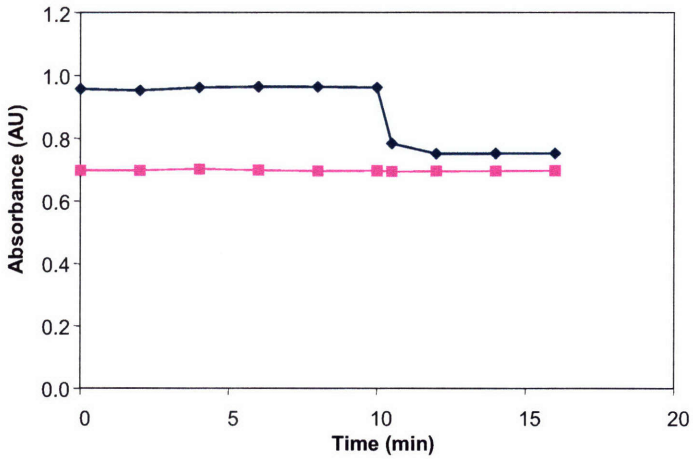

Fig. 4.11. Effect of galactose addition on the turbidity of paclitaxel-loaded particles with galactose substitutions of (■) 0% and (◆) 100%.

XRD was used to investigate the crystallinity of the encapsulated paclitaxel (Fig. 4.12). The polymers were amorphous and free paclitaxel was crystalline. XRD of the particles illustrated a lack of crystalline peaks, indicating that the paclitaxel solidified in an amorphous

form. The amorphous form has been reported to be slightly more soluble in aqueous media than the crystalline form [9]. It has been suggested that particles with higher drug loadings would be crystalline and would release drugs more slowly [31-33]. However, our particles with paclitaxel loadings as high as 39 wt% remained amorphous.

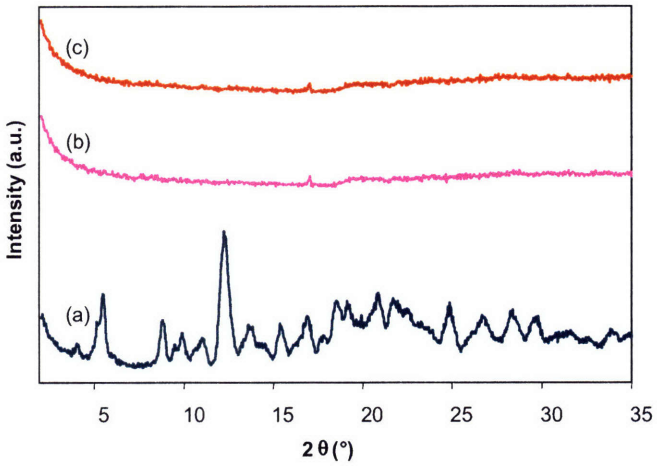

Fig. 4.12. XRD patterns of (a) paclitaxel, and paclitaxel-loaded particles with galactose substitutions of (b) 0% and (c) 100%.

4.3.2.3 pH-Sensitive Release of Paclitaxel

Paclitaxel-loaded particles were found to be stable in aqueous medium, and were not separated by centrifugation at the speeds and times used to isolate free paclitaxel. Release was measured at pH's of 7.4 and 5.0 at 37°C. Paclitaxel release at tumor or endosmal conditions was very rapid (Fig. 4.13), with at least 50% of the paclitaxel released within 1 h for all polymers examined. This was comparable to the rate of release from Cremophor EL [34]. As designed, our particles only released paclitaxel under the appropriate temperature and pH. After 24 h, the release at a pH of 7.4 was only ~ 20%, whereas ~ 100% release was achieved at a pH of 5.0. Since the particles did not aggregate and there was no burst release at a pH of 7.4, we could presume that there was little or no paclitaxel on the surface of the particles. Fig. 4.14 shows the release at a pH of 5.0 at 37°C for the different polymer MW's studied. Release from polymeric particles of lower MW was slightly faster. Since all our particles were amorphous, the faster release was attributed to the lower polymer MW and the smaller size of the resulting particles.

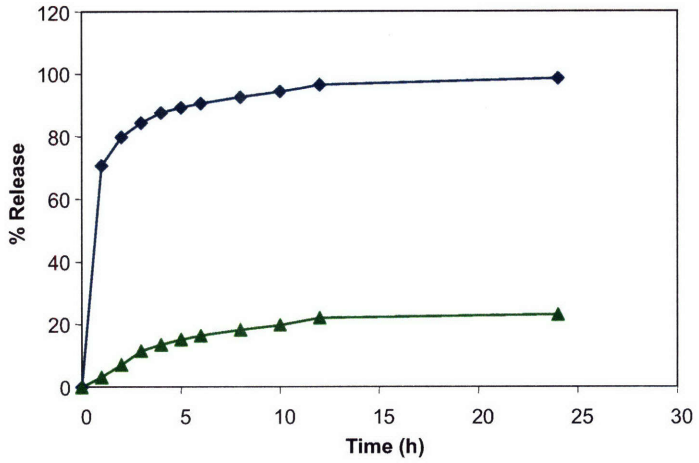

Fig. 4.13. Paclitaxel release at 37°C and pH's of (◆) 5.0 and (▲) 7.4 from particles synthesized from the 4.8 kDa polymer with 100% galactose substitution.

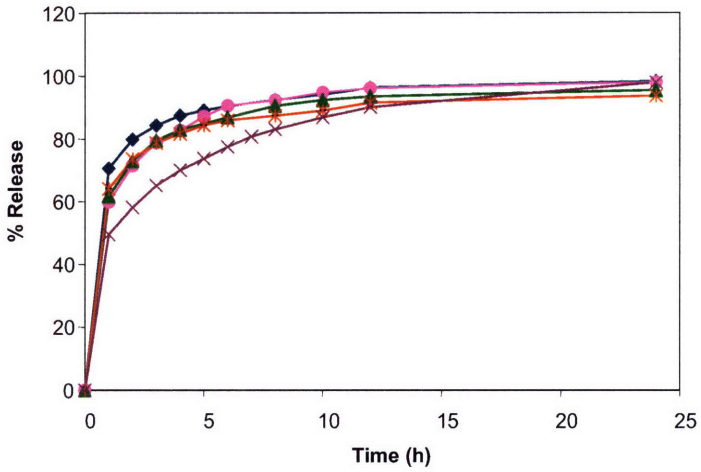

Fig. 4.14. Paclitaxel release at 37°C and a pH of 5.0 from particles synthesized from polymers with MW's of (◆) 4.8, (●) 6.5, (▲) 8.8, (✳) 9.6, and (×) 11.9 kDa.

4.3.3 In Vitro Studies

4.3.3.1 Cytotoxicity Studies on Target Cell Line

The MTT assay was used to measure the viability of cells treated with paclitaxel or paclitaxel-loaded particles due to its high throughput nature and ease of use. Polymer and blank particles had no effect on cell viability (data not shown). The dose response curves for cells treated with the 4.8 and 6.5 kDa polymer particles with varying galactose substitutions are shown

in Fig. 4.15. The lethal median concentrations for particles of various MW's and galactose substitutions for the BNL CL.2 cell line are shown in Table 4.4.

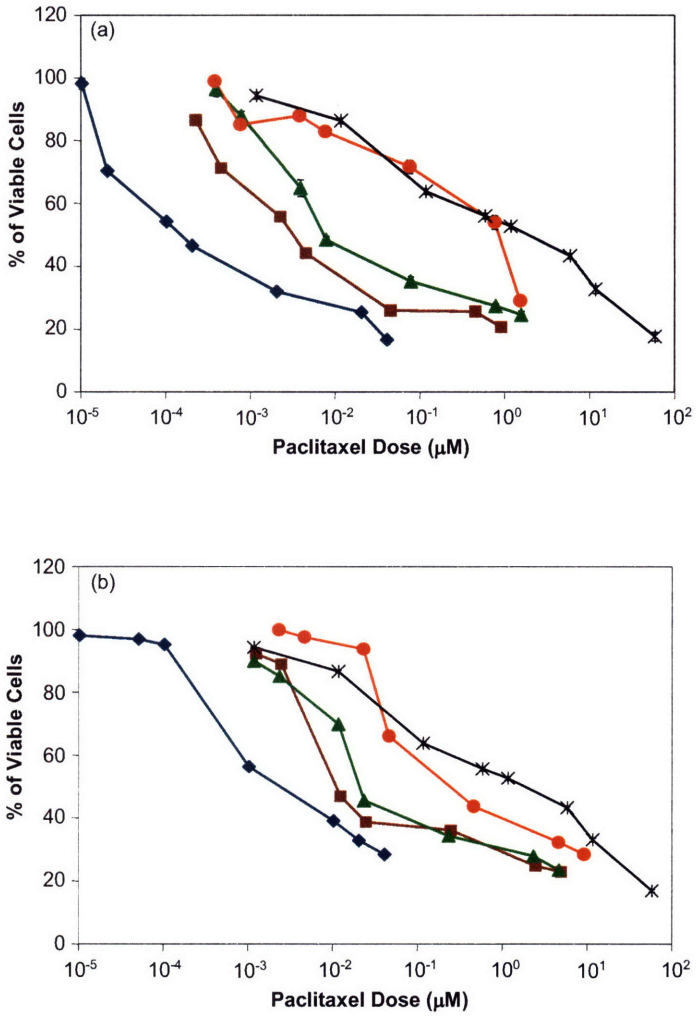

Fig. 4.15. Viability of BNL CL.2 cells incubated for 24 h with (∗) paclitaxel, and paclitaxel-loaded of (a) 4.8 kDa and (b) 6.5 kDa with galactose substitutions of (●) 0%, (▲) 50%, (■) 75% and (◆) 100%. Values are mean ± standard deviation; n = 3.

Table 4.4. LC_{50} (μM) of paclitaxel-loaded particles in BNL CL.2 cells.

% Galactose Substitution	MW (kDa)				
	4.8	6.5	8.8	9.6	11.9
0	4.7×10^{-1}	9.8×10^{-1}	9.0×10^{-1}	1.1×10^{0}	1.1×10^{0}
50	5.7×10^{-2}	1.3×10^{-1}	4.2×10^{-1}	6.7×10^{-1}	7.7×10^{-1}
75	1.0×10^{-2}	1.0×10^{-1}	1.0×10^{-1}	1.9×10^{-1}	2.7×10^{-1}
100	9.1×10^{-4}	7.0×10^{-3}	7.9×10^{-3}	7.5×10^{-3}	1.4×10^{-2}

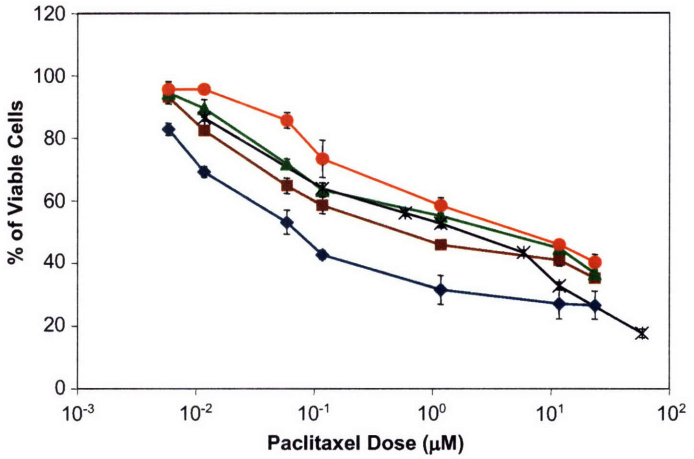

Fig. 4.16. Viability of BNL CL.2 cells incubated for 24 h with (✳) paclitaxel, and paclitaxel-loaded "control" or non-stimuli-responsive particles of 6.4 kDa with galactose substitutions of (●) 0%, (▲) 50%, (■) 75% and (◆) 100%. Values are mean ± standard deviation; n = 3.

The importance of stimuli-responsiveness was examined in cell culture experiments by measuring the cytotoxicity of "control" or non-stimuli-responsive particles that have an LCST of 44°C at a pH of 7.4, and an LCST of 39°C at a pH of 5.0. Ideally, these non-stimuli-responsive particles would not release in response to temperature and pH under cell culture conditions. However, in *in vitro* studies, they exhibited some cytotoxicity (Fig. 4.16), indicating that there was release of paclitaxel. There was some passive diffusion of paclitaxel out of the particles at 37°C at a pH of 7.4, as indicated in Fig. 4.13. The particles might also have been disrupted by proteins or various intracellular membranes, leading to the release of paclitaxel. The lethal median concentrations of these particles were 5.2, 3.1, 1.2 and 0.21 μM for 0, 50, 75 and 100%

galactose-substituted polymer, respectively. These values were one to two orders of magnitude higher than those for the stimuli-responsive particles at a similar molecular weight (6.5 kDa) (Table 4.4).

The cytotoxicity of the stimuli-responsive, non-targeted particles was slightly higher than that of free paclitaxel. The LC_{50} values of paclitaxel and paclitaxel-loaded stimuli-responsive particles (4.8 kDa, with 0% galactose substitution) for this cell line were 1.1 μM and 0.47 μM, respectively (Table 4.4). In contrast, the non-stimuli-responsive particles with 0% galactose substitution were less toxic than free paclitaxel. Since the polymer LCST was greater than 37°C, even if the non-stimuli-responsive particles were internalized by cells, only the portion of the drug that diffused out of the particles would become available to the cells.

As the galactose substitution was increased for the stimuli-responsive, targeted particles, there was a significant reduction in the LC_{50} at all MW's (Table 4.4). The same trend was observed for the non-stimuli-responsive particles, but to a lesser degree. At higher galactose substitutions, there would be greater particle uptake by the target cell line. For the stimuli-responsive particles, this led to a dramatic increase in toxicity since more particle uptake would result in greater drug release under the pH- and temperature-sensitive conditions. For the non-stimuli-responsive particles, this led to some increase in drug availability through diffusion from a larger number of particles uptaken, and thus a moderate increase in toxicity.

There was a small decrease in toxicity with increasing polymer MW due to the slightly slower release (Fig. 4.14). Since the effect of MW on the release was relatively minor, especially at 24 h, the effect in *in vitro* studies was not pronounced.

In clinical studies, the peak plasma concentration of paclitaxel ranged from 0.2 to 3.5 μM for a 24 h infusion [14, 35, 36]. Concentrations of 5×10^{-3} to 0.2 μM were found to cause mitotic arrest and cell death. In *in vitro* studies on the BNL CL.2 cell line, the lethal median concentration of the particles were in this clinically relevant range for particles formed with polymers that consisted of > 50% of galactose substitution (Table 4.4).

In a timed *in vitro* study, cytotoxicity was observed in cells incubated with paclitaxel-loaded particles for as short a period as 1 h (Fig. 4.17). This indicated that in spite of the large

size of the particles, uptake occurred very quickly. From the release studies (Fig. 4.13), we knew that the stimuli-responsive release would occur very rapidly after uptake by cells.

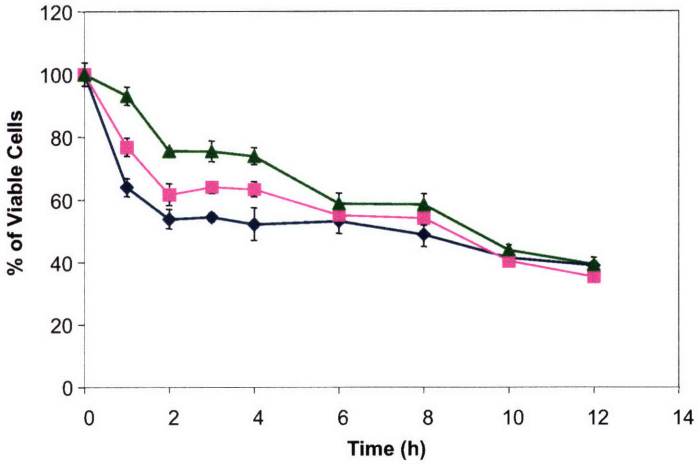

Fig. 4.17. Viability of BNL CL.2 cells incubated with (◆) paclitaxel, paclitaxel-loaded particles with 100% galactose substitutions and MW's of (■) 4.8 kDa and (▲) 11.9 kDa. Values are mean ± standard deviation.

BNL CL.2 cells treated with paclitaxel-loaded particles showed a rounded morphology in light microscopy images, as consistent with those treated with free paclitaxel [13]. The effect of paclitaxel or paclitaxel-loaded particles on the cytoskeleton was confirmed by staining microtubules with a fluorescent antibody (Fig. 4.18). DNA fragmentation was also confirmed with PI staining.

Paclitaxel is well-established as a mitotic inhibitor. The cell cycle analysis of cells treated with paclitaxel or paclitaxel-loaded particles confirmed G2/M phase arrest (see Table 4.5). Lin *et al.* also showed that cell viability in paclitaxel-treated hepatocytes was mediated through G2/M phase arrest and DNA fragmentation [13].

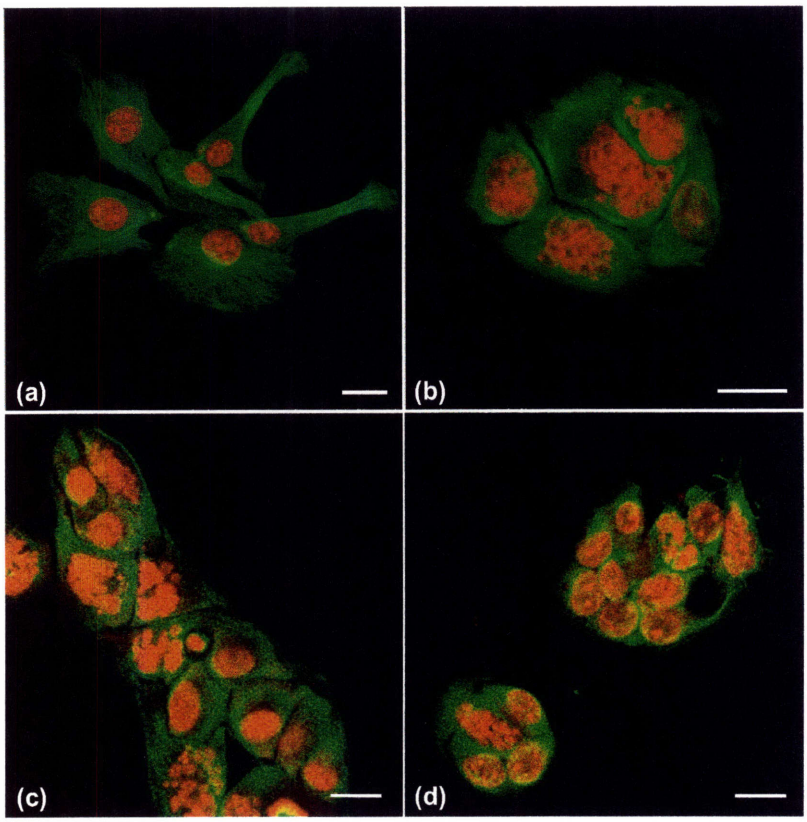

Fig. 4.18. BNL CL.2 cells incubated with (a) no treatment, (b) paclitaxel, and paclitaxel-loaded particles with galactose substitutions of (c) 0% and (d) 100% for 24 h. Nominal paclitaxel concentration = 0.1 μg/mL. Polymer MW = 4.8 kDa. Scale bar = 20 μm.

Table 4.5. Percentage of BNL CL.2 cell population in different phases of the cell cycle before or after treatment with paclitaxel or paclitaxel-loaded particles. Nominal paclitaxel concentration = 0.1 μM. Polymer MW = 4.8 kDa, galactose substitution = 100%.

Phase	Untreated	Treated with Paclitaxel	Treated with Paclitaxel-Loaded Particles
G0/G1	82	22	23
S	5	15	9
G2/M	13	62	65

4.3.3.2 Cytotoxicity Studies on Control Cell Line

Fig. 4.19 showed the cytotoxicity of paclitaxel and paclitaxel-loaded particles in the control NIH/3T3 cell line. The LC_{50} values of all the particles were comparable to that of free

paclitaxel (1.2 μM) (Table 4.6). There was no effect due to the galactose substitution in the polymer, since NIH/3T3 cells do not over-express ASGP receptors.

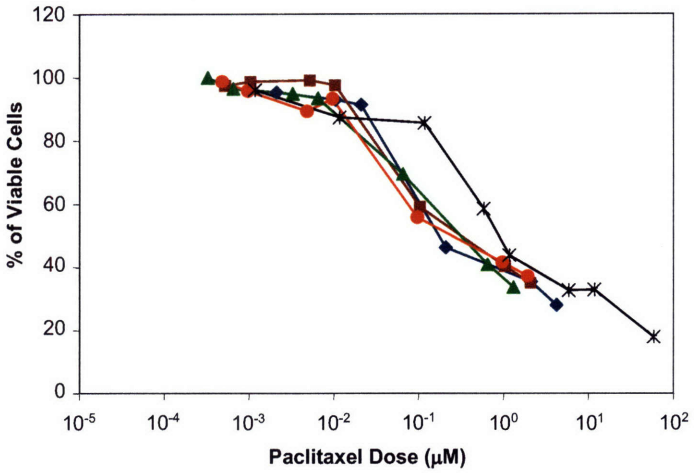

Fig. 4.19. Viability of NIH/3T3 cells incubated for 24 h with (✳) paclitaxel, and paclitaxel-loaded particles of 4.8 kDa with galactose substitutions of (●) 0%, (▲) 50%, (■) 75% and (◆) 100%. Values are mean ± standard deviation; n = 3.

Table 4.6. LC_{50} (μM) of paclitaxel-loaded particles in NIH/3T3 cells.

% Galactose Substitution	MW (kDa)				
	4.8	6.5	8.8	9.6	11.9
0	1.5×10^{-1}	3.0×10^{-1}	3.5×10^{-1}	8.3×10^{-1}	1.0×10^{0}
50	2.0×10^{-1}	2.6×10^{-1}	3.9×10^{-1}	3.8×10^{-1}	7.0×10^{-1}
75	2.3×10^{-1}	3.7×10^{-1}	5.2×10^{-1}	5.0×10^{-1}	7.9×10^{-1}
100	3.5×10^{-1}	4.5×10^{-1}	3.5×10^{-1}	5.0×10^{-1}	5.6×10^{-1}

4.3.4 Effect of Galactose Substitution on LC_{50} in Target and Control Cell Lines

The expression of galactose had a significant effect on the cytotoxicity of the paclitaxel-loaded particles in the target BNL CL.2 cell line. Fig. 4.20 showed the ratio of the LC_{50} of targeted particles to that for non-targeted particles synthesized from the same MW polymer as a function of the percentage of galactose substituted polymer used to form the targeted particles. The paclitaxel dosage needed to achieve the same cytotoxic effect was reduced by ~ 1–3 orders of magnitude using the targeted particles with galactose substitution.

In contrast, the presence of galactose had no effect on the cytotoxicity towards the control NIH/3T3 cell line. Fig. 4.21 shows the ratio of LC_{50} of targeted particles to that for non-targeted particles synthesized from 4.8 kDa polymer as a function of the galactose substitution in the targeted particles. Unlike for the BNL CL.2 cells, there was no appreciable change or trend in toxicity due to galactose substitution on the polymer for the NIH/3T3 cells. This confirmed the successful targeting of BNL CL.2 cells by the galactose-expressing particles.

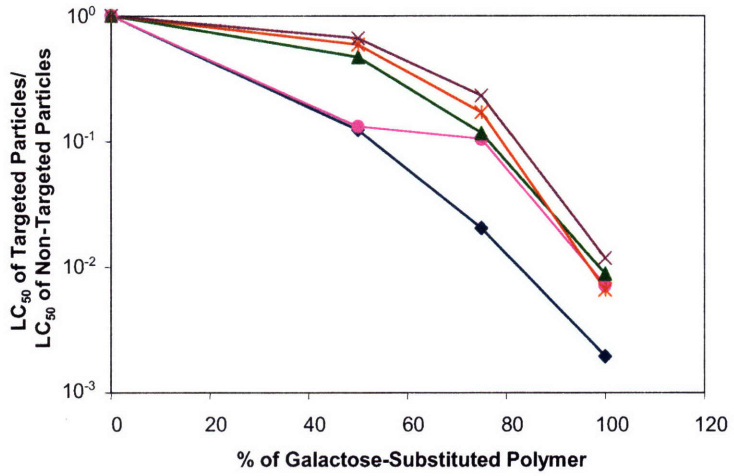

Fig. 4.20. Change in LC_{50} in BNL CL.2 cells incubated for 24 h with paclitaxel-loaded particles with polymer MW's of (◆) 4.8, (●) 6.5, (▲) 8.8, (✳) 9.6, and (×) 11.9 kDa, as a function of galactose substitution in the targeted particles.

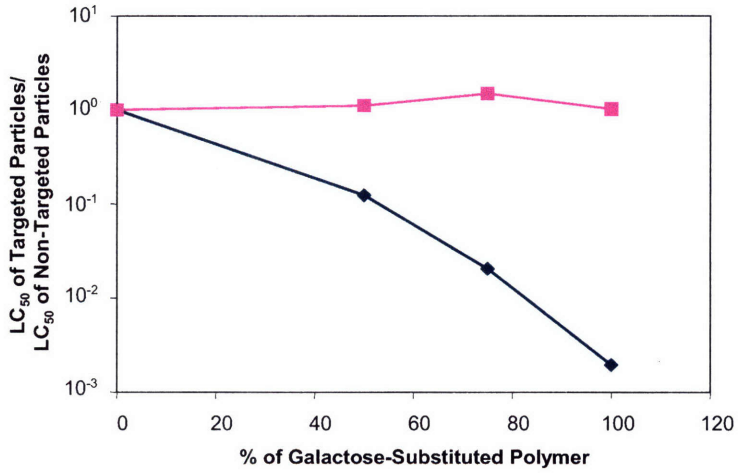

Fig. 4.21. Change in LC_{50} in (◆) BNL CL.2 and (■) NIH/3T3 cells incubated for 24 h with paclitaxel-loaded particles with a polymer MW of 4.8 kDa, as a function of galactose substitution in the targeted particles.

4.4 Summary and Conclusions

Various synthesis parameters for a temperature- and pH-sensitive random copolymer of NIPAAm, DMAAm and UA have been optimized to spontaneously form particles in an aqueous medium. A range of compositions that yielded polymers with physical properties appropriate for drug delivery has been identified. The desired LCST was obtained by adjusting the content of DMAAm and UA to change the hydrophilicity of the polymer. The hydrophilicity of UA was dependent on pH, and thus, made the polymer pH-sensitive. Galactose was attached to the end-group of the polymer to target it to hepatocytes. MW was found to be an important property of these polymers. The drug loading, particle size and release rate were affected by the polymer MW.

Paclitaxel was encapsulated in stimuli-responsive particles that released nearly 100% of the drug within 24 h at a pH of 5.0 at 37°C. The cytotoxicity of the stimuli-responsive, non-targeted particles was slightly higher than that of free paclitaxel. In contrast, the non-stimuli-responsive particles with no galactose substitution were less toxic than free paclitaxel. Since the polymer LCST was greater than 37°C, even if the non-stimuli-responsive particles were internalized by cells, only the portion of the drug that diffused out of the particles would become available to the cells.

In the target hepatocyte cell line, the galactose-expressing particles had LC_{50} values that were 1–3 orders of magnitude lower than the non-targeted particles and free paclitaxel. At higher galactose substitutions, there would be greater particle uptake by the target cell line. For the stimuli-responsive particles, this led to a dramatic increase in toxicity since more particle uptake would result in greater drug release under the pH- and temperature-sensitive conditions. In the control cell line, as expected, the presence of galactose did not have any effect on cytotoxicity.

4.5 References

[1] K. Ulbrich, T. Etrych, M. Jelinkova, B. Rihova, HPMA copolymers with pH-controlled release of doxorubicin: *In vitro* cytotoxicity and *in vivo* antitumor activity, J. Control. Release 87 (2003) 33–47.

[2] J. A. Champion, Y. K. Katare, S. Mitragotri, Particle shape: A new design parameter for micro- and nanoscale drug delivery carriers, J. Control. Release 121 (2007) 3–9.

[3] J. Sudimack, R. Lee, Targeted drug delivery via the folate receptor, Adv. Drug. Deliv. Rev. 41 (2000) 147–162.

[4] H.-S. Yoo, E. Lee, T. Park, Folate receptor targeted biodegradable polymeric doxorubicin micelles, J. Control. Release 96 (2004) 273–283.

[5] E. Lee, K. Na, Y. H. Bae, Polymeric micelle for tumor pH and folate-mediated targeting, J. Control. Release 91 (2003) 103–113.

[6] D. Saraydin, E. Koptagel, S. Unver-Saraydin, E. Karada, O. Guven, *In vivo* biocompatibility of radiation induced acrylamide and acrylamide/maleic acid hydrogels, J. Mater. Sci. 36 (2001) 2473–2481.

[7] S. Fernandez-Cossío, M. T. Castano-Oreja, Biocompatibility of two novel dermal fillers: Histological evaluation of implants of a hyaluronic acid filler and a polyacrylamide filler, Plast. Reconstr. Surg. 117 (2006) 1789–1796.

[8] H. Wei, X.-Z. Zhang, H. Cheng, W.-Q. Chen, S.-X. Cheng, R.-X. Zhuo, Self-assembled thermo- and pH-responsive micelles of poly(10-undecenoic acid-*b*-*N*-isopropylacrylamide) for drug delivery, J. Control. Release 116 (2006) 266–274.

[9] S. Q. Liu, Y. W. Tong, Y.-Y. Yang, Thermally sensitive micelles self-assembled from poly(*N*-isopropylacrylamide-*co*-*N*,*N*-dimethylacrylamide)-*b*-poly(D,L-lactide-*co*-glycolide) for controlled delivery of paclitaxel, Molecular BioSystems 1 (2005) 158–165.

[10] K. S. Soppimath, L.-H. Liu, W. Y. Seow, S.-Q. Liu, R. Powell, P. Chan, Y.-Y. Yang, Multifunctional core/shell nanoparticles self-assembled from pH-induced thermosensitive polymers for targeted intracellular anticancer drug delivery, Adv. Funct. Mater. 17 (2007) 355–362.

[11] K. S. Soppimath, D. C.-W. Tan, Y.-Y. Yang, pH-triggered thermally responsive polymer core-shell nanoparticles for drug delivery, Adv. Mater. 17 (2005) 318–323.

[12] G. Chen, A. S. Hoffman, Graft copolymers that exhibit temperature-induced phase transitions over a wide range of pH, Nature 373 (1995) 49–52.

[13] H.-L. Lin, T.-Y. Liu, G.-Y. Chau, W.-Y. Lui, C.-W. Chi, Comparison of 2-methoxyestradiol-induced, docetaxel-induced, and paclitaxel-induced apoptosis in

hepatoma cells and its correlation with reactive oxygen species, Cancer 89 (2000) 983–994.

[14] E. Rowinsky, R. Donehower, Paclitaxel (Taxol), New Engl. J. Med. 332 (1995) 1004–1014.

[15] T. K. Yeung, C. Germond, X. Chen, Z. Wang, The mode of action of Taxol: Apoptosis at low concentration and necrosis at high concentration, Biochem. Bioph. Res. Co. 263 (1999) 398–404.

[16] H. Feil, Y. H. Bae, J. Feijen, S. W. Kim, Mutual influence of pH and temperature on the swelling of ionizable and thermosensitive hydrogels, Macromolecules 25 (1992) 5528–5530.

[17] M. Wilhelm, C.-L. Zhao, Y. Wang, R. Xu, M. Winnik, J.-L. Mura, G. Riess, M. Croucher, Poly(styrene-ethylene oxide) block copolymer micelle formation in water: A fluorescence probe study, Macromolecules 24 (1991) 1033–1040.

[18] X.-Q. Zhang, X.-L. Wang, P.-C. Zhang, Z.-L. Liu, R.-X. Zhuo, H.-Q. Mao, K. W. Leong, Galactosylated ternary DNA/polyphosphoramidate nanoparticles mediate high gene transfection efficiency in hepatocytes, J. Control. Release 102 (2005) 749–763.

[19] M. Dubois, K. A. Gilles, J. K. Hamilton, P. A. Rebers, F. Smith, Colorimetric method for determination of sugars and related substances, Anal. Chem. 28 (1956) 350–356.

[20] G. Bokias, A. Durand, D. Hourdet, Molar mass control of poly(*N*-isopropylacrylamide) and poly(acrylic acid) in aqueous polymerizations initiated by redox initiators based on persulfates, Macromol. Chem. Phys. 199 (1998) 1387–1392.

[21] K. Huh, S. C. Lee, Y. W. Cho, J. Lee, J. H. Jeong, K. Park, Hydrotropic polymer micelle system for delivery of paclitaxel, J. Control. Release 101 (2005) 59–68.

[22] L. A. Bauer, N. S. Birenbaum, G. J. Meyer, Biological applications of high aspect ratio nanoparticles, J. Mater. Chem. 14 (2004) 517–526.

[23] L. E. Euliss, J. A. DuPont, S. Gratton J. DeSimone, Imparting size, shape, and composition control of materials for nanomedicine, Chem. Soc. Rev. 35 (2006) 1095–1104.

[24] J. A. Champion, Y. K. Katare, S. Mitragotri, Making polymeric micro– and nanoparticles of complex shapes, Proc. Natl. Acad. Sci. U. S. A. 104 (2007) 11901–11904.

[25] D. S. T. Hsieh, W. D. Rhine, R. Langer, Zero-order controlled-release polymer matrices for micromolecules and macromolecules, J. Pharm. Sci. 72 (1983) 17–22.

[26] P. Decuzzi, M. Ferrari, The adhesive strength of non-spherical particles mediated by specific interactions, Biomaterials 27 (2006) 5307–5314.

[27] Y. Geng, P. Dalhaimer, S. Cai, R. Tsai, M. Tewari, T. Minko, D. Discher, Shape effects of filaments versus spherical particles in flow and drug delivery, Nat. Nanotech. 2 (2007) 249–255.

[28] P. Kohli, C. R. Martin, Smart nanotubes for biotechnology, Curr. Pharm. Biotechnol. 6 (2005) 35–47.

[29] L. M. Roberts, F. I. Lamb, D. J. C. Pappin, J. M. Lord, The primary sequence of Ricinus communis agglutinin: Comparison with ricin, J. Biol. Chem. 260 (1985) 15682–15686.

[30] L. L. Houston, T. P. Dooley, Binding of two molecules of 4-methylumbelliferyl galactose or 4-methylumbelliferyl *N*-acetylgalactosamine to the B chains of ricin and Ricinus communis agglutinin and to purified ricin B chain, J. Biol. Chem. 257 (1982) 4147–4151.

[31] R. Gref, Y. Minamitake, M. Peracchia, V. Trubetskoy, V. Torchilin, R. Langer, Biodegradable long-circulating polymeric nanospheres, Science 261 (1994) 1600–1603.

[32] Y.-I. Jeong, J.-B. Cheon, S.-H. Kim, J.-W. Nah, Y.-M. Lee, Y.-K. Sunge, T. Akaikef, C.-S. Cho, Clonazepam release from core-shell type nanoparticles *in vitro*, J. Control. Release 51 (1998) 169–178.

[33] K. Na, K.-H. Park, S. Kim, Y. H. Bae, Self-assembled hydrogel nanoparticles from curdlan derivatives: Characterization, anti-cancer drug release and interaction with a hepatoma cell line (HepG2), J. Control. Release 69 (2000) 225–236.

[34] C. Zhang, P. Qineng, H. Zhang, Self-assembly and characterization of paclitaxel-loaded *N*-octyl-*O*-sulfate chitosan micellar system, Colloid. Surface. B 39 (2004) 69–75.

[35] S. Gagandeepa, P. M. Novikoffa, M. Otta, S. Gupta, Paclitaxel shows cytotoxic activity in human hepatocellular carcinoma cell lines, Cancer Lett. 136 (1999) 109–118.

[36] E. K. Rowinsky, P. J. Burke, J. E. Karp, R. W. Tucker, D. S. Ettinger, R. C. Donehower, Phase I and pharmacodynamic study of Taxol in refractory acute leukemias, Cancer Res. 49 (1989) 4640–4647.

Chapter 5 – Recommendations for Future Work

5.1 Further Enhancement of Drug Delivery Systems

Several researchers have performed binding studies with various molecules that were thought to mimic the binding site of the native asialoglycoprotein receptor ligand. These studies have shown that the binding affinity increases significantly when the number of terminal galactose residues was increased from one to three [1, 2]. The increase in affinity observed with a tri-galactose substituted molecule is greater than what can be expected from a simple collision theory effect. The multivalent structure is a general characteristic of carbohydrate ligands, and is known as the "cluster effect" [3, 4]. Additionally, increasing the flexibility of the galactose residues by putting a spacer molecule between the delivery vehicle and the targeting ligand also improves the affinity by increasing the chances of binding in a specific orientation [5]. Attaching galactose or a tri-galactose molecule through a spacer, such as poly(ethylene glycol) would improve the binding affinity of our drug delivery systems.

5.2 Mechanism of Action

It is important to identify the mechanism of action of a drug delivery vehicle. We measured the cytotoxicity using the MTT assay and performed some preliminary mechanistic studies with cell cycle analysis. However, assays that directly measure the effect of the drugs being delivered would provide more detailed information about the influence of the delivery vehicle. Doxorubicin leads to apoptosis by stabilizing an intermediate complex between DNA and topoisomerase II [6]. Additionally, an increase in p53 expression is often associated with the induction of apoptosis [7]. The levels of topoisomerase II and p53 can be measured to investigate the direct effect of doxorubicin.

Paclitaxel acts by various mechanisms in different cell types at different concentration ranges [8-10]. Since it stabilizes microtubules, the most direct measurement of the effect would be to study the number of asters of mitotic spindles, which should increase after treatment. Several proteins have also been associated with paclitaxel-mediated cell death, including Raf-1, p53 and p21 [8]. The expression of these proteins could also be studied to investigate the mechanism of action of the delivery vehicle.

5.3 Applications to Other Drugs and Therapeutics

Several other anthracycline chemotherapeutic agents such as epirubicin, daunorubicin and idarubicin can be conjugated to dextran through the same synthesis procedures given in Chapters 2 and 3 [11, 12]. Docetaxel is a hydrophobic chemotherapeutic agent similar to paclitaxel, which can be encapsulated in the polymer particles described in Chapter 4 [13]. Rifabutin (for advanced HIV treatment) and rifapentine (for pulmonary tuberculosis) are also hydrophobic drugs that can be delivered using these particles.

Cancerous cells often are or can become resistant to a wide variety of exogenous toxins. One mechanism is an over-expression of P-glycoprotein, which is a membrane transporter that can bind many drugs and pump them out of the cell [14]. Attachment of a drug to polymers or delivery through particles reduces the effect of multidrug resistance since the transporter cannot expel anything larger than a small molecule drug. The drug delivery systems developed in this work can be tested for effectiveness in *in vitro* studies using multidrug resistant cell lines.

Other than drug delivery, targeted delivery systems can also be utilized in gene delivery and biomedical imaging. Fluorescent or radio-labeled markers can be encapsulated in the polymer particles for imaging purposes [15].

5.4 References

[1] L. Seymour, Soluble polymers for lectin-mediated drug targeting, Adv. Drug. Deliv. Rev. 14 (1994) 89–111.

[2] A. Kichler, F. Schuber, Comparative affinity of synthetic multi-antennary galactosyl derivatives for the Gal/GalNAc receptor of rat hepatocytes and peritoneal macrophages, J. Drug Target. 6 (1998) 201–205.

[3] R. Roy, Syntheses and some applications of chemically defined multivalent glycoconjugates, Current Opinion in Structural Biology 6 (1996) 692–702.

[4] Y. Ohya, H. Oue, K. Nagatomi, T. Ouchi, Design of macromolecular prodrug of cisplatin using dextran with branched galactose units as targeting moieties to hepatoma cells, Biomacromolecules 2 (2001) 927–933.

[5] R. Lee, P. Lin, Y. Lee, New synthetic cluster ligands for galactose/N-acetylgalactosamine-specific lectin of mammalian liver, Biochemistry 23 (1984) 4255–4261.

[6] K. M. Tewey, T. C. Rowe, L. Yang, B. Halligan, L. F. Liu, Adriamycin-induced DNA damage mediated by mammalian DNA topoisomerase II, Science 226 (1984) 466–468.

[7] O. Hovorka, M. St'astny, T. Etrych, V. Subr, J. Strohalm, K. Ulbrich, B. Rihova, Differences in the intracellular fate of free and polymer-bound doxorubicin, J. Control. Release 80 (2002) 101–117.

[8] H.-L. Lin, T.-Y. Liu, G.-Y. Chau, W.-Y. Lui, C.-W. Chi, Comparison of 2-methoxyestradiol-induced, docetaxel-induced, and paclitaxel-induced apoptosis in hepatoma cells and its correlation with reactive oxygen species, Cancer 89 (2000) 983–994.

[9] K. Torres, S. B. Horwitz, Mechanisms of Taxol-induced cell death are concentration dependent, Cancer Res. 58 (1998) 3620–3626.

[10] T. K. Yeung, C. Germond, X. Chen, Z. Wang, The mode of action of Taxol: Apoptosis at low concentration and necrosis at high concentration, Biochem. Bioph. Res. Co. 263 (1999) 398–404.

[11] N. T. Zaman, J. Y. Ying, Synthesis, characterization and *in vitro* studies of dextran-galactose conjugates for targeted doxorubicin delivery to hepatocytes, To be submitted to J. Control. Release.

[12] N. T. Zaman, J. Y. Ying, Synthesis, characterization and *in vitro* studies of acid-labile dextran conjugates for doxorubicin delivery, To be submitted to J. Control. Release.

[13] N. T. Zaman, Y.-Y. Yang, J. Y. Ying, Synthesis, characterization and *in vitro* studies of a temperature- and pH-sensitive polymer and its use in targeted delivery of paclitaxel to hepatocytes, To be submitted to Adv. Mater.

[14] M. Yamazaki, H. Suzuki, Y. Sugiyama, Recent advances in carrier-mediated hepatic uptake and biliary excretion of xenobiotics, Pharm. Res. 13 (1996) 497–513.

[15] J. Reddy, L.-C. Xu, N. Parker, M. Vetzel, C. Leamon, Preclinical evaluation of 99mTc-EC20 for imaging folate receptor-positive tumors, J. Nucl. Med. 45 (2004) 857–866.

Chapter 6 – Conclusions

Cancer is a highly variable disease occurring in many organs. There is a need for delivery systems that are easily adaptable for a number of targets in different forms of cancers, and that can accommodate various cytotoxic drugs. The motivation of this project was to develop flexible synthesis procedures for the targeted delivery of chemotherapeutic agents. In this thesis, we have designed and tested three drug delivery systems.

A simple, efficient synthesis scheme was developed to conjugate doxorubicin to dextran with varying degrees of galactose substitution to target hepatocytes. The synthesis scheme was simple, efficient and easily adaptable to other therapeutic agents and targeting moieties with free amine groups. In cell culture studies on the target cell line, the dextran-doxorubicin-galactose (DDG) conjugates showed lower toxicity compared to doxorubicin, increased toxicity with higher molecular weight (MW) polymers, and greater toxicity with higher degree of galactose substitution. Experiments in the control cell lines showed increased toxicity for higher MW polymers; however, there was no effect due to the presence of galactose. At diameters of 15–40 nm, the polymer conjugates were too large to enter the cell nuclei in large quantities, but sufficient conjugates entered the nuclei to cause cell death. The higher MW polymers were more effective since they had a higher chain loading of doxorubicin.

In spite of successful targeting, the cytotoxicity of the first system was limited since the doxorubicin remained attached to the polymer. In the second system, we synthesized pH-sensitive dextran-doxorubicin conjugates of different MW's. Doxorubicin was attached through a hydrazone bond to the dextran backbone. These polymer conjugates were stable at a physiological pH of 7.4, but released over 70% of the attached doxorubicin within 24 h at a pH of 5.0. The rate of release was found to be faster for the lower MW polymers. In cell culture studies, the conjugates showed significant cytotoxicity. The effect of lower chain loading of doxorubicin for the lower MW polymers was offset by the rapid initial release, and they showed slightly greater toxicity. Uptake of the conjugates occurred within minutes after incubation, and since release occurred over hours, the conjugates might have gone through multiple endocytosis and exocytosis cycles before the doxorubicin was released. Doxorubicin from the dextran-hydrazone-doxorubicin (DHD) conjugates was found to localize almost exclusively in the nuclei

of cells. Since doxorubicin attached to dextran with a stable bond showed limited localization in the nuclei, this confirmed that doxorubicin from the acid-labile conjugates was released after internalization by cells. The cytotoxicity of the DHD conjugates was significantly greater than the stable DDG conjugates due to the release of doxorubicin inside cells.

In the third drug delivery system, the targeting and stimuli-responsive functionalities were combined using an amphiphilic copolymer of *N*-isopropylacrylamide (NIPAAm), *N*,*N*-dimethylacrylamide (DMAAm) and 10-undecenoic acid (UA). A range of compositions that yielded polymers with physical properties appropriate for drug delivery has been identified. The appropriate lower critical solution temperature (LCST) was obtained by adjusting the content of DMAAm and UA to change the hydrophilicity of the polymer. The hydrophilicity of UA was dependent on pH, and thus, rendered the polymer pH-sensitive. Galactose was attached to the end-group of the copolymer to target it to hepatocytes. The drug loading, particle size and release rate were affected by the polymer MW. Paclitaxel was encapsulated in particles that released nearly 100% of the drug within 24 h at a pH of 5.0 at 37°C. In the target hepatocyte cell line, these stimuli-responsive, galactose-expressing particles had LC_{50} values that were 1 order of magnitude lower than the non-stimuli-responsive particles, and 1 to 3 orders of magnitude lower than the non-targeted particles. In the control cell line, as expected, the presence of galactose did not have any effect on cytotoxicity.